Determination of Lipid Peroxidation Associated with a Focal Seizure Model through *In Vivo* Microdialysis Sampling

By

Justin Carl Cooley
B.S University of Northern Colorado
Greeley, CO

Submitted to the graduate degree program in Chemistry and the Graduate Faculty of the University of Kansas in partial fulfillment of the requirements for the degree of Doctor of Philosophy.

_____
Craig Lunte (Chairperson)

_____
Heather Desaire

_____
Mario Rivera

_____
Mike Johnson

_____
Audrey Lamb

Date Defended: September 7th 2012

The Thesis Committee for Justin Carl Cooley

certifies that this is the approved version of the following thesis:

Determination of Lipid Peroxidation Associated with a Focal Seizure Model through *In Vivo* Microdialysis Sampling

_____

Chairperson Craig E Lunte

Date approved: December 12th, 2012

Abstract

Justin Carl Cooley Ph.D
Ralph N. Adams Institute for Bioanalytical Chemistry
University of Kansas, 2012

Two methods were developed to evaluate the extent of lipid peroxidation in an animal model of focal seizures. Microdialysis was used to sample from the extracellular fluid in specific regions of the hippocampus. The first method was a CE-fluorescence method for the thiobarbituric acid derivatized malondialdehyde (MDA) fluorophore. The second was an HPLC-MS method for seven eicosanoids; five products of the cyclooxygenase (COX) pathway (6-ketoprostaglandin $F_{1\alpha}$, thromboxane B_2, prostaglandin F_2, prostaglandin E_2 and prostaglandin D_2), one product of the lipooxygenase pathway (leukotriene B_4), and one free radical byproduct of prostaglandin formation (8-isoprostaglandin F_2). In a focal seizure model, a microdialysis probe was implanted in either the CA1 or CA3 region of the hippocampus. The chemical convulsant 3-mercaptopropionic acid (3-MPA) was dosed directly into the hippocampus by perfusion through the microdialysis probe for 50 minutes to produce a focal seizure.

There were significant increases ($p > 0.001$ compared to control) in MDA from 20 minutes after the start through 30 minutes after the end of dosing. It is hypothesized that these increases in MDA were related to the COX pathway. Therefore, an LC-MS method was developed and applied to the same animal model. Interestingly, there were decreases in the detectable prostaglandins (E2, D2, F2, and TXB2) during the 3-MPA dosing followed by immediate increases after dosing. It is thought that these prostaglandins are rapidly depleted during dosing from excessive oxidative damage.

Acknowledgements

I would first like to thank my parents, Jim and Maria who have been so supportive over the past 30 years, along with my sisters Brianne and Jennica and brothers-in-law Kevin and Brian. Although they kept asking that dreadful question "When are you going to be done?" I know they just wanted me to be happy, and of course to go on a celebratory vacation.

The first time I actually enjoyed learning science was from two of my high school teachers, Mr. Hall and Mr. Richardson (chemistry and human anatomy, respectively). It is because of them that I pursued a degree in science.

I still find myself thinking of the words of wisdom from my undergraduate analytical professor Dr. Pringle, "think about what is happening on a chemical level." It is because of him I try to keep things simple and understand that just because a technique is old that doesn't mean that it is still not good chemistry (*i.e.* the qual scheme).

I certainly would not be here if it were not for my mentor Dr. Craig Lunte. Your mentoring style with me may not be conventional (I'll never forget seeing you downtown after the Jayhawks final four win in 2008), but it certainly kept me on my toes. Your vernacular provided a barrage of verbiage to cogitate but it usually left me with a dearth of rejoinder. I feel as though over the past 6 years I have matured not only as a scientist but also as a person thanks to your tutelage. Working for you has been a wonderful experience (for the most part) and I will be forever grateful.

To all my dearest friends (Tommy, Steve, Brian, Nevin, Hannah, Troy, Phil, Maggie, Matt, Megen, Heath, Tom, Dan, and the countless others) thank you for all the wonderful memories of evenings and weekends of great times with little drama.

Of course I have to thank my wonderful fiancée Megan (because if I don't…hell hath no fury). She was the voice of reason through all my moments of insane panic and distress. She put up with all my little (*i.e.* big) annoyances including but not limited to; dancing, hand-chopping, singing (beautifully I might add), stupid noises, and awkward looks. Every time she rolls her eyes at me, I know it's out of love. You bring so much joy and happiness to my life, I love you with all my heart.

Table of Contents

Chapter 1: Introduction to Oxidative Stress

1.1 Oxidative Stress 1

1.1.1 Reactive Oxygen Species 1

1.1.2 Necrosis/Apoptosis 4

1.1.3 Antioxidants 4

1.2 Lipid Peroxidation 5

1.2.1 Lipid Release and Metabolism 5

1.2.2 Lipid Peroxidation Biomarkers 6

1.3 Ischemia/Reperfusion 9

1.3.1 Ischemia/Hypoxia 9

1.3.2 Reperfusion 9

1.4 Seizure 10

1.4.1 Propagation of Neuronal Signal 10

1.4.2 Excitatory and Inhibitory Mechanisms 11

1.4.3 Development of Epilepsy 14

1.4.4 Chemically Induced Seizure Models 14

1.5 Microdialysis Sampling 16

1.5.1 Principle of Microdialysis 16

1.5.2 Microdialysis Calibration 18

1.5.3 Advantages/Disadvantages of Microdialysis 19

1.5.4 Analytical Consideration When Using Microdialysis 20

1.6 Conclusions 21

1.7 References 22

Chapter 2: Capillary Electrophoresis-Fluorescence Method for Malondialdehyde

Introduction 25

2.1 Capillary Electrophoresis 26

2.1.1 Basic Principles 26
2.1.2 CE Detection Methods 29
2.1.3 CE with Microdialysis Samples 30
2.2 Method 31
2.2.1 Chemicals 31
2.2.2 Reaction Conditions 31
2.2.3 CE Method 31
2.2.4 Mass Spectrometry 32
2.2.5 Microdialysis Probe Fabrication 33
2.2.6 Liver Animal Model 33
2.2.7 Antipyrine LC-UV Method 34
2.3 Discussion 34
2.3.1 Reaction 34
2.3.2 CE Conditions 38
2.3.3 Peak Identification 38
2.3.4 Mass Spectrometric Identification 41
2.4 MDA in Microdialysis 44
2.4.1 Relative Recovery 44
2.4.2 *In Vivo* Application 48
2.5 Conclusion 52
2.6 References 54

Chapter 3: Malondialdehyde as a Measure for Lipid Peroxidation in Local 3-MPA Dosing Model

Introduction 57
3.1 Brain Model of Seizures 57
3.1.1 Hippocampus 60
3.1.2 Systemic Dosing Model 60
3.1.3 Focal Dosing Model 61

3.2 Methods 64
3.2.1 Chemicals 64
3.2.2 CE-Fluorescence Method 64
3.2.3 Animal Surgery 64
3.3 MDA from Local Dosing of 3-MPA 67
3.3.1 MDA Reaction Modification 67
3.3.2 Delivery of 3-MPA through Microdialysis Probe 67
3.3.3 Varying 3-MPA Concentrations between Regions 68
3.3.4 Statistical Difference in MDA between Dosing Regimens 68
3.4 Glu/GABA from Local Dosing of 3-MPA 71
3.4.1 LC-Fluorescence Method of Glutamate and GABA 71
3.4.2 Increases in both Glutamate and GABA 73
3.4.3 GAD Isoforms 75
3.5 Neuromechanisms 76
3.5.1 MDA in the Hippocampus 76
3.5.2 GABAergic Neuronal Projections 81
3.5.3 Enzymatic Pathways Leading to MDA 81
3.6 Conclusion 82
3.7 References 84

Chapter 4: LC/MS Method Development for Eicosanoid7

Introduction 87
4.1 Mass Spectrometry 89
4.1.1 Ionization 90
4.1.2 Mass Analyzers 92
4.2 Methods 94
4.2.1 Chemicals 94
4.2.2 LC Conditions 94
4.2.3 MS Conditions 95

4.2.4 Microdialysis Application 97
4.2.4.1 *In Vitro* 97
4.2.4.2 *In Vivo* Animal Model 97
4.3 Separation 98
4.3.1 Column Selection 98
4.3.2 Mobile Phase 98
4.3.3 Gradient Profile 99
4.4 Tandem MS 99
4.4.1 Full-Scan MS1 99
4.4.2 MRM Development 100
4.4.3 S/N Optimization 100
4.5 Validation 109
4.5.1 Ionization Suppression 109
4.5.2 Reproducibility 112
4.6 Microdialysis 116
4.6.1 *In Vitro* Sample Switching 116
4.6.2 *In Vivo* 3-MPA Local Dosing 116
4.7 Conclusion 122
4.8 References 124

Chapter 5: Conclusions and Future Directions

5.1 Conclusions 127
5.2 Future Directions 129
5.3 References 131

Tables

Table 1.1 Leading causes of epilepsy in the US 15

Table 3.1 Data from microdialysis plots for CA1 and CA3 regions 80

Table 4.1 MS/MS settings for scans from individual segments 96

Table 4.2 Intra-day reproducibility of the seven eicosanoids 113

Table 4.3 Inter-day reproducibility of the seven eicosanoids 114

Table 4.4 Recoveries for eicosanoids during the sample switching *in vitro* 118

Figures

Figure 1.1 Biological pathways of ROS formation leading to cellular damage 2

Figure 1.2 Reactions involving iron leading to production of ROS 3

Figure 1.3 Pathway of lipid peroxidation forming secondary products 7

Figure 1.4 Prostaglandin versus isoprostane and MDA formation 8

Figure 1.5 Propagation of signal along a neuron 12

Figure 1.6 Depiction of a synapse with release of neurotransmitters 13

Figure 1.7 Illustration of linear microdialysis probe 17

Figure 2.1 Representation of the fixed and mobile layers in CE separation along with characteristic migration vectors for anions, cations and EOF 28

Figure 2.2 Derivatization scheme of MDA with fluorescence spectrum 36

Figure 2.3 MDA versus impurity with reaction time 37

Figure 2.4 Effects of Ringer's solution and surfactant on MDA peak efficiency 39

Figure 2.5 MDA peak verification with UV and fluorescence detection 40

Figure 2.6 MDA standards and calibration curve 42

Figure 2.7 MS spectra of MDA and TBA impurity 43

Figure 2.8 Electropherograms of dialysate samples in various tissues 45

Figure 2.9 Microdialysis calibration curves for MDA 47

Figure 2.10 Time course of liver ischemia experiments 49

Figure 2.11 Liver histology compared to respective MDA time plots 51

Figure 3.1 Synthesis of GABA from glutamate via glutamic acid decarboxylase 59

Figure 3.2 Data from systemic dosing method of 3-MPA 62

Figure 3.3 Data from local dosing model of 3-MPA 63

Figure 3.4 Diagram of CA1 and CA3 regions with probe placement 66

Figure 3.5 MDA in CA3 region with 10, 1 and 0.1 mM 3-MPA dosing 69

Figure 3.6 MDA in CA1 region with 10 and 1 mM 3-MPA dosing 70

Figure 3.7 Example chromatograms of NDA/CN derivatized amino acids 72

Figure 3.8 Glu and GABA in CA3 region with 10 mM 3-MPA dosing 74

Figure 3.9 MDA in CA1 and CA3 with 10 mM 3-MPA dosing 78

Figure 3.10 MDA in CA1 and CA3 with 1 mM 3-MPA dosing 79

Figure 4.1 Eicosanoids of interest involved in the arachidonic acid cascade 88

Figure 4.2 Illustration of electrospray ionization 91

Figure 4.3 Illustration of the linear ion trap with dual detector 93

Figure 4.4 CID spectra for 6-keto PGF 101

Figure 4.5 CID spectra for TXB 102

Figure 4.6 CID spectra for 8-isoPGF 103

Figure 4.7 CID spectra for PGF 104

Figure 4.8 CID spectra for PGE 105

Figure 4.9 CID spectra for PGD 106

Figure 4.10 CID spectra for LTB 107

Figure 4.11 Extracted ion chromatograms of each eicosanoid 108

Figure 4.12 Total ion chromatograms to examine the effects of ionization suppression with elution time 110

Figure 4.13 Ionization depression of Ringer's solution 111

Figure 4.14 Freeze-thaw data 115

Figure 4.15 Comparing 6-keto and LTB with *in vitro* sample switching 117

Figure 4.16 3-MPA in dialysate samples with 10 mM dosing 119

Figure 4.17 TXB, PGF, PGE, and PGD in CA3 region with 10 mM 3-MPA dosing 121

Chapter 1:

Introduction to Oxidative Stress

1.1 Oxidative Stress

1.1.1 Reactive Oxygen Species

Oxidative stress is the process by which free radicals, in particular reactive oxygen species (ROS), react with biological components such as DNA, proteins, and lipids. Oxidative stress occurs when high concentrations of ROS lead to an imbalance in the redox state of the cell. ROS such as super oxide and hydrogen peroxide can undergo neucleophilic reactions with thiols, amines and polyunsaturated fatty acids (PUFAs) found in biological systems. Super oxide radical ($O_2^{\bullet -}$) is formed through enzymatic (*e.g.* NADH oxidase) and nonenzymatic (*e.g.* ubiquinone) one electron redox reactions [1, 2]. Superoxide dismutase (SOD) reduces super oxide into hydrogen peroxide and singlet oxygen. Hydrogen peroxide can then be farther reduced to water or react with biological electrophiles. Superoxide can also combine with nitric oxide to form peroxynitrite [3]. Figure 1.1 shows these biological pathways.

Transition metal ions also play an important role in radical production. Metal ions (particularly iron) participate in one electron reactions in the Haber-Weiss cycle where hydrogen peroxide (or alkyl-hydroperoxide) is catalyzed by the metal ion to produce hydroxyl radical ($OH^{\bullet}$) (or alkyl-$O^{\bullet}$) [4]. These electron processes are shown in Figure 1.2. The continued production of ROS will eventually overwhelm the antioxidant defenses of the cell, ultimately causing cellular damage and death.

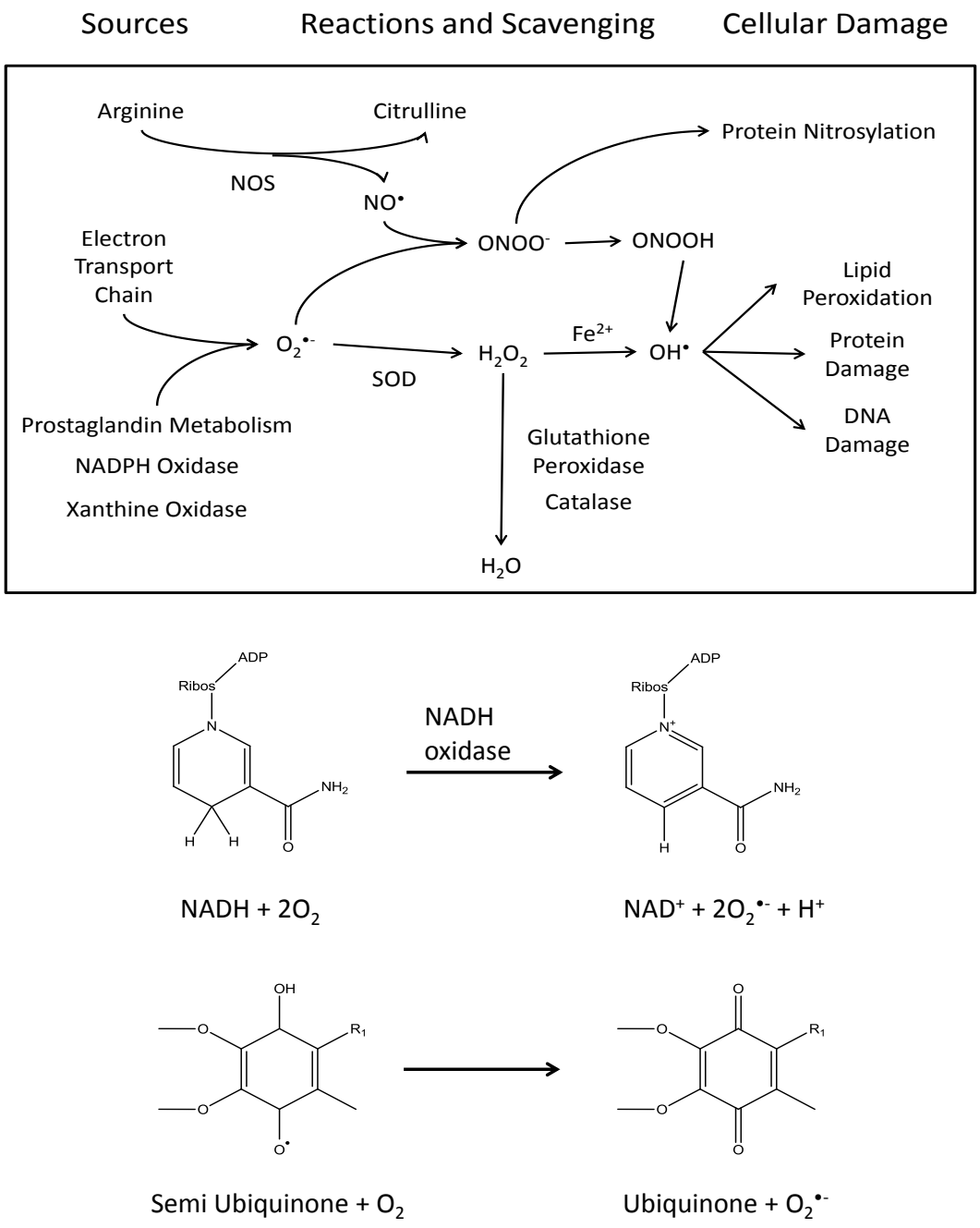

Figure 1.1: Biological pathways of ROS formation leading to cellular damage.

Haber-Weiss cycle

$$Fe^{3+} + O_2^{\bullet -} \longrightarrow Fe^{2+} + O_2$$
$$Fe^{2+} + H_2O_2 \longrightarrow Fe^{3+} + OH^- + OH^{\bullet}$$

Net $$O_2^{\bullet -} + H_2O_2 \longrightarrow OH^{\bullet} + OH^- + O_2$$

Fenton Reaction

$$Fe^{2+} + H_2O_2 \longrightarrow Fe^{3+} + OH^- + OH^{\bullet}$$
$$Fe^{3+} + H_2O_2 \longrightarrow Fe^{2+} + OOH^{\bullet} + H^+$$

Net $$H_2O_2 \longrightarrow OH^{\bullet} + OOH^{\bullet} + H_2O$$

Figure 1.2: Reactions involving iron leading to production of ROS.

1.1.2 Necrosis/Apoptosis

There are two physiological processes leading to cellular death, necrosis and apoptosis. Necrosis is the irreversible loss of metabolic function resulting from injury, while apoptosis is programmed cell death resulting in membrane-bound fragments of the whole cell containing viable organelles [5]. Necrosis occurs from a direct insult on the cell which is the case for an oxidative stress event, such as ischemia/reperfusion or seizure. Apoptosis is initiated through cellular messaging activating the cascade for cell death.

Cell death is a result of either interference with ATP synthesis or loss in plasma membrane function [6]. For example, during ischemia ATP is rapidly depleted due to a lack of energy and oxygen getting to the cell. A drop in ATP production alone does not necessarily cause necrosis but can result in acidosis as well as loss in ion homeostasis [5, 6]. The changes in cytosolic ion concentrations, particularly Ca^{2+}, can lead to very detrimental effects. Increases in Na^{+} can lead to cell swelling and, in the case of neurons, the inability to produce an action potential, but this damage is reversible. An increase in Ca^{2+}, however, causes an increase in mitochondrial membrane permeability leading to a further drop in ATP production and release of reactive oxygen [7]. Calcium can come from extracellular influx, release from endoplasmic reticulum, or drop in Ca^{2+} removal [5]. The Ca^{2+} overload does not solely lead to mitochondrial permeability. Only when in conjunction with the dearth of ATP will Ca^{2+} cause the permeability transition pore to open [7]. Leakage across the mitochondrial membrane from the transition pore causes a further decline in ATP production.

1.1.3 Antioxidants

When free radical species formed outweigh the antioxidant measures major cellular damage will occur. Thiols, particularly glutathione (GSH), play an important role in free radical scavenging. Defense systems that protect against these ROS include superoxide dismutase, which converts superoxide into hydrogen peroxide; catalase, which catalyzes the reduction of hydrogen peroxide to water and oxygen; and glutathione peroxidase, which helps eliminate hydrogen peroxide.

1.2 Lipid Peroxidation

1.2.1 Lipid Release and Metabolism

The brain is highly susceptible to oxidative damage because of its large consumption of oxygen, limited antioxidant capacity and high concentration of PUFAs. Arachidonic acid (AA) comprises about half of the PUFA phospholipids found in the brain [8]. AA is stored in membranes through esterification as phospholipids and is enzymatically released by phospholipase A_2 [9]. The activity of phospholipase A_2 increases upon the influx of Ca^{2+} during ischemia or seizure as well as with a drop in pH [10]. AA is involved in the synthesis of ceramide (through sphingomyelinase) which inhibits the electron transport chain (complex I and II) leading to an increase in hydrogen peroxide, generating more ROS [11]. AA can be metabolized by cyclooxygenase (COX), forming prostaglandins (PGs); lipooxygenase (LOX), producing leukotrienes and hydroperoxyeicosatetraenoic acids; or cytochrome P450, forming epoxyeicosatrienoic acids [12]. PGs are synthesized through a 2-step enzymatic oxidation of AA via COX, leading to the formation of PGH_2 and superoxide [13]. COX-2 (an isoform of COX) is highly expressed in glutaminergic neurons and plays a role in neuronal plasticity. COX-2 is upregulated by stimuli and cellular stress including that from excitatory amino acids [13].

Enzymatic reactions make up only a portion of lipid peroxidation; PUFAs are highly susceptible to radical attack and oxidation (Figure 1.3). The C-H bond on a methylene group located between two double bonds is weakened, which can easily go through hydrogen abstraction creating a carbon radical [4]. The lipid radicals can react with oxygen or hydrogen peroxide creating lipid hydroperoxides which can degrade and rearrange into short chain aldehydes (*e.g.* the three carbon dialdehyde, malondialdehyde (MDA)) and radical alkenes (Figure 1.3) [14]. Work by Morrow *et al.* revealed that the formation of prostaglandin F2-like compounds formed *in vivo* resulted from non-COX free radical peroxidation of AA and when dosed produced biological activity [15]. Clearly both enzymatic and non-enzymatic products of AA metabolism should be gauged when studying biological processes associated with lipid peroxidation.

1.2.2 Lipid Peroxidation Biomarkers

The subsequent release of AA by PLA_2 results in formation of the enzymatic products PG and thromboxane, and non-enzymatic lipid peroxidation products isoprostane, MDA, 4-hydroxynonenal (4-HNE), and acrolein [16]. Prostaglandins can stimulate heme oxygenase to breakdown heme into iron, carbon monoxide and biliverdin [17]. Fe^{2+} is a strong lipid peroxidation agent through Fenton chemistry leading to further degradation of PUFAs [4].

F_2-IsoP is one of the most common isoprostane (IsoP) products formed from AA. The only difference between IsoPs and PGs is that the chains from the prostane ring in IsoP are cis while those of PGs are trans (Figure 1.4 A) [18]. Because of the degree of oxidation of the PGs and IsoPs they can easily undergo further degradation to form more stable products such as MDA, 4-HNE and acrolein. MDA formation could also be the result of a destructive intermediate in the COX mechanism [19] (Figure 1.4 B).

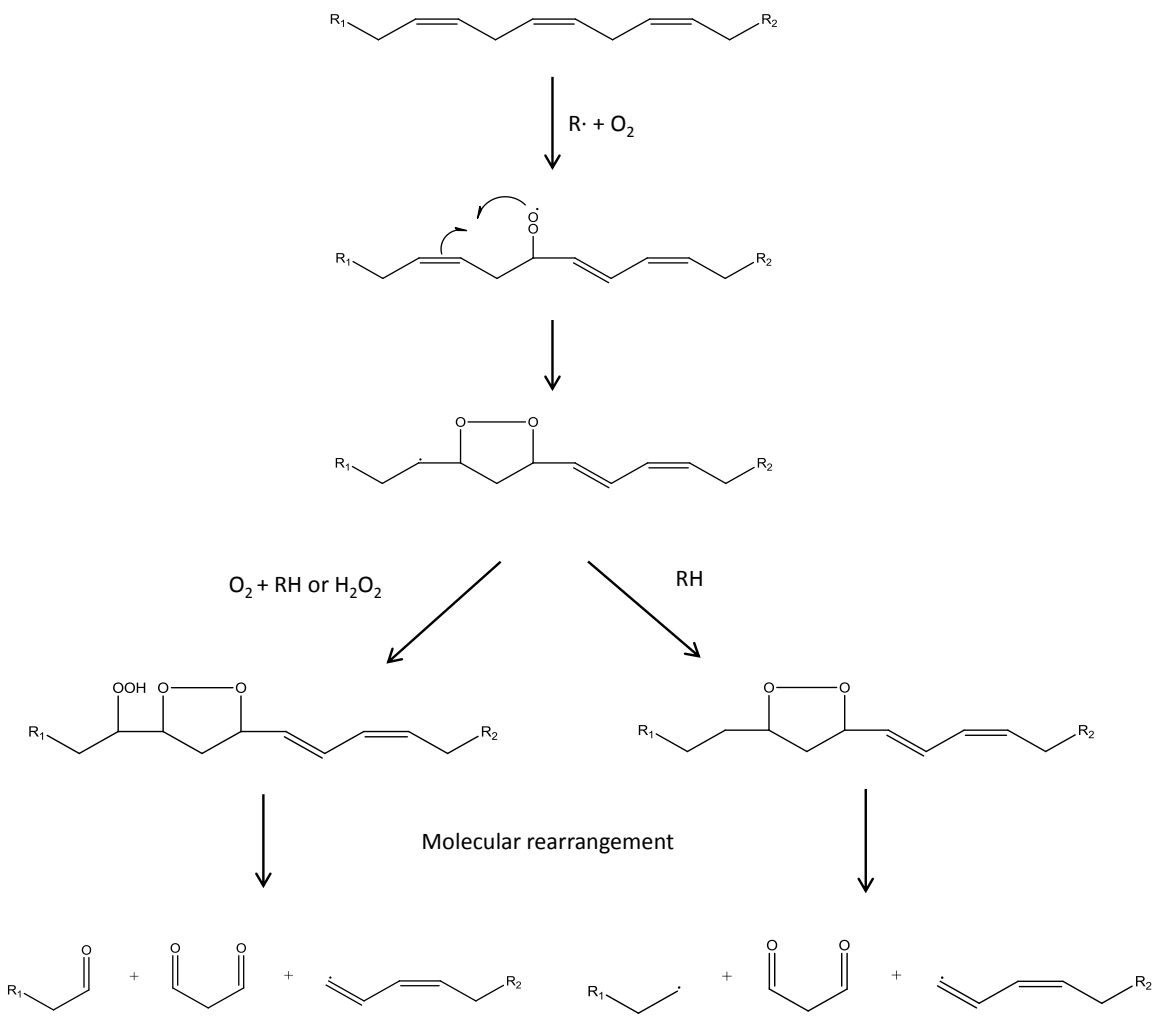

Figure 1.3: Pathway of lipid peroxidation for a PUFA with free radial propagation forming MDA along with other aldehydes. R1 and R2 represent either end of the fatty acid. Adapted from [14]

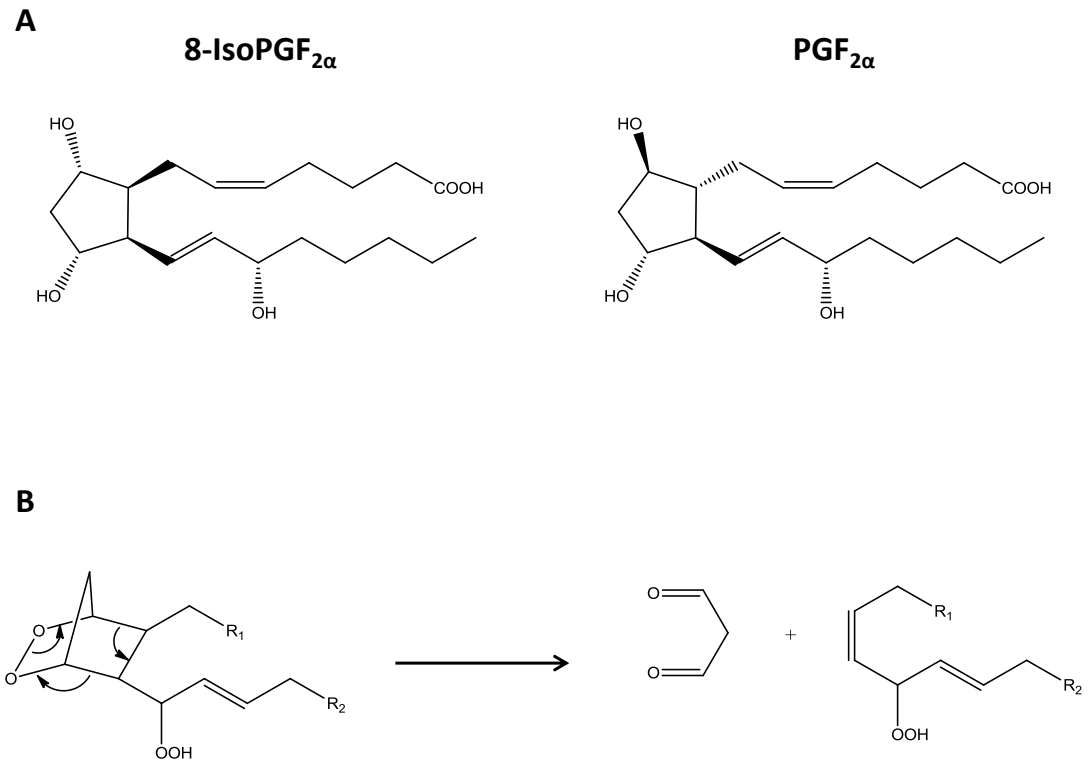

Figure 1.4: A) Structural differences between isoprostanes and prostaglandins, note the stereochemistry of the chains about the ring. Shown here are 8-isoprostaglandin $F_{2\alpha}$ and prostaglandin F_2. B) Proposed mechanism of MDA formation through prostaglandin ring intermediate.

1.3 Ischemia/Reperfusion

1.3.1 Ischemia/Hypoxia

Ischemia is the deprivation of blood flow to a portion of tissue via arterial blockage leading to hypoxia which is a severe (but not complete) drop in cellular oxygen [4]. During ischemia ATP is consumed producing hypoxanthine and converting xanthine dehydrogenase to xanthine oxidase [20]. The activities of cytochrome oxygenase found in the mitochondria are also reduced during ischemia because of the requirement of oxygen [21]. This lack of activity from the cytochromes in the mitochondria adds to the drop in ATP production. Cells begin anaerobic metabolism due to the lack of oxygen producing lactic acid, abandoning ATP production through the mitochondria. There is a decrease in both glutathione synthesis and reduction of glutathione disulfide during hypoxia [22].

1.3.2 Reperfusion

A secondary insult of cellular injury occurs during the resurgence of oxygen to tissue not damaged from the initial ischemic event. Upon reperfusion, xanthine oxidase catalyzes the production of super oxide and hydrogen peroxide from excess oxygen and hypoxanthine [20]. During ischemia the pH of the tissue drops (becoming acidotic) as a result of anaerobic glycolysis, while during reperfusion the pH of the hypoxic tissue returns to normal (~7). This phenomenon is known as the pH paradox and causes accelerated cell death [23]. However, the absence of oxygen during reperfusion can still cause necrosis. Interestingly, it has been shown that tumor cells which are well-perfused were hypoxic and had a lower pH than surrounding tissue [24]. A sub-family of the epithelial Na^+ channels/degenirin, known as the acid-sensing ion channels (ASICs) have recently been of interest for studying the effects of the decrease in pH

during ischemia. The drop in pH causes the ASICs to open, allowing Na^+ and Ca^{2+} into the cell [25]. The blocking of ASICs have shown glutamate independent drops in infarct volumes and neuroprotection during cerebral ischemia [25, 26].

It has been shown *in vitro* that AA metabolites are responsible for the irreversible depolarization of neurons after ischemia [27]. AA plays a central role in the increase of Ca^{2+} which has been shown to evoke the release of glutamate in neuronal cells [28, 29]. This could result in the generation of seizures and epilepsy after ischemia/reperfusion injury.

1.4 Seizure

1.4.1 Propagation of Neuronal Signal

Neurons are specialized cell types which transmit external stimuli from one cell to the next through synaptic junctions. Signal travels through a neuron by polarization of the membrane. This occurs via transmembrane gated ion channels through which Na^+, K^+, Ca^{2+}, and Cl^- cross the cell membrane. Under resting conditions, the neuron is considered to be polarized, meaning that the potential difference from inside to outside the membrane is negative (about -60 mV) [21]. A stimulus at the synaptic junction will cause influx of Na^+ or Ca^{2+} into the dendritic spine of a neuron depolarizing the cell membrane about the ion channel, while K^+ channel activation prevents the initiation of action potential [30]. This localized depolarization (about +30 mV) causes nearby Na^+ channels to open allowing more Na^+ to enter the cell, propagating the signal along the neuron. The direction of the action potential is conserved by the more slowly opened K^+ channels, however, there is evidence of backpropogation where the action potential travels retrogradely toward the dendrite [31]. The efflux of K^+ causes the cell membrane potential to become more negative to the point of hyperpolarization [32]. The resting

potential is then restored by Na^+, K^+-ATPase pumps. Figure 1.5 illustrates the propagation of signal along an neuronal body and the resulting membrane potentials.

1.4.2 Excitatory and Inhibitory Mechanisms

Seizures occur when there is an imbalance between the excitatory and inhibitory mechanisms within the brain. The initial reasons as to why a seizure event begins are unknown, and the aftermath can be quite detrimental to the neurons involved which leads to ineffective therapies for patients suffering from epilepsy [33]. Glutamate is the most abundant excitatory neurotransmitter and γ-amino butyric acid (GABA) the most abundant inhibitory neurotransmitter in the brain [34, 35]. Signal propagation from one neuron to the next occurs in the synapse. When the neuronal signal travels down the axon of a neuron and reaches the synapse, the depolarization causes a release of vesicular neurotransmitters. The neurotransmitters cross the synapse to the post-synaptic neuron (dendritic spine) and elicit a response via transmembrane receptors (Figure 1.6).

Excitation through glutamate release involves glutamate receptors that are either G-protein coupled, opening Ca^{2+} channels, or ionotropic, allowing the influx of Na^+ and Ca^{2+} [36]. Such receptors include: N-methyl-D-aspartate (NMDA), α-amino-3-hydroxy-5-methyl-4-isoxzaole propionate (AMAP), and kainate [37]. Signal inhibition through GABA release involves opening of K^+ or Cl^- channels, causing a repolarization of the neuron back to resting potential, stopping signal propagation. Glutamate is vital for signal transmission and neuronal plasticity; however, during prolonged release, excitotoxicity occurs causing a continuous neuronal transmission [38]. Cells experiencing constant stimuli can undergo apoptosis.

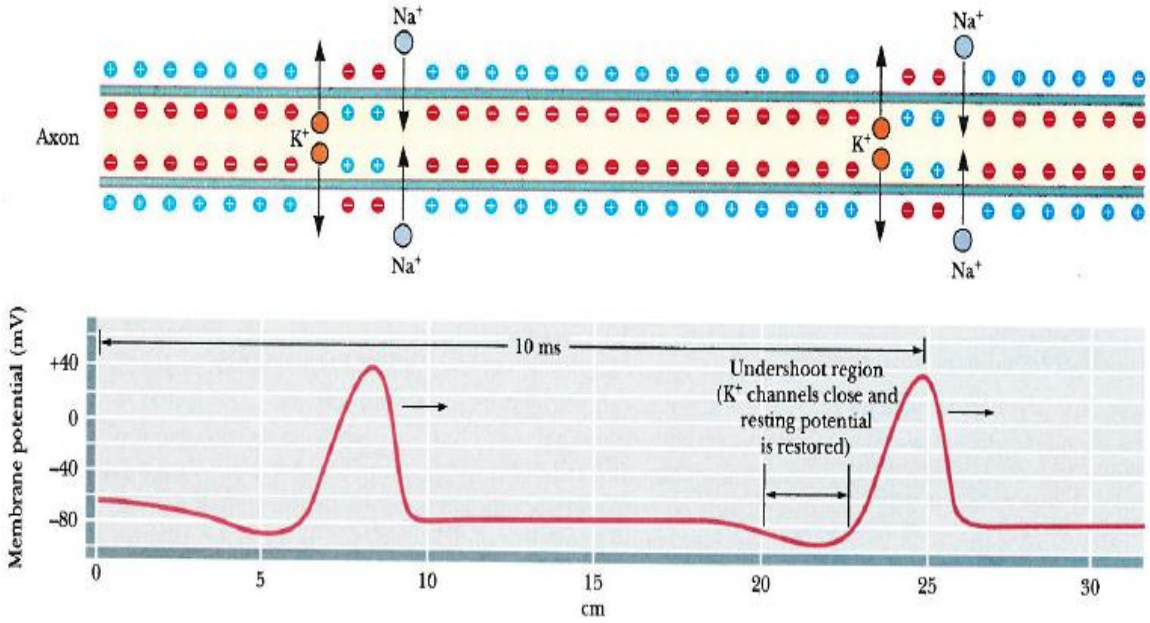

Figure 1.5: Propagation of signal along the neuron represented by influx of Na^+ and efflux of K^+ and the membrane potential associated with each. The slower opening K^+ channels allow the propagation of signal in one direction. With permission from [32] page s-45.

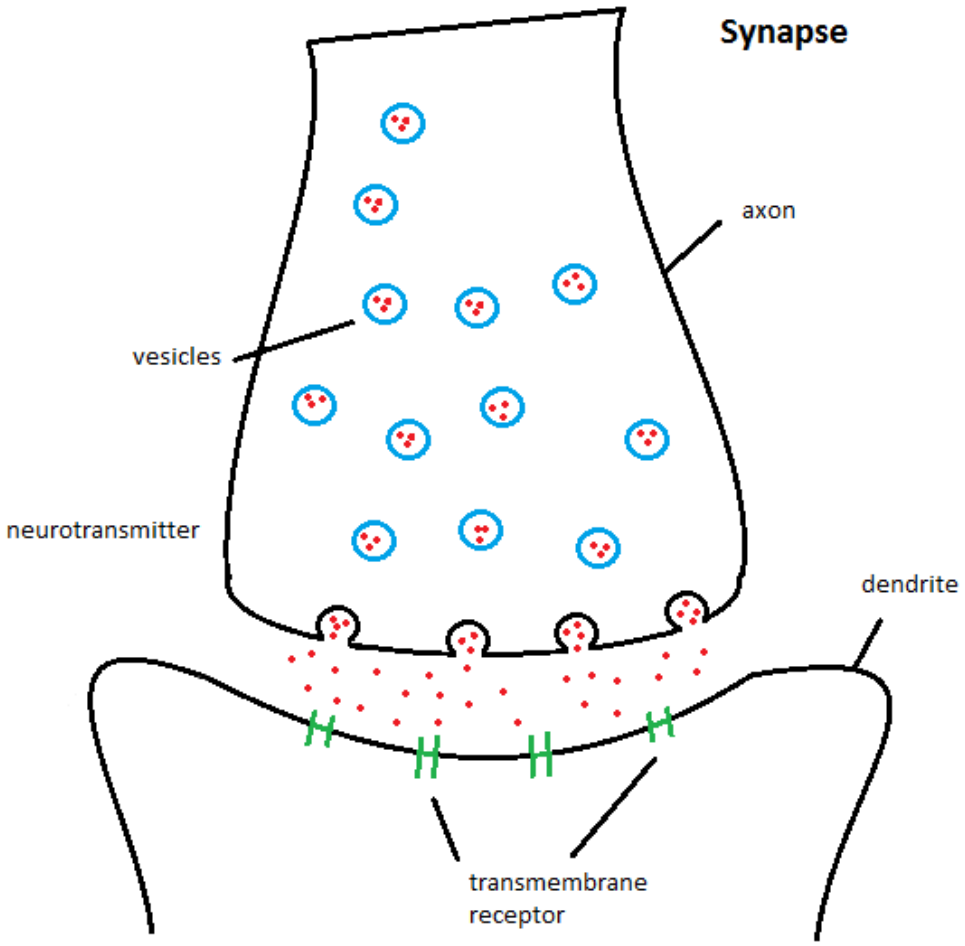

Figure 1.6: Depiction of a synapse with release of neurotransmitters from synaptic vesicles

1.4.3 Development of Epilepsy

The onset of epilepsy is not clearly understood. Epilepsy is defined as having two or more seizure events and affects nearly 3 million people in the US and 50 million people worldwide [39]. The majority of epilepsy patients develop symptoms from an unknown cause of origin (Table 1.1). Most common therapeutics used to treat epilepsy focus on the inhibitory mechanisms in the brain, either blocking sodium channels or increasing GABA synthesis or reuptake [40]. However, because these therapeutics merely treat the symptoms and not the underlying cause, upwards of 30% of patients do not have remission and anywhere between 12-66% who appear symptom free relapse [33].

1.4.4 Chemically Induced Seizure Models

There are a number of chemical seizure models which vary based on the type of seizure desired. There are two fundamental types of seizures; generalized and focal [41]. Generalized seizures distribute bilaterally across multiple brain networks. Focal seizures are localized to one specific network and do not cross hemispheres. To induce a generalized seizure, a chemical convulsant is dosed systemically either as a bolus or by constant infusion. A local seizure is produced through a microinjection of the convulsant or delivery through a microdialysis probe to the to the specific brain region. Details of two seizure models related to this research are described in Chapter 3 of this dissertation.

Cause	Percent of Cases
Unknown	62
Stroke	9
Head Trauma	9
Alcohol	6
Neurodegenerative disease	4
Static Encephalopathy	3.5
Brain Tumor	3

Table 1.1: Leading causes of epilepsy in the US [42].

1.5 Microdialysis Sampling

1.5.1 Principles of Microdialysis

Microdialysis is a diffusion-based sampling technique. Microdialysis sampling involves the implantation of a semipermeable membrane into a target tissue with perfusion of an isotonic solution [43, 44]. Small molecules in the extracellular space will diffuse across the membrane due to the concentration gradient and are then carried out by the perfusion solution and collected as dialysate (Figure 1.7). The perfusion solution is prepared to match the electrolyte composition (*e.g.* Ringer's solution, artificial cerebral spinal fluid (aCSF), *etc.*) of the tissue being studied. This is done to prevent a net exchange of water across the membrane keeping the volume of the tissue constant. Samples are collected over a specific period of time determined by the desired temporal resolution. Microdialysis provides clean, protein free samples without the strenuous workup required for tissue homogenates [45]; however, the samples are of high salt concentration and usually low volumes (µl).

The flow rate of the perfusate and length of membrane play a particularly important role in the extraction efficiency (EE) of analytes. EE is proportional to the concentration gradient across the membrane and can be determined by the ratio of the concentration in the dialysate to that in the sample/tissue [46]. EE is determined based on the following equation:

$$EE = \frac{Cp - Cd}{Cp - Cs} \qquad (1)$$

were *Cs* is the concentration in the sample (*e.g.* brain ECF), *Cp* is the concentration in the perfusate, and *Cd* is the concentration in the dialysate [47].

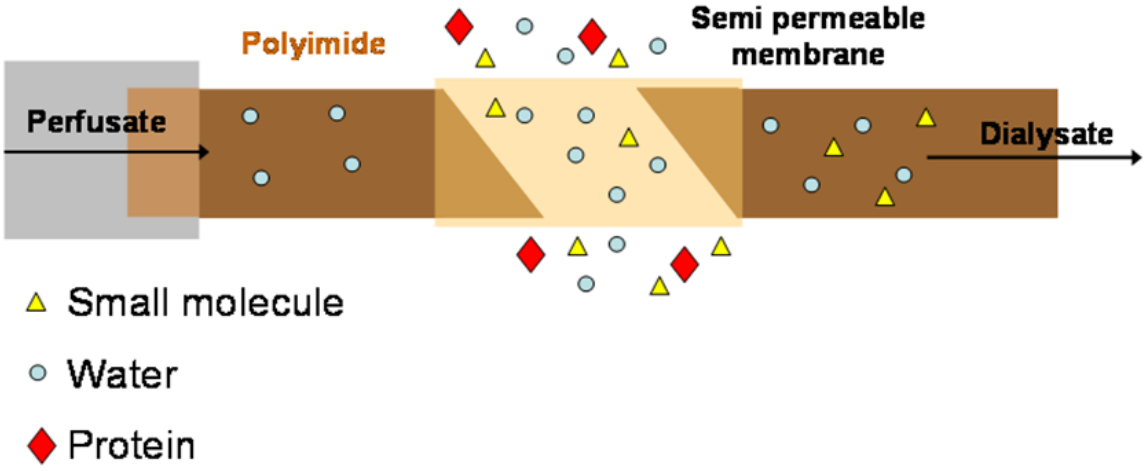

Figure 1.7: Diagram of a linear microdialysis probe. As demonstrated, small molecules are able to diffuse across the membrane and be collected as dialysate while macromolecules such as proteins remain in the extracellular space.

At low flow rates (0.1 µl/min) EE goes up; however, temporal resolution must be sacrificed in order to collect enough volume of sample [48]. The opposite is true for high flow rates. Microdialysis also provides the advantage of delivering chemicals to the site of implantation while collecting samples simultaneously. Delivery of a known analyte can be used to determine EE and probe calibration. The overall relative recovery (RR) for an endogenous chemical can be calculated by:

$$RR = \frac{Cd}{Cs} * 100 \qquad (2)$$

however, the *Cs* cannot be determined without performing calibration experiments [47, 49].

1.5.2 Microdialysis Calibration

Microdialysis is a continual flow technique; therefore, equilibrium for compounds between the extracellular space and across the membrane is not achieved at relevant flow rates or membrane lengths [44]. In order to accurately evaluate *in vivo* concentrations EE needs to be determined through probe calibration. The most common *in vivo* calibration method is the no-net flux (NNF) experiment where varying concentrations of the analyte of interest are perfused. A graph of (*Cp-Cd*) vs. *Cp* is constructed where the EE is the negative of the slope of a linear regression line and *Cs* is the x-intercept [47, 50]. The NNF can easily determine if recovery across the membrane is dependent on concentration. However, the NNF experiment is very time consuming, taking up to 8 hours (five perfusion concentration with 50 minute collection periods plus re-equilibration between).

Calibration can also be performed by constant delivery, also known as retrodialysis. In this case, the calibrant is perfused for the entire experiment [47]. The

equation for calculating delivery (D) is similar to equation (1) except here, *Cs* equals zero:

$$D = \frac{Cp - Cd}{Cp} \qquad (3)$$

The assumption here is that the delivery and recovery of an analyte are equal across both directions of the probe [51]. The difficulty, however, is finding a calibrant that is chemically similar to the biomarker of interest without inducing a biological response. Therefore retrodialysis is usually performed using compounds which have limited biological activity (*e.g.* Adriamycin), and it is the relative changes in probe performance which are monitored during the experiment and on the exact delivery.

Another form of retrodialysis can be performed using the analyte of interest as the calibrant. This technique involves perfusing the analyte before and after the experiment, and if the EE is the same then it is assumed the probe performance was maintained throughout the experiment [51]. Of course an allotted amount of time before the experiment is required to not only perfuse the analyte long enough to calculate EE, but also to allow the complete flushing and clearing as to not skew the results. This technique can be troublesome if the analyte causes a biological response when dosed and therefore great care needs to be taken when interpreting results.

1.5.3 Advantages/Disadvantages of Microdialysis

Microdialysis offers excellent selectivity with regards to sampling, providing site specific, real time samples which are protein free. Microdialysis probes have been implanted in virtually every organ in the body. By implanting probes in selected regions, biological processes happening at the site of incidence can be monitored. This cannot be accomplished by sampling blood or urine. Microdialysis is a continuous sampling

technique, which allows for collection of basal samples prior to and after perturbation of a system. Each experiment not only acts as its own control, but also provides the temporal resolution and lowered variability (animal to animal) that tissue harvesting cannot accomplish [52]. The molecular weight cutoff (MWC) for membranes can range anywhere from 5 to 100 kDa. This MWC range affords experimental design to be more selective with protein extraction than tissue harvesting.

However, microdialysis sampling has many limitations such as sample volume, sample matrix composition, and analyte recovery. Because microdialysis is a diffusion based technique, the sample volume collected is limited to the extraction efficiency of the analyte of interest. If the analyte has low EE, then flow rate should be decreased in order to improve recovery, however, a slower flow rate leads to small collection volumes. Sample volumes can be increased by increasing sampling time but with a sacrifice in temporal resolution. Other *in vivo* monitoring techniques such as biosensors or electrochemical voltammetry can provide better temporal and spatial resolution than microdialysis. However, their selectivity limits them to analytes that are either enzyme specific (*i.e.* glucose) or electroactive (*i.e.* dopamine) [53, 54]. Microdialysis is more conducive to the range of biomarkers to be studied here.

1.5.4 Analytical Considerations When Using Microdialysis

A good analytical technique for use with microdialysis samples should have the following characteristics: 1) be robust, 2) have short analysis times, 3) be compatible with high salt matrices, and 4) require small volumes. The most common analytical techniques used for microdialysis samples are separation based techniques (HPLC or CE) coupled to a general detection method (UV/vis, fluorescence, electrochemical or mass spectrometry). These methods are well suited for microdialysis samples because

they do not require large volumes and have throughput on the minute time scale. However, when developing a method it is important to not only consider the sample matrix but the volume required as well.

In microdialysis, sample volume is inversely proportional to temporal resolution. If the analytical method requires 5 µl of sample, then sampling and/or flow rate must be sufficient to meet this need. For instance, if drug A has a half-life of 2 minutes, then the sampling rate must be 1 minute or less in order to have enough data points for pharmacokinetic studies. A common microdialysis flow rate of 1 µL/min would allow a maximum of 1 µL for analysis. If the microdialysis flow rate must be increased to meet the volume requirements and temporal resolution, then there will be a sacrifice in the EE of the analyte.

1.6 Conclusions

Lipid peroxidation is involved in multiple cellular processes during oxidative stress events. The purpose of this research project was to develop methods to detect biomarkers of lipid peroxidation, specifically, MDA and eicosanoids (PGF_2, PGE_2, PGD_2, LTB_4, 6-keto-$PGF_{1\alpha}$, TXB_2, and 8-iso-$PGF_{2\alpha}$), and to apply these methods to evaluate their formation *in vivo*. Microdialysis was used to sample the extracellular fluid in animal models of induced oxidative stress. The goal of this work is to aid in the understanding of the molecular mechanisms associated with lipid degradation during a chemically induced model of epilepsy.

1.7 References

1. Droge, W., Free radicals in the physiological control of cell function. *Physiol. Rev.* **2002,** *82* (1), 47-95.
2. Adibhatla, R. M.; Hatcher, J. F., Phospholipase A2, reactive oxygen species, and lipid peroxidation in cerebral ischemia. *Free Radic. Biol. Med.* **2006,** *40* (3), 376-387.
3. Adibhatla, R. M.; Hatcher, J. F., Lipid Oxidation and Peroxidation in CNS Health and Disease: From Molecular Mechanisms to Therapeutic Opportunities. *Antioxid. Redox Signal.* **2010,** *12* (1), 125-169.
4. Roberfroid, M.; Calderon, P. B., *Free Radicals and Oxidation Phenomena in Biological Systems*. Marcel Dekker, Inc: New York, 1995.
5. Rosser, B. G.; Gores, G. J., Liver-Cell Necrosis - Cellular Mechanisms and Clinical Implications. *Gastroenterology* **1995,** *108* (1), 252-275.
6. Trump, B. F.; Berezesky, I. K., The role of cytosolic Ca2+ in cell injury, necrosis and apoptosis. *Current opinion in cell biology* **1992,** *4* (2), 227-232.
7. Crompton, M., The mitochondrial permeability transition pore and its role in cell death. *Biochem. J.* **1999,** *341*, 233-249.
8. Contreras, M. A.; Greiner, R. S.; Chang, M. C. J.; Myers, C. S.; Salem, N.; Rapoport, S. I., Nutritional deprivation of alpha-linolenic acid decreases but does not abolish turnover and availability of unacylated docosahexaenoic acid and docosahexaenoyl-CoA in rat brain. *J. Neurochem.* **2000,** *75* (6), 2392-2400.
9. Katsuki, H.; Okuda, S., Arachidonic-Acid as as Neurotoxic and Neurotrophic Substance. *Prog. Neurobiol.* **1995,** *46* (6), 607-636.
10. Karmazyn, M., *Myocardial Ischemis: Mechanisms, Reperfusion, Protection*. Birkhauser Verlag: Basel, 1996.
11. GarciaRuiz, C.; Colell, A.; Mari, M.; Morales, A.; FernandezCheca, J. C., Direct effect of ceramide on the mitochondrial electron transport chain leads to generation of reactive oxygen species - Role of mitochondrial glutathione. *J. Biol. Chem.* **1997,** *272* (17), 11369-11377.
12. Masoodi, M.; Eiden, M.; Koulman, A.; Spaner, D.; Volmer, D. A., Comprehensive Lipidomics Analysis of Bioactive Lipids in Complex Regulatory Networks. *Anal. Chem.* **2010,** *82* (19), 8176-8185.
13. Lajtha, A.; Chan, P., *Handbook of Neurochemistry and Molecular Biology*. 3rd ed.; Plenum Press: New York, 2007.
14. Pryor, W. A.; Stanley, J. P.; Blair, E., Autoxidation of Polyunsaturated Fatty-Acids .2. Suggested Mechanism for Formation of TBA-Reactive Materials from Prostaglandin-Like Endoperoxides. *Lipids* **1976,** *11* (5), 370-379.
15. Morrow, J. D.; Hill, K. E.; Burk, R. F.; Nammour, T. M.; Badr, K. F.; Roberts, L. J., A Series of Prostaglandin-F2-Like Compounds are Produced Invivo in Humans by a Noncyclooxygenase, Free Radical-Catalyzed Mechanism. *Proc. Natl. Acad. Sci. U. S. A.* **1990,** *87* (23), 9383-9387.
16. Rink, C.; Khanna, S., Significance of Brain Tissue Oxygenation and the Arachidonic Acid Cascade in Stroke. *Antioxid. Redox Signal.* **2011,** *14* (10), 1889-1903.
17. Zhuang, H.; Pin, S.; Li, X. L.; Dore, S., Regulation of heme oxygenase expression by cyclopentenone prostaglandins. *Exp. Biol. Med.* **2003,** *228* (5), 499-505.
18. Roberts, L. J.; Morrow, J. D., Measurement of F-2-isoprostanes as an index of oxidative stress in vivo. *Free Radic. Biol. Med.* **2000,** *28* (4), 505-513.

19. Hemler, M. E.; Lands, W. E. M., Evidence for a Peroxide-Initiated Free-Radical Mechanism of Prostaglandin Biosynthesis. *J. Biol. Chem.* **1980,** *255* (13), 6253-6261.
20. Granger, D. N., Role of Xanthine-Oxidase and Granulocytes in Ischemia-Reperfusion Injury. *Am. J. Physiol.* **1988,** *255* (6), H1269-H1275.
21. Nelson, D. L.; Cox, M. M., *Lehninger Principles of Biochemistry*. 4th ed.; W.H. Freeman and Company: New York, 2005.
22. Clerch, L. B.; Massaro, D. J., *Oxygen, Gene Expression, and Cellular Function*. Marcel Dekker: New York, 1997.
23. Lemasters, J. J.; Nieminen, A. L.; Qian, T.; Trost, L. C.; Elmore, S. P.; Nishimura, Y.; Crowe, R. A.; Cascio, W. E.; Bradham, C. A.; Brenner, D. A.; Herman, B., The mitochondrial permeability transition in cell death: a common mechanism in necrosis, apoptosis and autophagy. *Biochim. Biophys. Acta-Bioenerg.* **1998,** *1366* (1-2), 177-196.
24. Helmlinger, G.; Yuan, F.; Dellian, M.; Jain, R. K., Interstitial pH and pO(2) gradients in solid tumors in vivo: High-resolution measurements reveal a lack of correlation. *Nat. Med.* **1997,** *3* (2), 177-182.
25. Xiong, Z. G.; Zhu, X. M.; Chu, X. P.; Minami, M.; Hey, J.; Wei, W. L.; MacDonald, J. F.; Wemmie, J. A.; Price, M. P.; Welsh, M. J.; Simon, R. P., Neuroprotection in ischemia: Blocking calcium-permeable acid-sensing ion channels. *Cell* **2004,** *118* (6), 687-698.
26. Pignataro, G.; Simon, R. P.; Xiong, Z. G., Prolonged activation of ASIC1a and the time window for neuroprotection in cerebral ischaemia. *Brain* **2007,** *130*, 151-158.
27. Tanaka, E.; Niiyama, S.; Sato, S.; Yamada, A.; Higashi, H., Arachidonic acid metabolites contribute to the irreversible depolarization induced by in vitro ischemia. *J. Neurophysiol.* **2003,** *90* (5), 3213-3223.
28. Ruehr, M. L.; Zhang, L.; Dorman, R. V., Lipid-dependent modulation of Ca2+ availability in isolated mossy fiber nerve endings. *Neurochem. Res.* **1997,** *22* (10), 1215-1222.
29. Yue, H. Y.; Fujita, T.; Kumamoto, E., Phospholipase A(2) activation by melittin enhances spontaneous glutamatergic excitatory transmission in rat substantia gelatinosa neurons. *Neuroscience* **2005,** *135* (2), 485-495.
30. Hoffman, D. A.; Magee, J. C.; Colbert, C. M.; Johnston, D., K+ channel regulation of signal propagation in dendrites of hippocampal pyramidal neurons. *Nature* **1997,** *387* (6636), 869-875.
31. Vetter, P.; Roth, A.; Hausser, M., Propagation of action potentials in dendrites depends on dendritic morphology. *J. Neurophysiol.* **2001,** *85* (2), 926-937.
32. Garrett, R. H.; Grisham, C. M., *Biochemistry*. 2nd ed.; Saunders College Publishing: Fort Worth, 1999.
33. Kwan, P.; Brodie, M. J., Early identification of refractory epilepsy. *N. Engl. J. Med.* **2000,** *342* (5), 314-319.
34. Timmerman, W.; Westerink, B. H. C., Brain microdialysis of GABA and glutamate: What does it signify? *Synapse* **1997,** *27* (3), 242-261.
35. Bradford, H. F., Glutamate, GABA and epilepsy. *Prog. Neurobiol.* **1995,** *47* (6), 477-511.
36. Coyle, J. T.; Puttfarcken, P., Oxidative Stress, Glutamate, and Neurodegenerative Disorders. *Science* **1993,** *262* (5134), 689-695.
37. Phillis, J. W.; Horrocks, L. A.; Farooqui, A. A., Cyclooxygenases, lipoxygenases, and epoxygenases in CNS: Their role and involvement in neurological disorders. *Brain Res. Rev.* **2006,** *52* (2), 201-243.

38. McEwen, B. S., Stress and hippocampal plasticity. *Annu. Rev. Neurosci.* **1999,** *22*, 105-122.
39. http://www.epilepsyfoundation.org/ (accessed 2011).
40. Brodie, M. J., Monostars: An aid to choosing an antiepileptic drug as monotherapy. *Epilepsia* **1999,** *40*, S17-S22.
41. Berg, A. T.; Scheffer, I. E., New concepts in classification of the epilepsies: Entering the 21st century. *Epilepsia* **2011,** *52* (6), 1058-1062.
42. French, J. A.; Pedley, T. A., Initial management of epilepsy. *N. Engl. J. Med.* **2008,** *359* (2), 166-176.
43. Ungerstedt, U., Microdialysis - Principles and Applications for Studies in Animals and Man. *J. Intern. Med.* **1991,** *230* (4), 365-373.
44. Elmquist, W. F.; Sawchuk, R. J., Application of microdialysis in pharmacokinetic studies. *Pharm. Res.* **1997,** *14* (3), 267-288.
45. Lloyd, D. K., Capillary electrophoretic analyses of drugs in body fluids: Sample pretreatment and methods for direct injection of biofluids. *J. Chromatogr. A* **1996,** *735* (1-2), 29-42.
46. Chen, K. C.; Hoistad, M.; Kehr, J.; Fuxe, K.; Nicholson, C., Theory relating in vitro and in vivo microdialysis with one or two probes. *J. Neurochem.* **2002,** *81* (1), 108-121.
47. Song, Y.; Lunte, C. E., Calibration methods for microdialysis sampling in vivo: muscle and adipose tissue. *Anal. Chim. Acta* **1999,** *400*, 143-152.
48. Plock, N.; Kloft, C., Microdialysis - theoretical background and recent implementation in applied life-sciences. *Eur. J. Pharm. Sci.* **2005,** *25* (1), 1-24.
49. Yang, Z.; Brundage, R. C.; Barbhaiya, R. H.; Sawchuk, R. J., Microdialysis studies of the distribution of stavudine into the central nervous system in the freely-moving rat. *Pharm. Res.* **1997,** *14* (7), 865-872.
50. Song, Y.; Lunte, C. E., Comparison of calibration by delivery versus no net flux for quantitative in vivo microdialysis sampling. *Anal. Chim. Acta* **1999,** *379* (3), 251-262.
51. Bouw, M. R.; Hammarlund-Udenaes, M., Methodological aspects of the use of a calibrator in in vivo microdialysis - Further development of the retrodialysis method. *Pharm. Res.* **1998,** *15* (11), 1673-1679.
52. Westerink, B. H. C., Brain Microdialysis and its Application for the Study of Animal Behavior. *Behav. Brain Res.* **1995,** *70* (2), 103-124.
53. Murphy, L., Biosensors and bioelectrochemistry. *Curr. Opin. Chem. Biol.* **2006,** *10* (2), 177-184.
54. Kondepati, V. R.; Heise, H. M., Recent progress in analytical instrumentation for glycemic control in diabetic and critically ill patients. *Anal. Bioanal. Chem.* **2007,** *388* (3), 545-563.

Chapter 2:

Capillary Electrophoresis-Fluorescence Method for Malondialdehyde

Introduction

Malondialdehyde (MDA) is a three carbon dialdehyde produced as a secondary product of lipid peroxidation. MDA was originally studied in the late 1950's as a measure of food rancidity [1, 2] but recently has become viewed as a biomarker for lipid peroxidation [3]. During oxidative stress, polyunsaturated fatty acids can be attacked by ROS to form lipid hydroperoxides which readily decompose to form secondary products such as MDA, 4-hydroxynonenal, and dienals [4, 5]. MDA is used as a reliable biomarker to determine the extent of lipid peroxidation [6-8]. Although MDA absorbs at 245 nm and 267 nm in acidic and basic solutions respectively, the most common method for detection is by derivatization to produce a fluorophore, in particular through the thiobarbituric acid (TBA) assay (for review see Janero [3] and Grotto [9]). Briefly, TBA reacts with MDA in a 2:1 ratio in acidic media and at high temperatures to form a pink product which absorbs at 530 nm and emits at 550 nm. It should be noted, however, that the TBA assay is not specific for MDA and will react with dialdehydes and pyrimidines producing similar absorbance spectra [10]. However, MDA is comparatively more reactive and has greater fluorescence intensity than other TBA products per molar ratio [11]. Therefore, coupling fluorescence detection with a separation technique must be employed in order to increase selectivity and more accurately quantify MDA.

MDA has been studied in such matrixes as plasma [12, 13], breath condensate [14] and tissue homogenate [15, 16]; in conjunction with separation techniques such as HPLC-UV/fluorescence [16-19] GC-MS [20], and CE-UV/fluorescence [12, 13, 19]. Although MDA has been monitored previously in microdialysis samples using HPLC

methods [21, 22], the sample volume required greatly limited the temporal resolution during animal experimentation. In this chapter the development of a CE-fluorescence method for the detection of MDA in microdialysis samples through derivatization with the TBA assay is described.

2.1 Capillary Electrophoresis

2.1.1 Basic Principles

Capillary electrophoresis (CE) is a separation method in which a potential is applied across a fused silica capillary containing a conducting solution (background electrolyte (BGE)) and analytes are separated based on their electrophoretic mobility (a function of their hydrodynamic radius and charge). Two factors affect the direction and velocity of analytes in CE, migration of the ion μ_{ion} and electroosmotic flow (EOF) μ_{EOF}. The sum of these two vectors along with the electric field strength *E* determines the total migration velocity of the analyte given by

$$v = \mu E = \frac{\mu V}{L} \qquad (1)$$

where *v* is the velocity, μ is the electrophoretic mobility, *E* is the electric field strength, *V* is the applied voltage and *L* is the length of the capillary [23, 24]. Electrophoretic mobility is limited by the frictional forces of the medium as described by

$$\mu = \frac{q}{6\pi\eta r} \qquad (2)$$

were *q* is the ion charge, *r* is the solvated radius, and η is the viscosity of the solution [25]. Note the denominator is the frictional coefficient from Stokes' Law. If no EOF was present, all charged analytes would migrate toward their respective counter electrode

(cations to the cathode, anions to the anode) and neutrals would remain stationary. EOF is the driving force for all species to migrate in a unilateral direction.

EOF is a result of the interaction of the solution with the surface wall of the capillary [24]. At basic pHs the silanol groups on the surface of the capillary will become negatively charged at which point cations in solution will attract to it creating a double layer, consisting of a fixed and mobile layer [26]. Under normal polarity conditions, where the outlet is the cathode, the cations in the mobile layer will migrate toward the outlet pulling bulk solution with them creating EOF (Figure 2.1). The magnitude of the EOF is dependent on the pH of the BGE as determined by the deprotonation of silanol groups along the capillary wall [26]. At higher pHs the EOF will have a greater magnitude than most other species creating a net migration toward the outlet where the detector is situated.

CE however, is ineffective at separating neutral compounds which will simply migrate with the EOF. To resolve this issue surfactants are added to the BGE in order to create a secondary mode of separation at concentrations above their critical micelle concentration (CMC) [27]. These micelles will migrate toward the outlet but at a different rate than the EOF [28]. Neutral analytes will partition in and out of the micelle based on their hydrophobicity giving them a net mobility between that of the EOF and micelles. This type of separation is termed micellar electrokinetic chromatography (MEKC).

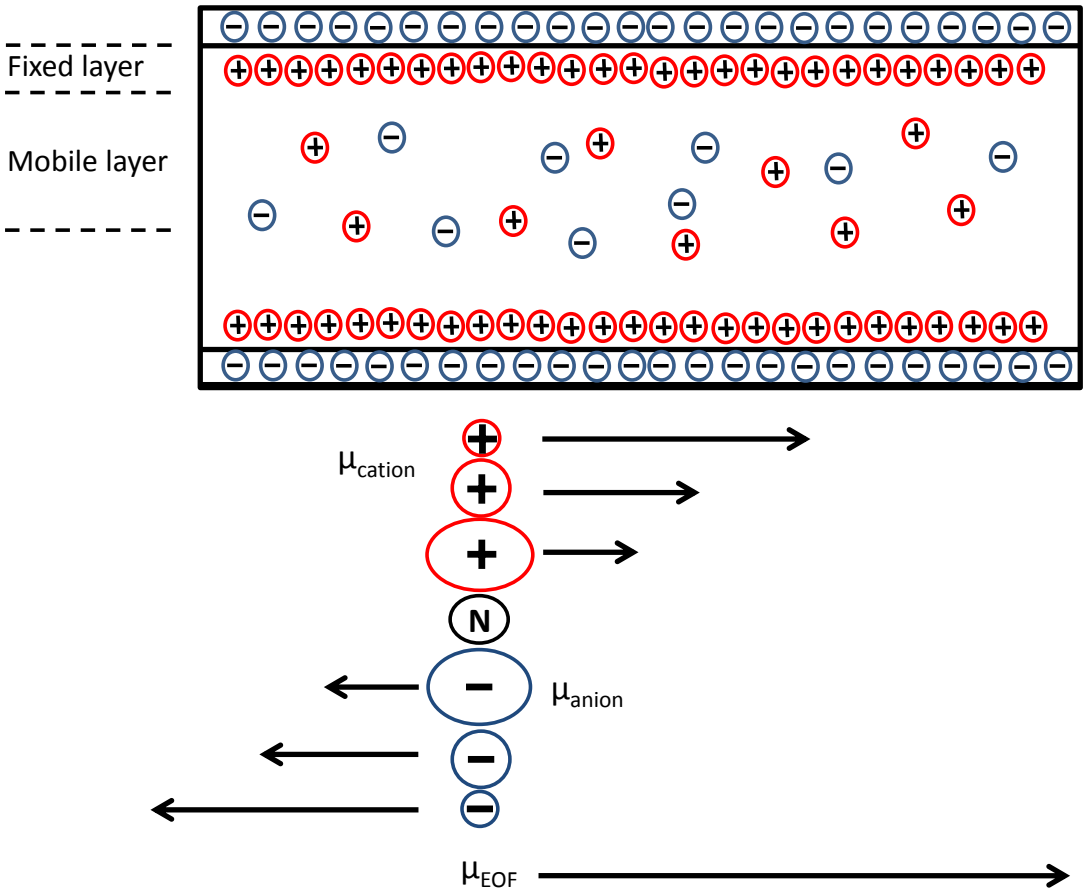

Figure 2.1: Representation of the fixed and mobile layers in CE separation along with characteristic migration vectors for anions, cations and EOF. The EOF migration vector is greater in magnitude than the anion vectors providing a total vector towards the outlet (detector).

2.1.2 CE Detection Methods

The detector is attached to the capillary at the outlet end, usually the cathode, in which the buffer solution will create an EOF toward the cathode and pull all species (positive, neutral, and negative) in that direction. Several types of detectors can be used depending on the analyte of interest; absorbance, fluorescence, electrochemical, or mass spectrometric.

UV/Vis spectrophotometric detection is simple and relatively inexpensive to use, and because of its nondestructive characteristics, it can easily be used in tandem with other detectors [29]. A spectrophotometric UV detector for CE has the same components as those used in HPLC. A major limitation to using UV detectors, however, is in the detection cell. Since the path length is no more than 100 μm, the capillary has to be manipulated/bent at the detector window in order to improve detection limits [30].

Fluorescence detection is considered one of the most sensitive detection techniques used for CE, particularly laser-induced fluorescence (LIF) capable of detection on the nM and subnanomolar scale. Several designs for LIF detector units are available one of which is the “ball lens” Picometrics arrangement [29]. Fluorescence is a very attractive detection setup for CE because the signal (emission) is determined, in part, by the intensity of excitation source making the use of lasers extremely advantageous. The major pitfall, however, is the ability to match the laser wavelength with the excitation wavelength of the analyte or fluorophore, greatly limiting the variety of derivatizing agents applicable to CE-LIF.

With the small flow rates associated with CE it would be effective to integrate mass spectrometric detectors to the end of a capillary due to their high selective and sensitive analysis. The coupling of CE and MS, however, is more complicated than

coupling with LC [31]. Because CE produces a high background current (associated with the separation voltage) and has such low flow rates, it cannot be directly coupled into the MS. To circumvent the high CE current, a terminating voltage is indirectly applied to the buffer leaving the capillary by using a sheath liquid [29, 31]. The sheath liquid merges with CE effluent along with a nebulizing gas to facilitate ESI prior to MS analysis.

2.1.3 CE with Microdialysis Samples

The major difficulty when analyzing microdialysis samples with CE is the vast difference in conductance between the sample and the BGE. Most CE buffers are at concentrations in the low mM range (10-40 mM); however, microdialysis samples have a salt concentration of about 150 mM. When voltage is applied across the capillary, there is a drop in field strength across the sample plug due to high conductance. This results in analytes migrating faster once they cross the sample/BGE boundary causing destacking (peak broadening).

Using micelles for sweeping in CE is ideal when the sample matrix is of low conductivity and the analytes are relatively hydrophobic [32]. However, this does not mean that the addition of micelles is only useful for separation purposes. Landers *et al.* described how micelles will stack at the detector side of an injection plug when the sample matrix is of higher conductivity than the BGE [33]. In this instance, the micelles stack because of the decrease in electric field at the sample plug. Essentially, field amplification occurs in the buffer and not in the sample zone. Analytes will stack at the sample/micelle boundary as a result of the reduced velocity from the high micelle concentration.

2.2 Method

2.2.1 Chemicals

MDA (malondialdehyde tetrabutylammonium salt), boric acid, 3-mercaptopropionic acid (3-MPA) and TBA were purchased from Sigma-Aldrich (St. Louis, MO). TBA was also purchased from Cayman Chemical (Ann Arbor, MI). Brij 35 was purchased from MP Biomedicals (Solon, OH). Sulfuric acid and salts for Ringer's solution were purchased from Fisher (Fair Lawn, NJ). Ringer's solution composition was: 147 mM NaCl, 3 mM KCl, 1 mM $MgCl_2$, and 1.2 mM $CaCl_2$. All solutions were made using nanopure water obtained from a Labconco Water Pro Plus purification system (Kansas City, KS).

2.2.2 Reaction Conditions

All MDA standards were made in Ringer's solution. TBA was made fresh daily at a concentration of 0.4% (w/v) in nanopure water. TBA was dissolved using a stir bar in a scintillation vial. Sulfuric acid was diluted with nanopure water to a concentration of 0.4% (v/v) and could be used for several months. For the reaction, an MDA:TBA:acid ratio of 8:2:1 was used. TBA and sulfuric acid were mixed (60:30) and 3 µL of that mixture was added to 8 µL of MDA standard or sample in a 200 µL microcentrifuge tube. TBA and sulfuric acid were pre-mixed to reduce pipetting error. The reaction mixture was vortex for ~3 seconds then placed in a 90-95°C water bath for 20 minutes. After heating, the standards/samples were immediately placed in liquid nitrogen for flash freezing then stored at -80°C until used.

2.2.3 CE Method

MDA was separated by capillary electrophoresis with fluorescence detection. A 75 µm inner diameter (ID) capillary was cut to 55 cm total length and a window of about 2 mm in length was burned at the middle of the 45 cm mark. The background electrolyte (BGE) was a 200 mM boric acid solution with 4.5 mM brij 35 adjusted to pH 8.4 with NaOH. The capillary was flushed between runs with methanol (2 min), NaOH (2 min) and BGE (3 min) at 20 psi each. Prior to injection, the derivatized standard/sample was removed from the freezer and allowed to warm to room temperature for about 5 min and vortexed for about 5 sec. Any water adhered to the lid of the microcentrifuge tube was pipetted back to the mixture using a micropipette and re-vortexed. The solution was hydrodynamically injected with 0.5 psi for 5 seconds and the separation voltage was set at 10 kV. It should be noted that since a hydrodynamic injection method is being used, it was important to ensure the inlet of the capillary was cut straight. A jagged end at the inlet will lead to peak tailing.

The separation was performed on a Beckman Coulter P/ACE MDQ CE system with a 488 nm Laser Module as the excitation source and a 560 nm band pass emission filter. The data were collected and analyzed using 32-Karat software. The gain of the instrument could be adjusted by changing the range setting in the 32-Karat software. The range was set at 100 for all experiments. This setting prevented peak plateauing from high MDA concentrations at a low range (10) and limited noise associated with a high range (1000). The Calibration Correction Factor (CCF) could also be slightly adjusted to give optimal S/N; here it was set a 1.

2.2.4 Mass Spectrometry

To identify an unknown contaminate, a blank and standard solutions were analyzed using flow injection mass spectrometry. The same reaction conditions as

mentioned above were used, but scaled up 50 times. After derivatization, the 10 µM MDA-TBA standard and TBA blank were extracted using n-butanol to remove salt and sulfuric acid which are detrimental to the mass spectrometer. Other organic solvents such as ethyl acetate and hexanes were unable to extract the TBA-MDA fluorophore. Three 200 µL aliquots were used for extraction and the butanol was evaporated under argon stream. The dried extracts were reconstituted with 50:50 methanol:water. The butanol extracted constituents from both a blank and MDA standard were analyzed by collision induced dissociation in a linear ion trap (Thermo LTQ XL) using ESI in negative ion mode with syringe pump flow injection at 2 µL/min.

2.2.5 Microdialysis Probe Fabrication

Microdialysis probes were implanted into multiple tissue sites to help validate the application of the MDA method. For liver, heart, and muscle implantation, polyacrylonitrile (PAN) membrane (Hospal, Lakewood, CO) of dimensions 350 µm outer diameter (OD) and 260 µm ID with a molecular weight cutoff of 20 kDa was used as the microdialysis window. The PAN membrane was cut and attached using UV curing glue to two strips of polyimide tubing (MicroLumen, Tampa, FL) of dimensions 160 µm OD and 120 µm ID. A 2 cm piece of Tygon tubing was attached to the inlet tube in order to affix the probe to a syringe. The probe window was 10 mm for liver and muscle and 2 mm for heart. For brain implantation, a CMA 12 Elite (CMA, N. Chelmsford, MA) 2 mm probe with a cutoff of 20 kDa was implanted into the hippocampus at coordinates -3.3 A/P, +1.7 L/M, -3.7 D/V reference from bregma line.

2.2.6 Liver Animal Model

Male Sprague Dawley rats were anesthetized with isoflurane followed by a subcutaneous injection of ketamine/xylazine/acepromazine mixture (67.5 / 3.4 / 0.67

mg/kg respectively). The animal's stomach was shaved and a midline incision was made below the sternum opening the abdominal cavity. Adjustable retractors were used to hold the cavity open during surgery. A 23 gauge needle was inserted in to the left liver lobe to guide the microdialysis probe in place. The needle was removed and tissue glue was applied to secure the probe. Ischemia was produced by securing a set of tissue forceps around left hepatic artery for 30 minutes. All animal experiments were performed in accordance with the local Institutional Animal Care and Use Committee (IACUC) and follow the principles stated in the Guide for the Care and Use of Laboratory Animals (National Academy of Sciences, 1996). All chemical solutions used for microdialysis experiments were diluted in Ringer's solution. The probe was perfused for a 1 hour recovery period before basal sample collection was started. Samples were collected over a 10 minute interval with a perfusion rate of 1 µL/min.

2.2.7 Antipyrine LC-UV Method

Antipyrine was detected at 241 nm using an LC-UV system (Shimadzu LC-10AD pump and SPD-10A UV/Vis detector). Liver samples (1 µL) were injected onto a Phenomenex Synergy Polar-RP (150 x 2 mm, 4 µm) column with a mobile phase of 25 mM acetic acid with 17% ACN (v/v). The pH was adjusted to 4.5 using NaOH and flow rate was set at 0.300 mL/min.

2.3 Discussion

2.3.1 Reaction

Although MDA absorbs at 245 and 267 nm in acidic and basic media respectively it has relatively low absorptivity [3]. MDA reacts with TBA in a neucliophilic condensation type reaction where one molecule of MDA reacts with two molecules of TBA. This product produces a fluorophore with excitation at 530 nm and emission at

560 nm (Figure 2.2). Varying concentrations of sulfuric acid provided no observable changes in peak area; however, a noticeable difference in sensitivity could be seen at lower concentrations of TBA. The majority of TBA methods call for 0.4-0.5 % TBA [3, 34]; however, in an attempt to reduce an observed TBA contaminant, the TBA concentration was decreased. With a decrease in the TBA concentration to 0.1%, the sensitivity only decreased by 0.5 and y-intercept by 2.5. Because the degree of MDA production resulting from oxidative stresses *in vivo* remained unclear, it would be more advantageous to use 0.4% TBA and have the added sensitivity even though the contaminant in the blank TBA decreased with lower concentrations.

The 20 minute reaction time was also examined. When a large volume of reaction mixture was used and aliquots were taken at specific time points, maximum peak intensity was achieved at around 60 minutes. However, calibration curves made at longer reaction times with low volume solutions were non-linear particularly at low MDA concentrations. At low volumes, water evaporates and condenses on the lid of the microcentrifuge tube, leaving a heavily salted solution changing reaction kinetics. The longer reaction times also had a larger contribution from the TBA impurity (Figure 2.3). A reaction time of 20 minutes, although not ideal, provided the most reproducible and linear standard curves. A 20 minute reaction time also had the largest difference between MDA-TBA and the TBA contaminant (Figure 2.3).

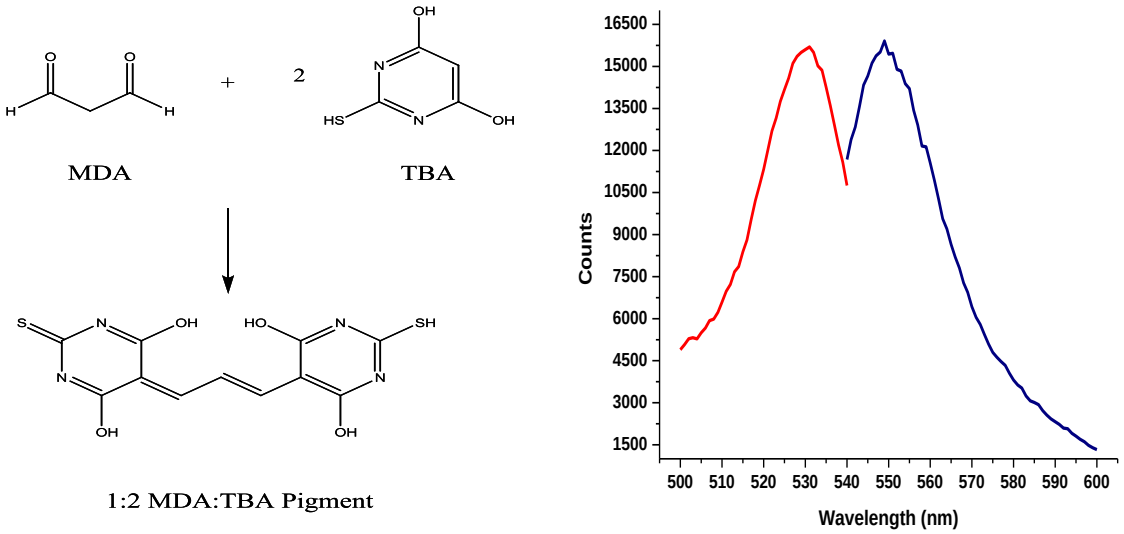

Figure 2.2: Derivatization scheme of MDA with 2 molecules of TBA. Fluorescence excitation and emission spectra showing maximum excitation at 530 nm and emission at 550 nm. With permission from [35]

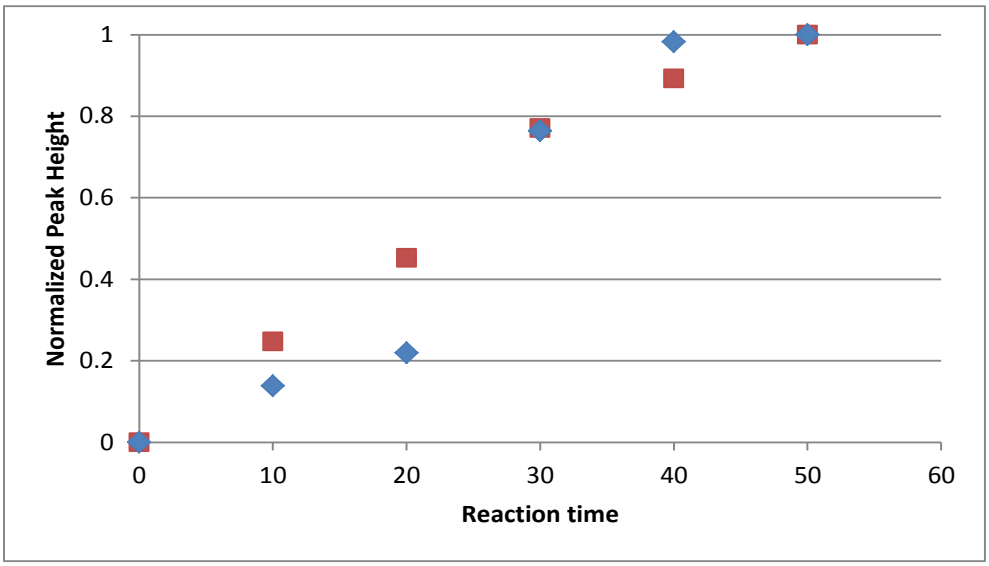

Figure 2.3: Graph of normalized peak height for the TBA impurity (-◆-) and a 50 nM MDA standard (-■-) for selected reaction times. At longer reaction times the impurity becomes more significant and greatly interferes with low concentrations of MDA.

2.3.2 CE Conditions

Separation conditions attempted using only boric acid were sufficient with water as the matrix; however, a substantial destacking effect with Ringer's solution as the matrix was observed due to high salt concentration (Figure 2.4). One possible remedy is to add a surfactant to the BGE at a concentration above its critical micelle concentration (CMC). When potential is applied, the micelles stack at the detector side of the sample plug which can help prevent the destacking of the analyte. Neither sodium dodecylsulfate (SDS) nor tetradodecylammonium bromide (TTAB) provided any advantage, above or below their respective CMC, over straight boric acid (data not shown). Another approach to this problem is to use a neutral surfactant (*i.e.* brij 35) to increase the viscosity of the BGE in order to slow the adduct based on its hydrophobicity as it crosses the sample plug boundary [15, 36]. Brij 35 was used at concentrations ranging from below the CMC to well above (0.5, 4.5, and 15 mM) and a large increase in sensitivity at 4.5 and 15 mM was observed (Figure 2.4). A concentration of 4.5 mM was chosen because there appeared to be no advantage to using a higher concentration.

2.3.3 Peak Identification

To identify the MDA peak an MDA-TBA standard was run first with a UV/Vis photodiode array detector connected to the CE system. The peak at 10.1 minutes was easily identified as the adduct based on the UV/Vis spectrum having peak absorbance at 530 nm, which matched well with literature [1, 10, 37]. The PDA detector was then replaced with the fluorescence module and another MDA-TBA standard was run on the same capillary producing a similar electropherogram. The UV data along with varying standard concentrations helped further identify the MDA-TBA formation as well as its migration time (Figure 2.5).

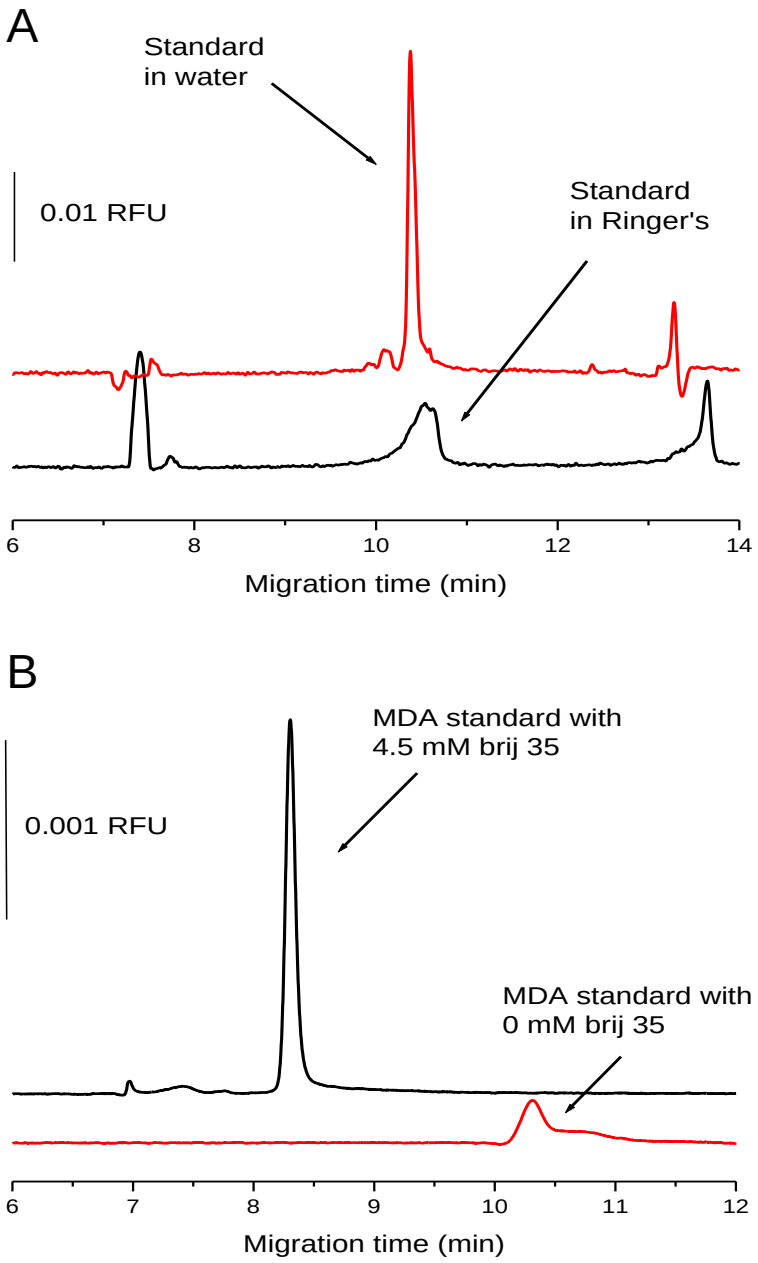

Figure 2.4: A) Electropherograms of 50 nM MDA standards showing destacking effects of Ringer's solution (BGE 200 mM boric acid pH 8.4). B) Electropherograms of 500 nM MDA standards showing the increase in efficiency with added brij 35 (runs were made using a Jasco fluorescence detector with a capillary of dimensions 55 (30).

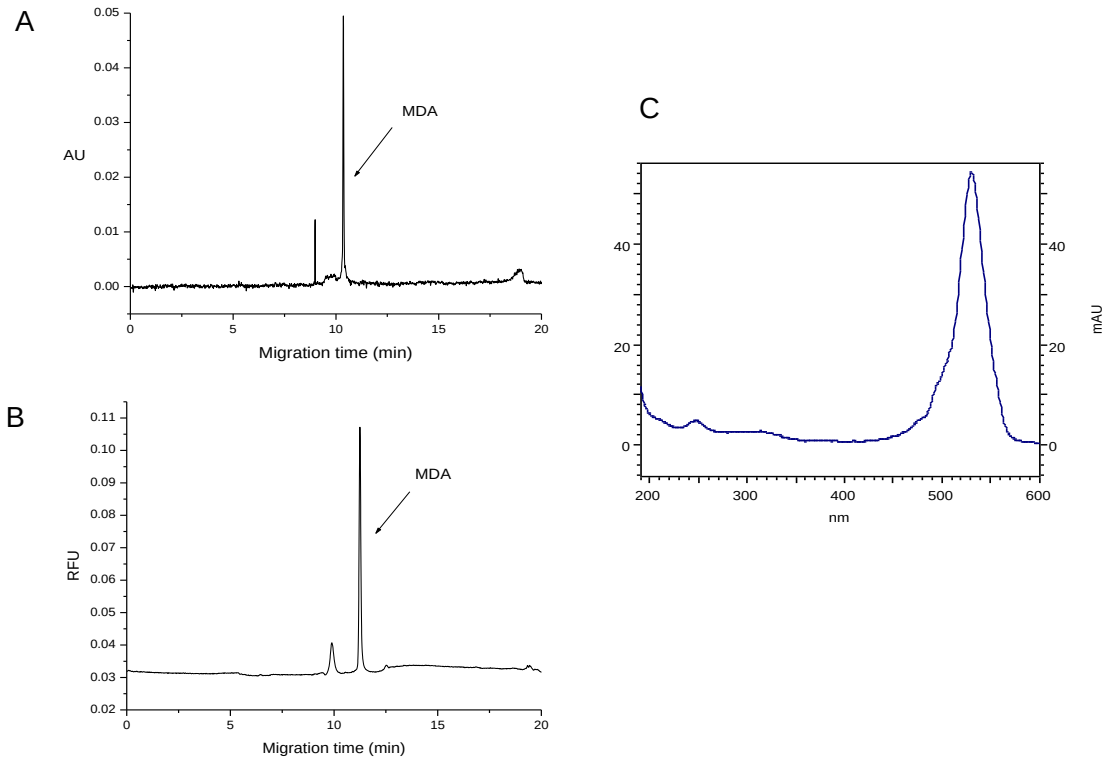

Figure 2.5: Electropherograms of (A) 25 µM MDA with PDA detector and (B) 500 nM MDA with fluorescence detection (ex 488 nm, em 560 nm). (C) UV spectrum of the peak at 10.1 minutes in plot A. With permission from [35]

This method provided a limit of detection of 25 nM (S/N = 3) and a linear range of 75-9600 nM (5.4-969 ng/ml). The inter-day coefficient of variance (CV) observed for standards ranging from 2500-25 nM were between 7-19% (n=8) ever a 3 month period (Figure 2.6). The high variance for low standards can be attributed to them being at the limits of detection for the method.

Unfortunately a contaminant in the TBA that was unresolvable from the MDA-TBA adduct. It was postulated that this contaminate could be a barbituric-thiobarbituric adduct formed during the heating. The barbituric acid contaminate has been previously observed and characterized using LC/MS [37].

2.3.4 Mass Spectrometric Identification

The 10 µM MDA standard had an expected $[M-H]^-$ peak at *m/z* 323 representing the MDA-TBA adduct (figure 2.7B). The subsequent collision induced dissociation (CID) produced fragments at *m/z* 264 $[M-59]^-$ and 143 $[M-180]^-$ which have been previously characterized [37]. The blank had a TBA peak *m/z* 143 which fragmented to m/z 58 $[M-85]^-$. Also, there was an unknown peak *m/z* 301 which fragmented to *m/z* 258 $[M-43]^-$, 157 $[M-144]^-$, and 143 $[M-158]^-$ ions, and further fragmentation of *m/z* 157 produced *m/z* 98 $[M-144-59]^-$. The loss of mass 59 (HSCN) from *m/z* 157 would indicate it has a similar structure to TBA and the MDA-TBA adduct. The fragmentation along with the methylene mass difference between *m/z* 157 and 143 would indicate that the contaminant could be residual formaldehyde in the purified TBA. During the flow injection analysis, peaks at *m/z* 269 and 285 were also identified as barbituric-thiobarbituric and thiobarbituric-thiobarbituric derivatives.

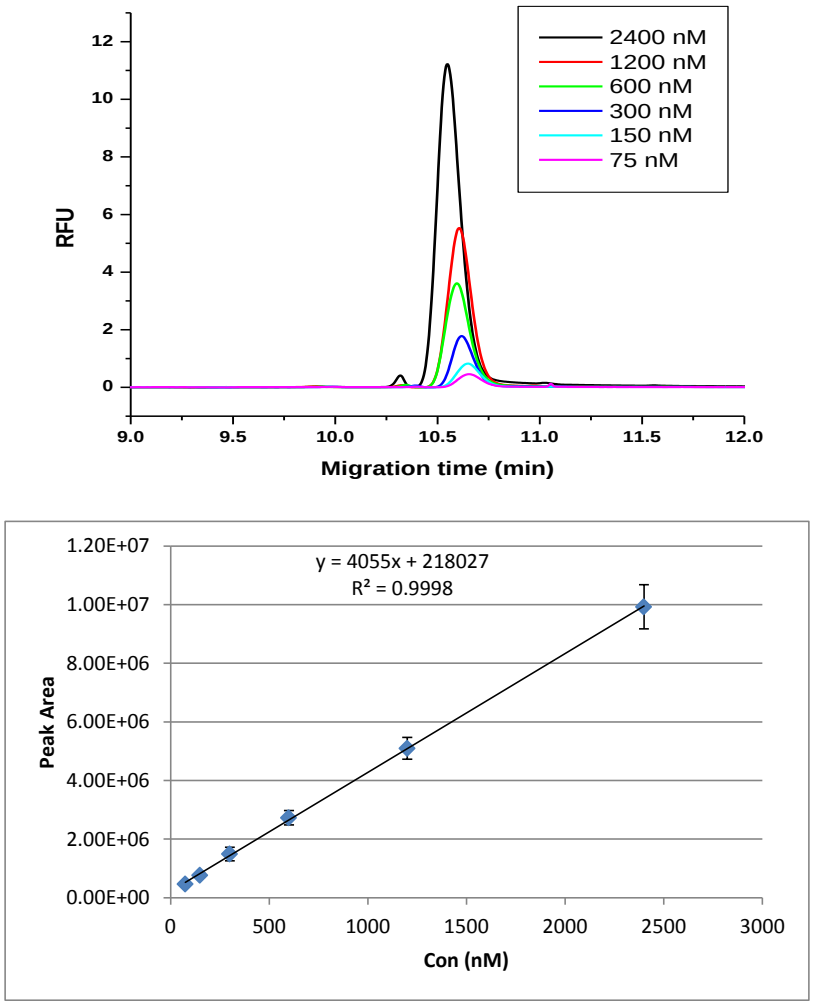

Figure 2.6: Electropherograms of MDA standards and subsequent calibration curve (n=8)

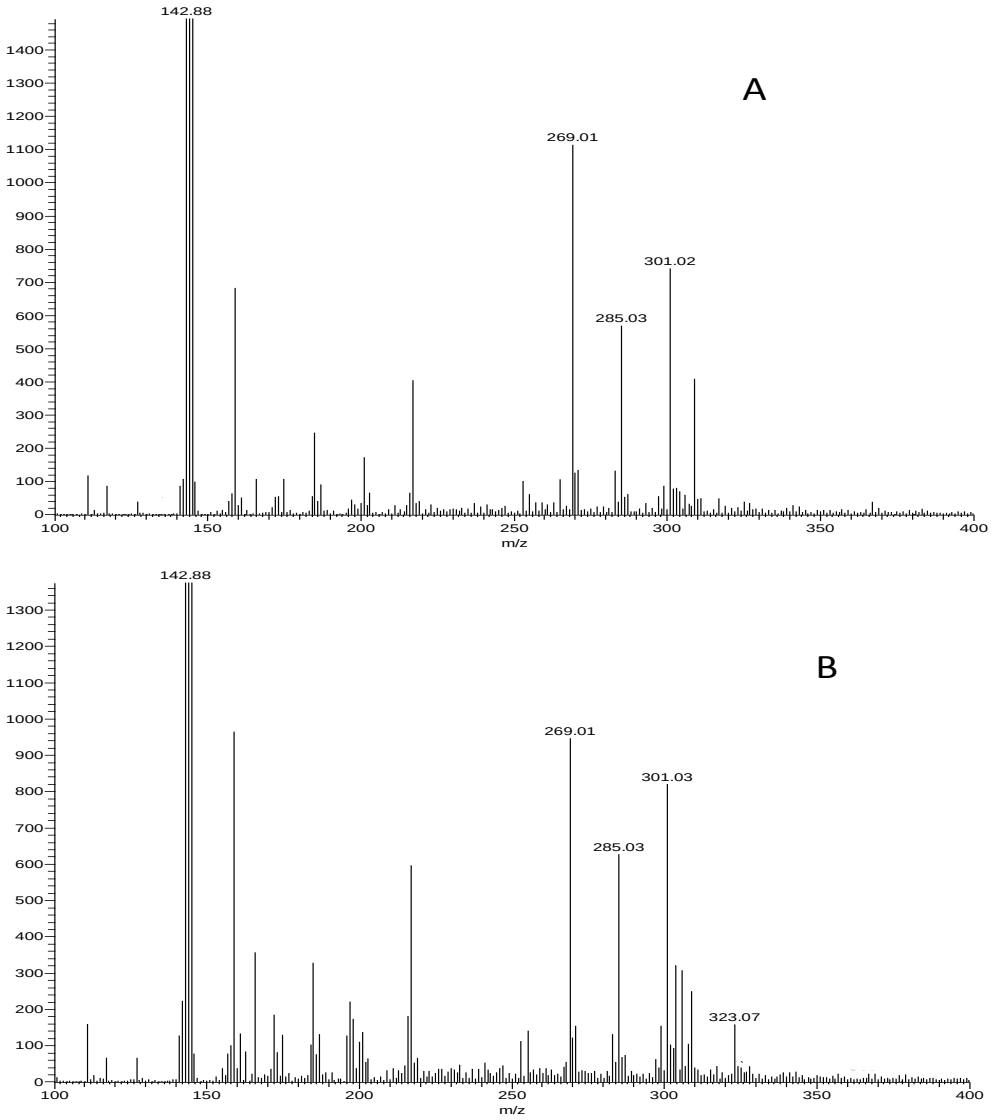

Figure 2.7: Mass spectra of (A) TBA reagent blank and (B) 10 µM MDA standard after derivatization and extraction with butanol. The *m/z* 142.8 correlates to TBA, 323 to MDA-(TBA), 269 to barbituric-TBA, 285 to TBA-TBA and 301 to the unknown. With permission from [35]

The interfering peak in the electropherogram could be resulting from the methylene-thiobarbituric acid product because it is more structurally similar to the MDA-TBA product. TBA was purchased from two venders (Sigma and Cayman) both with purity >98% to examine if there would be a difference in the formulation. Unfortunately, no difference in either mass spectra or electropherograms was seen from either vender. However, this interfering peak was observed to be consistent from every fresh TBA solution made and was less than 25% of the smallest basal MDA detected. Because MDA levels are expected to only increase from the induced oxidative stress, the blank was subtracted for quantitation and provided *y*-intercepts which were closer to zero.

2.4 MDA in Microdialysis

2.4.1 Relative Recovery

To demonstrate this method's applicability, MDA levels were monitor in a variety of rat organs (heart, muscle, and liver). *In vitro* studies using a linear microdialysis probe of 10 mm showed MDA had a relative recovery of 49 ± 6 % (n=6) at a flow rate of 1 µL/min which is a reasonable recovery considering MDA's low molecular weight, and with no evidence to suggest MDA will cause a probe failure from sticking to the membrane. MDA was detected in dialysate collected from probes implanted in liver, heart and leg muscle (Figure 2.8). The samples were derivatized as previously stated (Section 2.2.2) and compared to standards. The dialysate concentrations were calculated by a calibration curve with linear regression to be: 80 ± 20, 80 ± 8, and 48 ± 9 nM averaged over 5 basal samples for the liver, muscle and heart respectively. An unreacted dialysate sample was also run and showed no interferences with the MDA peak.

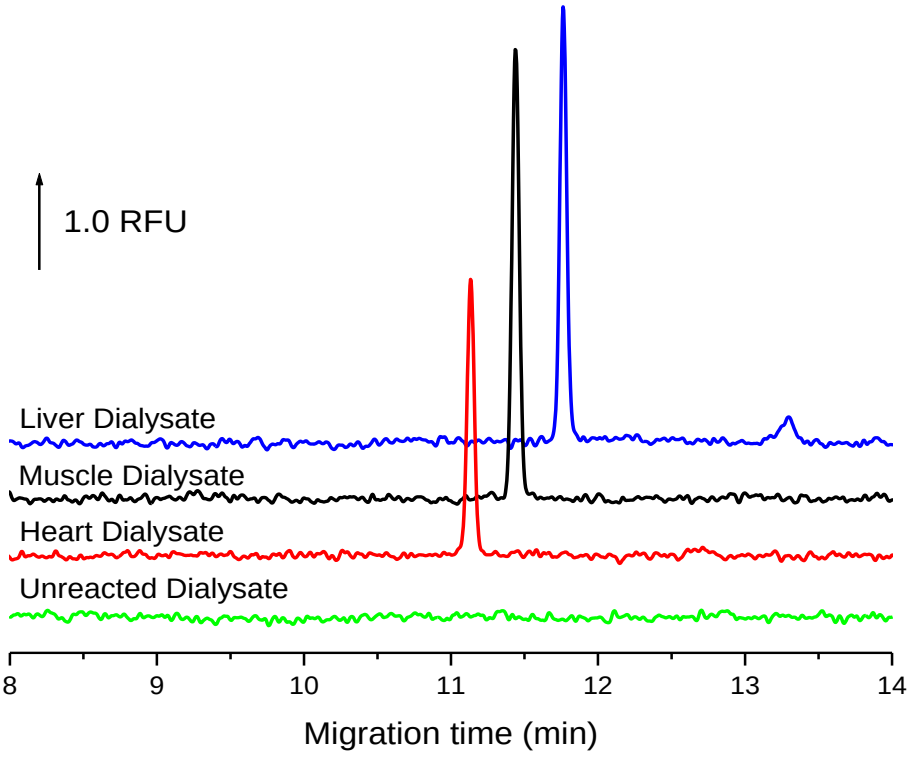

Figure 2.8: Electropherograms of microdialysis samples collected from liver, heart, and muscle and an unreacted (not heated) dialysate sample. With permission from [35]

Calibration of a CMA 12 brain probe was also performed. *In vitro* experiments were performed where the brain probe was submerged in a 500 nM MDA solution maintained at 37 °C. Six MDA standard solutions (0, 100, 250, 500, 750, and 1000 nM) were perfused for 50 minutes each, with Ringer's solution perfused for 30 minutes between standards (Figure 2.9). Samples were collected over 10 minute intervals and the last 30 minutes of each standard perfusion period were used to determine the MDA relative recovery. MDA had similar recovery (40%) with the CMA 12 probe as with the 10 mm linear probe.

For *in vivo* calibration, a two point no-net-flux experiment was performed. A basal sample was collected for reference prior to perfusion of 0.4 and 1 µM MDA standard solutions, still at 1 µL/min flow rate. Each standard was perfused for 1 hour to allow for equilibration with sample collection over 10 minute intervals. Ringer's solution was perfused between MDA standards for 30 minutes and basal samples were again collected. The last three samples for each standard were averaged and used to calculate MDA relative recovery. From this two-point calibration, it was determined that MDA had a recovery between 40-50% (Figure 2.9). In another experiment (not shown) the recovery was calculated to be 5%, but there was a noticeable decrease in dialysate volume indicative of probe failure. It was not surprising though to have a 10% difference within the *in vivo* calibrations experiments because of the added variable compared to *in vitro*. It is the purpose of these studies to observe changes relative to basal and control levels. Even with a difference in recovery of 10% or greater from probe to probe, the percent change in MDA will still be indicative of changes *in vivo*.

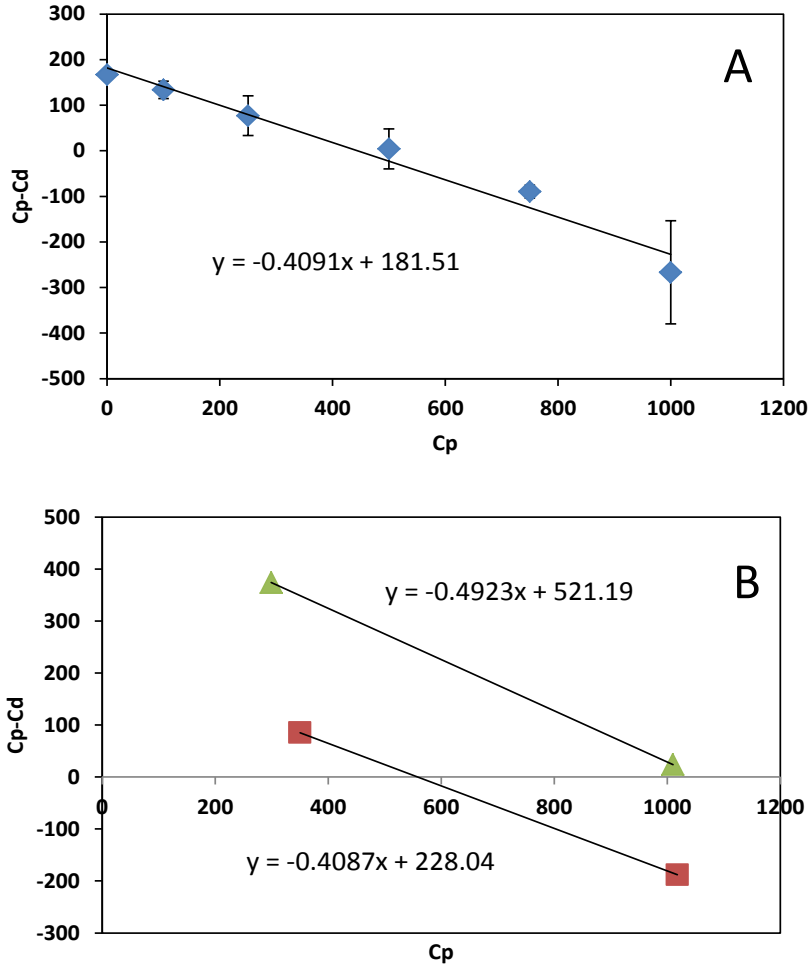

Figure 2.9: Relative recovery curves for *in vitro* (A) and *in vivo* (B) brain microdialysis experiments using a CMA 12 probe. The negative of the slope indicates a RR of about 40% and the x-intercept is the Cs (concentration in the sample)

2.4.2 *In Vivo* Application

The first attempt at inducing oxidative stress was by dosing doxorubicin (Adriamycin) through the microdialysis probe into the liver, as done previously in our laboratory [38]. However, doxorubicin has fluorescent characteristics matching that of the detection scheme used for MDA, and at the concentration being used had large peaks interfering with MDA detection. Solid phase extraction (SPE) using Ziptips (Millipore, Billerica, MA) was employed in order to remove doxorubicin from the samples. SPE was successful at removal of doxorubicin; however, samples collected during the dosing period were too heavily concentrated causing saturation of the Ziptip. The remaining doxorubicin during dosing still caused interferences preventing MDA quantitation. Therefore, a model of liver ischemia was used to validate the application of this method for *in vivo* oxidative stress. Models of liver ischemia/reperfusion are used to study injury from liver transplantation [39]; also, conditions of hemorrhaging, severe bleeding and infectious diseases can lead the liver to be vulnerable to I/R injury [40]. Partial ischemia/reperfusion was accomplished here by clamping the left hepatic artery for 30 minutes. Probe performance was monitored by retrodialysis of 5 µM antipyrine in Ringer's solution throughout the experiment as performed previously in our laboratory [41].

Increases in MDA were inconsistent for ischemia experiments and at first glance there appeared to be no correlation in MDA production and liver ischemia (Figure 2.10). Of the nine ischemia/reperfusion experiments, two showed no change from basal, five had sporadic jumps in MDA at single time points, and two had extended increases in MDA over multiple data points. From these data it can be concluded that either many factors are involved in MDA production in the liver or there are inconsistencies with the experimental design.

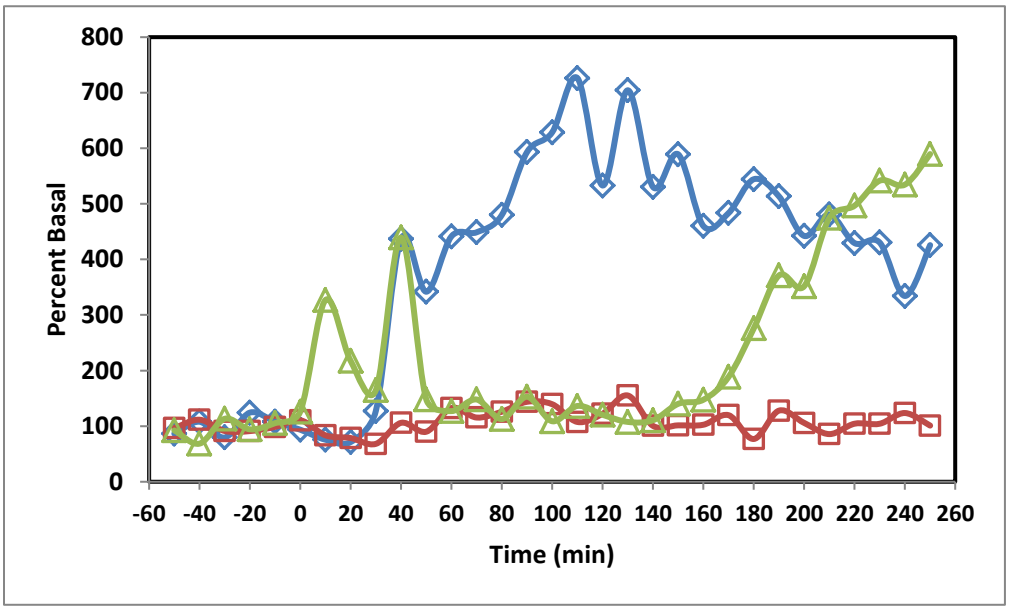

Figure 2.10: MDA time plots of three different liver ischemia experiments to illustrate the range of MDA produced. Time 0 represents the start of 30 minute ischemia. It is important to note the change in percent basal of MDA after ischemia and how vastly it varies between the three experiments.

However, comparing the histology results (cellular necrosis) to their respective MDA data for each experiment revealed a damage correlation. Those experiments which had no change in MDA production showed little to no damage to the liver (similar to controls) while the liver histology from the experiments with extended MDA production showed large amounts of damage and necrosis. These data would indicate problems with reproducibility of the ischemia in the animal model and that the analytical method is able to track those differences. The probe placement also had a factor in the MDA recovered. If the probe was inserted next to an artery or vein then whatever damage occurred at the start of reperfusion the probe was able to sample from that immediate area. However, when the probe was located further away from an artery the MDA recovered was either delayed because of the diffusion rate through the tissue or a result of damage to tissue outside the penumbra. Figure 2.11 shows three example experiments of varying damage in which probe placement could have affected MDA recovery results.

The liver receives blood from two sources, the portal vein and the hepatic artery [42]. The portal vein supplies the liver with blood from the gut, spleen, and pancreas as part of digestive processes. The hepatic artery supplies the liver with oxygenated blood from the heart. Blood exits the liver via the hepatic vein into the inferior vena cava (heading to the heart). Partial liver ischemia can be achieved by clamping the portal vein, hepatic artery and bile duct of a particular liver lobe [43]. In this work, only the hepatic artery was clamped. It has been stated that portal vein occlusion can lead to intestinal pooling of blood producing inflammatory metabolites in the gut [44]. Portal vein occlusion causes an increase in animal mortality, but models have been used to produce substantial liver injury with only hepatic occlusion [45].

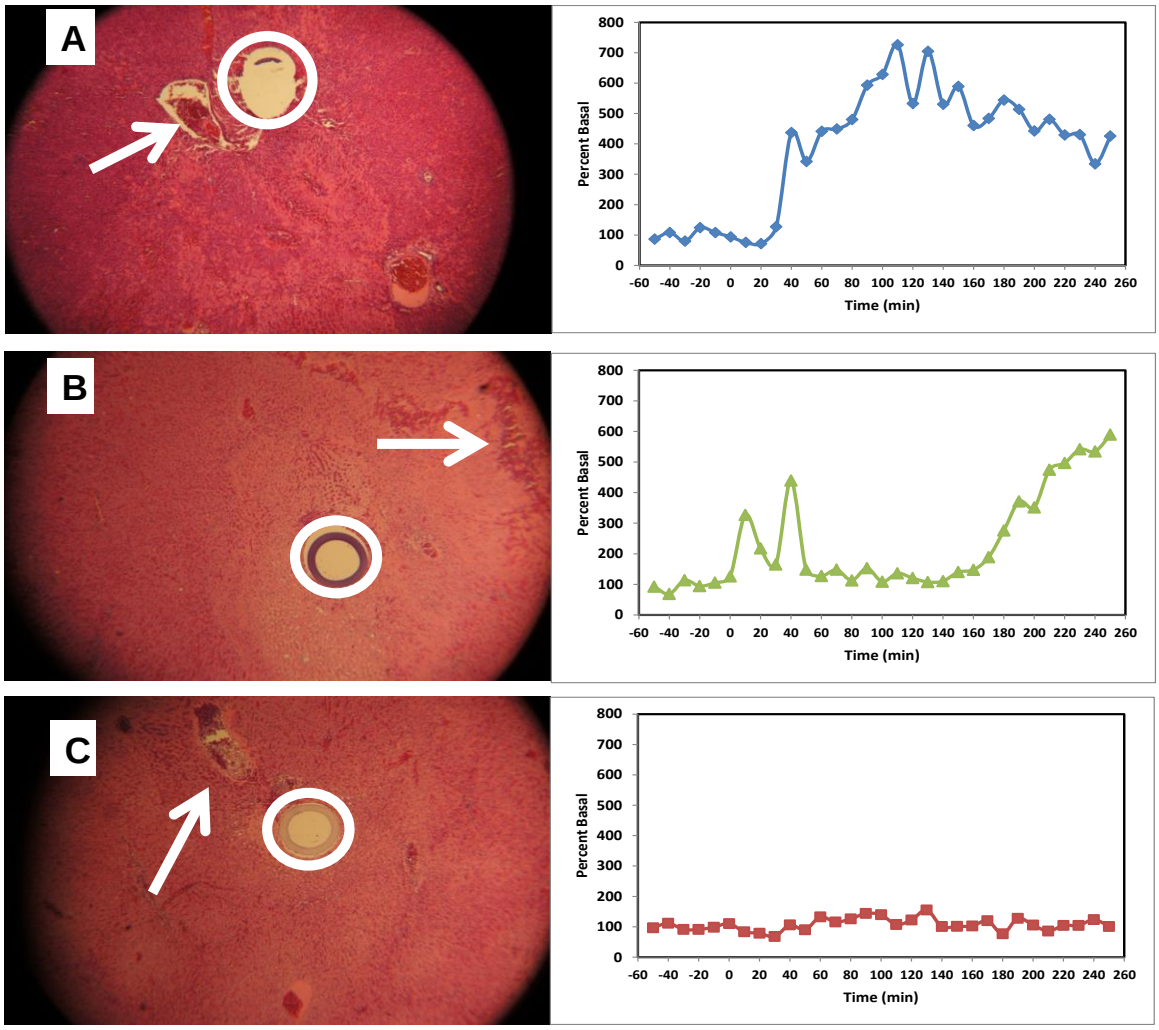

Figure 2.11: Liver histology pictures and their respective MDA time plots. A) Example of high damage experiment where the microdialysis probe is located near an artery, the time plot shows immediate increase in MDA after ischemia. B) Example of medium damage experiment where the microdialysis probe is located further from an artery, the time plot shows a delayed increase in MDA (~180 min) with sporadic increase in MDA around the ischemia. C) Example of low damage experiment where although microdialysis probe is located near an artery, little MDA or damage was produced. White circles highlight probe location, white arrows show artery.

In order to prevent a misinterpretation of the data and animal death from intestinal byproducts, the hepatic artery was the only blood supply occluded. However, if the hepatic artery is not fully clamped, then the leakage could still provide the liver with some oxygenated blood. A study by Brooks *et al.* [46] used microdialysis sampling to monitor the partial pressures of oxygen and carbon dioxide in patients undergoing liver resection surgery. During the 10 minute clamping of the hepatic vesicular inflow they observed a statistical difference in carbon dioxide; however, no significant difference in oxygen during the same time period [46]. This lack of statistical difference between basal and ischemia was due to a large variation in oxygen during the ischemic period.

Blood from the portal vein, although not fully oxygenated, could provide enough oxygen to prevent the cellular changes leading to oxidative stress. If for example the animal was fasting then little oxygen would be consumed in digestion prior to the blood reaching the liver via the portal vein. An interesting experiment would be to not allow the animal food several hours before surgery and compare those experiments to animals whom were recently feed.

2.5 Conclusion

A CE-LIF method was developed to detect MDA in microdialysis samples. This method was linear over 3 orders of magnitude. The method had an LOD adequate to detect MDA in microdialysis basal samples from probes implanted in multiple tissue sites. Although a contaminant in the derivatizing reagent was present, the electrophoretic interference was consistent within batch to batch reactions and could be accounted for in analysis. To show the applicability, this method was used in an animal model of liver ischemia. Although the resulting MDA data were inconsistent, the

variability was with the animal model and not the MDA method. The MDA results were a good indicator of damage and correlated well with the respective histology.

2.6 References

1. Sinnhuber, R. O.; Yu, T. C., 2-Thiobarbituric Acid Method for the Measurment of Rancidity in Fishery Products .2. The Quantitative Determination of Malonaldehyde. *Food Technol.* **1958,** *12* (1), 9-12.
2. Sinnhuber, R. O.; Yu, T. C.; Yu, T. C., Characterization of the red pigment formed in the 2-thiobarbituric acid determination of oxidative rancidity. *Food Res* **1958,** *23* ((6)), 626-634.
3. Janero, D. R., Malondialdehyde and Thiobarbituric Acid-Reactivity as Diagnostic Indexes of Lipid-Peroxidation and Peroxidative Tissue-Injury. *Free Radic. Biol. Med.* **1990,** *9* (6), 515-540.
4. Adibhatla, R. M.; Hatcher, J. F., Phospholipase A2, reactive oxygen species, and lipid peroxidation in cerebral ischemia. *Free Radic. Biol. Med.* **2006,** *40* (3), 376-387.
5. Mateos, R.; Bravo, L., Chromatographic and electrophoretic methods for the analysis of biomarkers of oxidative damage to macromolecules (DNA, lipids, and proteins). *J. Sep. Sci.* **2007,** *30* (2), 175-191.
6. Nielsen, F.; Mikkelsen, B. B.; Nielsen, J. B.; Andersen, H. R.; Grandjean, P., Plasma malondialdehyde as biomarker for oxidative stress: Reference interval and effects of life-style factors. *Clin. Chem.* **1997,** *43* (7), 1209-1214.
7. Akhgari, M.; Abdollahi, M.; Kebryaeezadeh, A.; Hosseini, R.; Sabzevari, O., Biochemical evidence for free radical-induced lipid peroxidation as a mechanism for subchronic toxicity of malathion in blood and liver of rats. *Hum. Exp. Toxicol.* **2003,** *22* (4), 205-211.
8. Mateos, R.; Lecumberri, E.; Ramos, S.; Goya, L.; Bravo, L., Determination of malondialdehyde (MDA) by high-performance liquid chromatography in serum and liver as a biomarker for oxidative stress - Application to a rat model for hypercholesterolemia and evaluation of the effect of diets rich in phenolic antioxidants from fruits. *J. Chromatogr. B* **2005,** *827* (1), 76-82.
9. Grotto, D.; Maria, L. S.; Valentini, J.; Paniz, C.; Schmitt, G.; Garcia, S. C.; Pomblum, V. J.; Rocha, J. B. T.; Farina, M., Importance of the Lipid Peroxidation Biomarkers and Methodological Aspects for Malondialdehyde Quantification. *Quim. Nova* **2009,** *32* (1), 169-174.
10. Knight, J. A.; Pieper, R. K.; McClellan, L., Specificity of the Thiobarbituric Acid Reaction - Its Use in Studies of Lipid Peroxidation. *Clin. Chem.* **1988,** *34* (12), 2433-2438.
11. Gutteridge, J. M. C.; Tickner, T. R., Charaterization of Thiobarbituric Acid Reactivity in Human-Plasma and Urine. *Anal. Biochem.* **1978,** *91* (1), 250-257.
12. Korizis, K. N.; Exarchou, A.; Michalopoulos, E.; Georgakopoulos, C. D.; Kolonitsiou, F.; Mantagos, S.; Gartaganis, S. P.; Karamanos, N. K., Determination of malondialdehyde by capillary electrophoresis, application to human plasma and relation of its levels with prematurity. *Biomed. Chromatogr.* **2001,** *15* (4), 287-291.
13. Wilson, D. W.; Metz, H. N.; Graver, L. M.; Rao, P. S., Direct method for quantification of free malondialdehyde with high-performance capillary electrophoresis in biological samples. *Clin. Chem.* **1997,** *43* (10), 1982-1984.
14. Larstad, M.; Ljungkvist, G.; Olin, A. C.; Toren, K., Determination of malondialdehyde in breath condensate by high-performance liquid chromatography with fluorescence detection. *J. Chromatogr. B* **2002,** *766* (1), 107-114.

15. Ji, L. L.; Fu, R. G.; Waldrop, T. G.; Liu, K. J.; Swartz, H. M., Myocardial Response to Regional Ischemia and Reperfusion In-Vivo in Rat Heart. *Can. J. Physiol. Pharmacol.* **1993,** *71* (10-11), 811-817.
16. Tatum, V. L.; Changchit, C.; Chow, C. K., Measurement of Malondialdehyde by High-Performance Liquid-Chromatography with Fluorescence Detection. *Lipids* **1990,** *25* (4), 226-229.
17. Fukunaga, K.; Yoshida, M.; Nakazono, N., A simple, rapid, highly sensitive and reproducible quantification method for plasma malondialdehyde by high-performance liquid chromatography. *Biomed. Chromatogr.* **1998,** *12* (5), 300-303.
18. Janssen, M.; Koster, J. F.; Bos, E.; Dejong, J. W., Malondialdehyde and Glutathione Production in Isolated-Perfused Human and Rate Hearts. *Circ.Res.* **1993,** *73* (4), 681-688.
19. Young, I. S.; Trimble, E. R., Measurement of Malondialdehyde in Plasma by High-Performance Liquid-Chromatography with Fluorometric Detection. *Ann. Clin. Biochem.* **1991,** *28*, 504-508.
20. Stalikas, C. D.; Konidari, C. N., Analysis of malondialdehyde in biological matrices by capillary gas chromatography with electron-capture detection and mass spectrometry. *Anal. Biochem.* **2001,** *290* (1), 108-115.
21. Fraser, M.; Bennet, L.; Van Zijl, P. L.; Mocatta, T. J.; Williams, C. E.; Gluckman, P. D.; Winterbourn, C. C.; Gunn, A. J., Extracellular amino acids and lipid peroxidation products in periventricular white matter during and after cerebral ischemia in preterm fetal sheep. *J. Neurochem.* **2008,** *105* (6), 2214-2223.
22. Qian, H.; Liu, D. X., The time course of malondialdlehyde production following impact injury to rat spinal cord as measured by microdialysis and high pressure liquid chromatography. *Neurochem. Res.* **1997,** *22* (10), 1231-1236.
23. Neubert, R.; Ruttinger, H., *Affinity Capillary Electrophoresis in Pharmaceutics and Biopharmaceutics*. Marcel Dekker: New York, 2003; Vol. 128.
24. Jorgenson, J. W.; Lukacs, K. D., Zone Electrophoresis in Open-Tubular Glass-Capillaries. *Anal. Chem.* **1981,** *53* (8), 1298-1302.
25. Harris, D. C., *Quantitative Chemical Analysis*. 6th ed.; W.H. Freeman: New York, 2003.
26. Schwer, C.; Kenndler, E., Electrophoresis in Fused-Silica Capillaries - The Influence of Organic-Solvents on the Electroosmotic Velocity and the Zeta-Potential. *Anal. Chem.* **1991,** *63* (17), 1801-1807.
27. Nishi, H.; Terabe, S., Optical Resolution Drugs by Capillary Electrophoresis Techniques. *J. Chromatogr. A* **1995,** *694* (1), 245-276.
28. Quirino, J. P.; Terabe, S., Exceeding 5000-fold concentration of dilute analytes in micellar electrokinetic chromatography. *Science* **1998,** *282* (5388), 465-468.
29. Pyrell, U., *Electrokinetic Chromatography: Theory, Instrumentation and Application*. John Wiley & Sons: West Sussex, 2006.
30. Walbroehl, Y.; Jorgenson, J. W., On-Column UV Absorption Detection for Open Tubular Capillary Zone Electrophoresis. *Journal of Chromatography* **1984,** *315* (DEC), 135-143.
31. Smith, R. D.; Barinaga, C. J.; Udseth, H. R., Improved Electrospray Ionization Interface for Capillary Zone Electrophoresis - Mass Spectrometry. *Anal. Chem.* **1988,** *60* (18), 1948-1952.
32. Quirino, J. P.; Terabe, S., Approaching a million-fold sensitivity increase in capillary electrophoresis with direct ultraviolet detection: Cation-selective exhaustive injection and sweeping. *Anal. Chem.* **2000,** *72* (5), 1023-1030.

33. Palmer, J.; Munro, N. J.; Landers, J. P., A universal concept for stacking neutral analytes in micellar capillary electrophoresis. *Anal. Chem.* **1999,** *71* (9), 1679-1687.
34. Esterbauer, H.; Schaur, R. J.; Zollner, H., Chemistry and Biochemistry of 4-Hydroxynonenal, Malonaldehyde and Related Aldehydes. *Free Radic. Biol. Med.* **1991,** *11* (1), 81-128.
35. Cooley, J. C.; Lunte, C. E., Detection of malondialdehyde in vivo using microdialysis sampling with CE-fluorescence. *Electrophoresis* **2011,** *32* (21), 2994-2999.
36. Matsubara, N.; Terabe, S., Separation of Closely Related Peptides by Capillary Electrophoresis with a Nonionic Surfactant. *Chromatographia* **1992,** *34* (9-10), 493-496.
37. Jardine, D.; Antolovich, M.; Prenzler, P. D.; Robards, K., Liquid chromatography-mass spectrometry (LC-MS) investigation of the thiobarbituric acid reactive substances (TBARS) reaction. *J. Agric. Food Chem.* **2002,** *50* (6), 1720-1724.
38. Price, K. E.; Larive, C. K.; Lunte, C. E., Tissue-targeted metabonomics: biological considerations and application to doxorubicin-induced hepatic oxidative stress. *Metabolomics* **2009,** *5* (2), 219-228.
39. Zhai, Y.; Busuttil, R. W.; Kupiec-Weglinski, J. W., Liver Ischemia and Reperfusion Injury: New Insights into Mechanisms of Innate-Adaptive Immune-Mediated Tissue Inflammation. *Am. J. Transplant.* **2011,** *11* (8), 1563-1569.
40. Boys, J. A.; Toledo, A. H.; Anaya-Prado, R.; Lopez-Neblina, F.; Toledo-Pereyra, L. H., Effects of Dantrolene on Ischemia-Reperfusion Injury in Animal Models: A Review of Outcomes in Heart, Brain, Liver, and Kidney. *J. Invest. Med.* **2010,** *58* (7), 875-882.
41. Price, K. E.; Lunte, C. E.; Larive, C. K., Development of tissue-targeted metabonomics. Part 1. Analytical considerations. *J. Pharm. Biomed. Anal.* **2008,** *46* (4), 737-747.
42. Clavien, P.; Petrowsky, H.; DeOliveira, M. L.; Graf, R., Medical progress: Strategies for safer liver surgery and partial liver transplantation. *N. Engl. J. Med.* **2007,** *356* (15), 1545-1559.
43. Jin, L. M.; Liu, Y. X.; Zhou, L.; Xie, H. Y.; Feng, X. W.; Li, H.; Zheng, S. S., Ischemic Preconditioning Attenuates Morphological and Biochemical Changes in Hepatic Ischemia/Reperfusion in Rats. *Pathobiology* **2010,** *77* (3), 136-146.
44. Winbladh, A.; Sandstrom, P.; Olsson, H.; Svanvik, J.; Gullstrand, P., Segmental Ischemia of the Liver - Microdialysis in a Novel Porcine Model. *Eur. Surg. Res.* **2009,** *43* (3), 276-285.
45. Asakawa, H.; Jeppsson, B.; Mack, P.; Hultberg, B.; Hagerstrand, I.; Bengmark, S., Acute Ischemic Liver Failure in the rat - A Reproducible Model not Requiring Protal Decompresion. *Eur. Surg. Res.* **1989,** *21* (1), 42-48.
46. Brooks, A. J.; Eastwood, J.; Beckingham, I. J.; Girling, K. J., Liver tissue partial pressure of oxygen and carbon dioxide during partial hepatectomy. *Br. J. Anaesth.* **2004,** *92* (5), 735-U738.

Chapter 3:

Malondialdehyde as a Measure for Lipid Peroxidation in Local 3-MPA Dosing Model

Introduction

Epilepsy, a neurological disorder affecting nearly 3 million people in the US and 50 million people worldwide, is defined as having 2 or more unprovoked seizure events [1]. It can arise from several mechanisms that include genetic disposition, small molecule excitotoxicity, and oxidative stress; however, the initiation of these mechanisms remains unclear. Studies have shown that upwards of 36% of patients with epilepsy continue to have uncontrolled seizures even with anti-epileptic therapeutic treatment [2]. The most common types of anti-epileptic medications focus on decreasing neuronal signal through inhibitory mechanisms such as blocking Na^+ channels or preventing GABA depletion. Evidence continues to grow for the role oxidative stress plays in the development of epilepsy (for review see Shin EJ [3] and Patel [4]), suggesting that oxidative stress and epilepsy have a cyclical nature. For example, oxidative stress caused by a stroke or brain trauma (the second and third leading causes of epilepsy) provokes a seizure event which causes more oxidative damage leading to further seizures [5]. The opposite would then be a seizure event causing oxidative damage followed by repetitive seizure events. The research goal in our laboratory is to monitor biomarkers of oxidative stress during chemically induced seizures.

3.1 Brain Model of Seizures

Animal models for seizures can be produced in several ways, the most common being through the addition of a chemical convulsant. The route through which the convulsant is dosed depends on the type of seizure desired, generalized or focal. A

generalized seizure originates at some point and rapidly distributes between networks and across hemispheres [6]. A generalized seizure can be produced by dosing a convulsant systemically, through *i.v.* or *i.p.,* and produces tonic-clonic seizures (body jerks and twitching). A focal seizure is limited to one hemisphere and usually within one network [6]. In this case, a convulsant is dosed by a microinjection directly into the brain or delivered through a microdialysis probe. An unpleasant smell or small motor movement are usually the only symptoms experienced from a focal seizure and because of this mild activity usually go undiagnosed.

3-Mercaptopropinoic acid (3-MPA) is a competitive inhibitor of glutamic acid decarboxylase (GAD) (Figure 3.1) preventing neurons from synthesizing gamma-aminobutyric acid (GABA), a major inhibitory neurotransmitter, from glutamate, the brains main excitatory neurotransmitter [7]. Glutamate release is involved in neuronal plasticity, memory formation, and excitotoxicity; therefore, its regulation is highly important. When 3-MPA is dosed systemically, there is a differential response to seizure induction across brain regions. Schneider *et al.* observed increases in muscarinic receptor binding in the hippocampus (a structure in the temporal lobe) at the early stages of 3-MPA induced seizures but not at post-seizure stages [8]. This suggests that the hippocampus has involvement in seizure onset and development but not in seizure maintenance as compared to other regions of the brain such as the cerebellum and striatum [8]. Animal seizure models in the hippocampus have been used to simulate temporal lobe epilepsy.

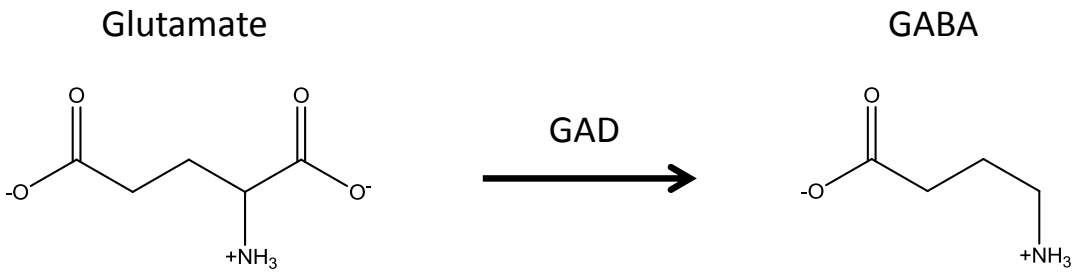

Figure 3.1: Synthesis of GABA from glutamate via glutamic acid decarboxylase (GAD). 3-MPA is an inhibitor for GAD.

3.1.1 Hippocampus

The most common human form of epilepsy involves the medial temporal/limbic network which includes the hippocampus, amygdala, entorhinal cortex, lateral temporal neocortex, medial thalamus and inferior frontal lobes [9]. Evidence points to the hippocampus as an origin for temporal lobe epilepsy, in particular, Ammon's horn sclerosis (or hippocampal sclerosis) with damage to the hippocampus pertaining to the *Cornu Ammonis* (CA) region [10]. The hippocampus is comprised of three distinct regions; the dentate gyrus, hippocampus proper, and subiculum. The hippocampus proper (CA region) consists of three sub-fields; CA1, CA2, and CA3 all made up of pyramidal neurons. The distinction between these regions comes from the size of the neurons (CA3 > CA1) and the direction of signal. Signaling in the hippocampus runs unidirectional, from dentate gyrus to CA3, CA3 to CA1, and CA1 to the stubiculum [11]. The CA2 field is a fusion between the CA3 and CA1; it has larger neurons like the CA3 but does not have mossy fiber connections like the CA1; however, the exact functionality of the CA2 is unclear. It has been postulated that seizure activity is a result of the hippocampal restructuring of surviving neurons (particularly inhibitory) after the death of pyramidal cells [10].

3.1.2 Systemic Dosing Model

A systemic dosing model of 3-MPA was previously developed in our laboratory by Eric Crick [12]. This model produced a steady state of 3-MPA in the brain for 50 minutes and produced status epilepticus during dosing (Figure 3.2). Status epilepticus is defined as a generalized seizure event where the individual experiences full body twitching (clonic-tonic). In this model, both 3-MPA and the neurotransmitters glutamate and GABA were monitored through a microdialysis probe implanted in the hippocampus

CA3 region (-5.6 A/P, +4.8 L/M, -7.0 D/V versus bregma). Glutamate increased about 200% during and following seizure induction, while GABA decreased during dosing but slowly returned to basal levels during recovery period. This trend follows what is expected based on the mechanism of 3-MPA.

3.1.3 Focal Dosing Model

To complement the systemic seizure model a local dosing method for 3-MPA was also developed in our laboratory by Andrew Meyer to simulate a focal seizure. In this model, 3-MPA was dosed through the microdialysis probe directly into the hippocampus CA1 region (-3.3 A/P, +1.7 L/M, -3.7 D/V versus bregma) [13]. Again, a steady-state delivery of 3-MPA to the brain was established for 50 minutes matching the conditions from the systemic dosing model (Figure 3.3). However, because the area of dosing was so small, it was difficult to detect seizure (electrical) activity. In this model, there was an increase in glutamate of about 600% during dosing (3 times that of the systemic model), but more interestingly GABA also increased during dosing unlike the systemic model.

In order to better understand the mechanisms associated with 3-MPA dosing, the extent of lipid peroxidation (as measured by MDA) was determined with local dosing between the CA3 and CA1 regions. Perfusion of glutamate through the microdialysis probe elicited a 6-fold increase in MDA production in the cortex [14]. It can be anticipated that the perfusion of 3-MPA (which indirectly increases glutamate) should also increase MDA production.

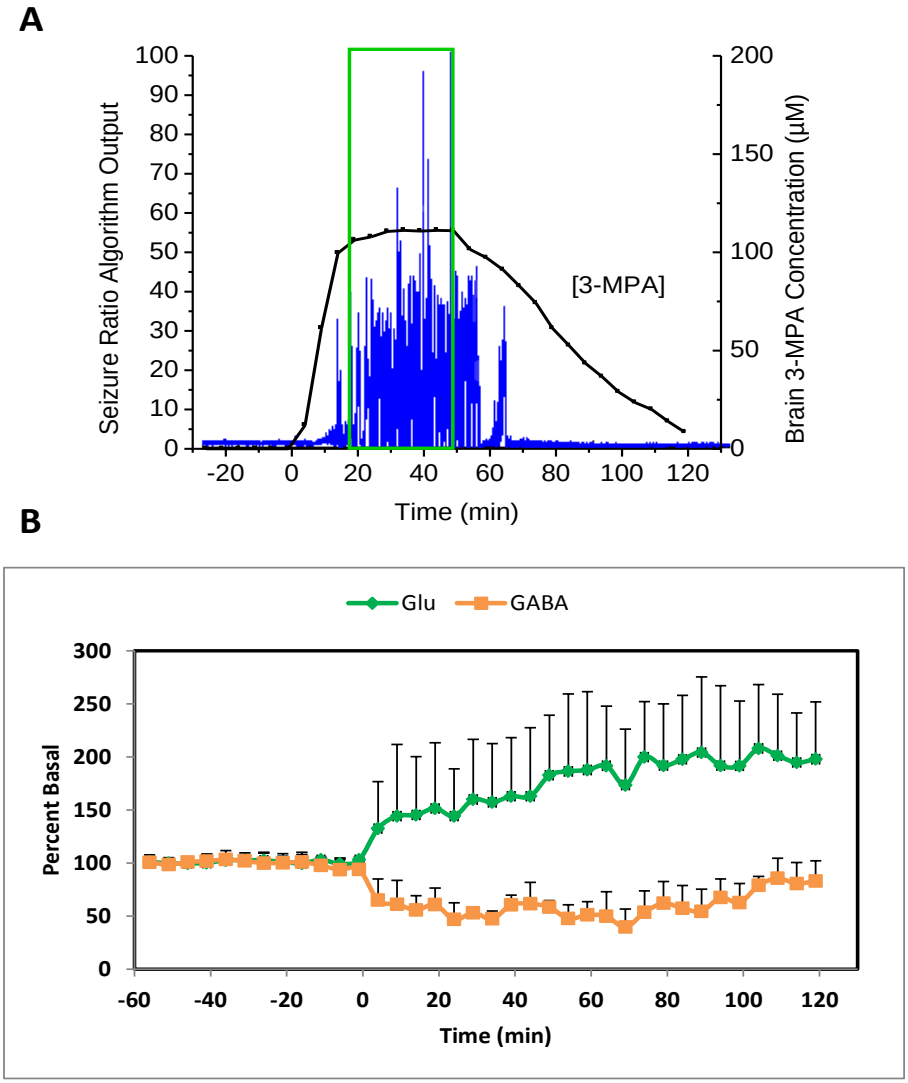

Figure 3.2: Data from systemic dosing method of 3-MPA: A) Box represents steady state of 3-MPA in the brain (line graph) and bar graph shows individual ECoG seizure activity, B) Microdialysis data from glutamate (Glu) and GABA as percent basal. Figures taken from Eric Crick, PhD dissertation [12].

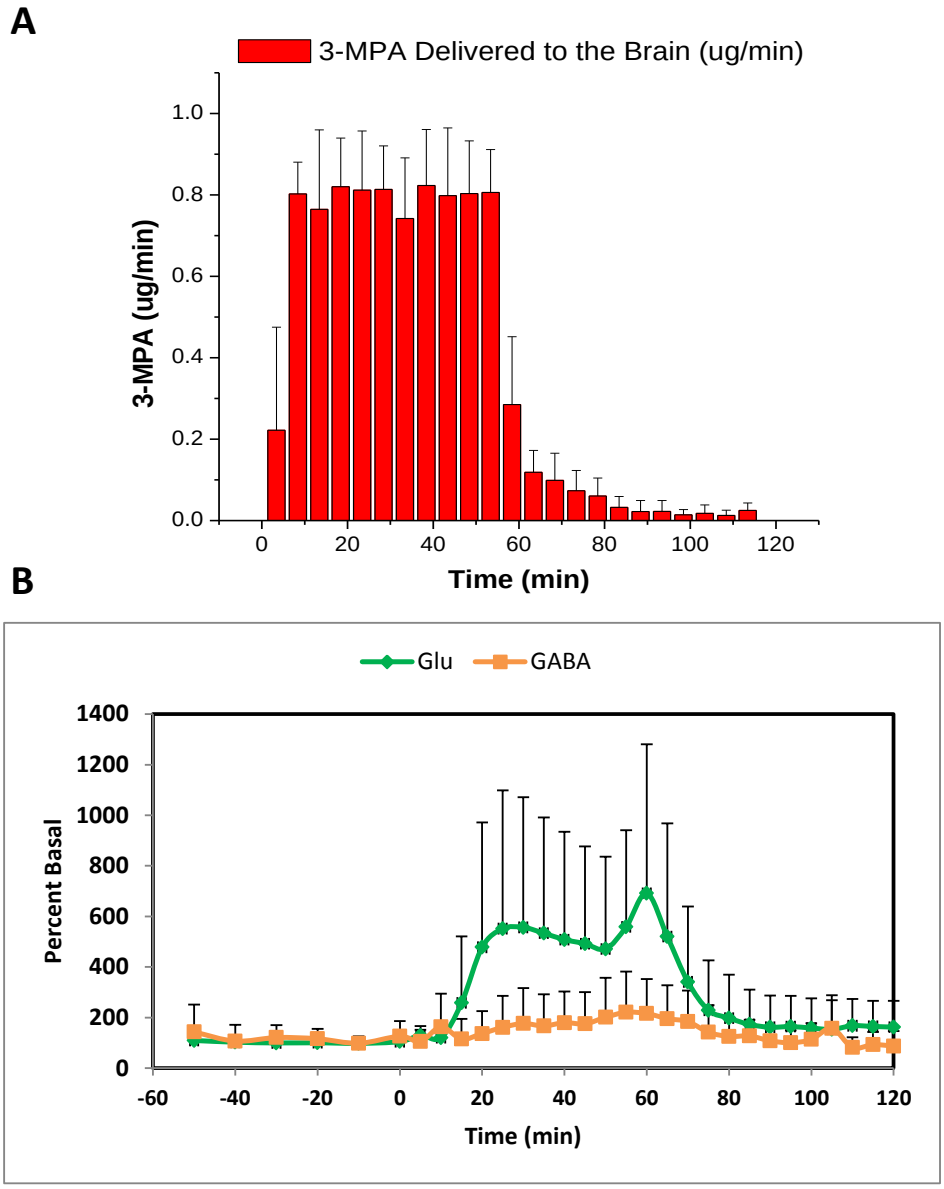

Figure 3.3: Data from local dosing model of 3-MPA: A) steady state delivery of 3-MPA through the microdialysis probe into the brain, B) Microdialysis data from glutamate (Glu) and GABA as percent basal. Figures taken from Andrew Meyer, PhD dissertation [13].

3.2 Methods

3.2.1 Chemicals

MDA (malondialdehyde tetrabutylammonium salt), boric acid, 3-mercaptopropionic acid (3-MPA) and TBA were purchased from Sigma-Aldrich (St. Louis, MO). TBA was also purchased from Cayman Chemical (Ann Arbor, MI). Brij 35 was purchased from MP Biomedicals (Solon, OH). Sulfuric acid and salts for Ringer's solution were purchased from Fisher (Fair Lawn, NJ). Ringer's solution composition was: 147 mM NaCl, 3 mM KCl, 1 mM $MgCl_2$, and 1.2 mM $CaCl_2$. All solutions were made using nanopure water obtained from a Labconco Water Pro Plus purification system (Kansas City, KS).

3.2.2 CE-Fluorescence Method

MDA was detected based on the CE-fluorescence method described in Chapter 2 of this dissertation. Briefly, 5 µl of microdialysate samples were derivatized with 3.75 µl of a 2:1 thiobarbituric acid (0.2% w/v) and sulfuric acid (0.2% v/v) mixture in a water bath at 90-95 °C for 20 minutes. The samples were flash frozen in liquid N_2 and stored at -80 °C until analyzed. Separation was carried out using a Beckman Coulter P/ACE MDQ CE system coupled with a 488 Ag laser module for excitation. Samples were hydrodynamically injected for 5 seconds at 0.5 psi. The separation was carried out at 10 kV with a BGE of 200 mM boric acid and 4.5 mM Brij 35 at pH 8.4. Fluorescence detection was achieved with excitation at 488 nm and emission at 560 nm.

3.2.3 Animal Surgery

All animal experiments were performed using male Wistar rats (Charles River) in the weight range of 300-500 g. Rats were housed under a 12 hr day/night cycle and given free access to food and water. All experiments were performed in the morning to

account for diurnal fluctuations. All animal experiments were performed in accordance with the local Institutional Animal Care and Use Committee and follow the principles stated in the Guide for the Care and Use of Laboratory Animals (National Academy of Sciences, 1996). All chemical solutions used for microdialysis experiments were diluted in Ringer's solution.

Rats were pre-anesthetized with isoflurane inhalation to effect and then fully anesthetized using a subcutaneous cocktail (ketamine (67.5 mg/kg), xylazine (3.4mg/kg), acepromazine (0.67 mg/kg)). Once under anesthesia, the top of the skull was shaved and the rat was placed in a stereotaxic instrument such that the bregma and lambda skull points were approximately at the same height. A lateral incision was made exposing the skull, and a CMA 12 microdialysis guide cannula (CMA, N. Chelmsford, MA) was slowly implanted into the rat's hippocampus CA3 region at stereotaxic coordinates -5.6 A/P, +4.8 L/M, and -5.0 D/V or CA1 region at -3.3 A/P, +1.7 L/M, and -1.7 D/V according to The Rat Brain in Stereotaxic Coordinates 2nd Ed [15] (Figure 3.4). The guide cannula was lowered to 2 mm above the desired location to account for the length of the microdialysis probe. The guide cannula was secured in place with dental cement and the animal was removed from the stereotaxic instrument. A CMA 12, 2 mm length microdialysis probe (CMA, N. Chelmsford, MA), which had been flushed with Ringer's solution for 1 hour, was placed through the guide cannula into the hippocampus. During the experiment animals were maintained under anesthesia with intramuscular booster doses of ketamine equal to one fourth the original dose. Animal body temperature was maintained at 37 °C using an electronically controlled heating pad.

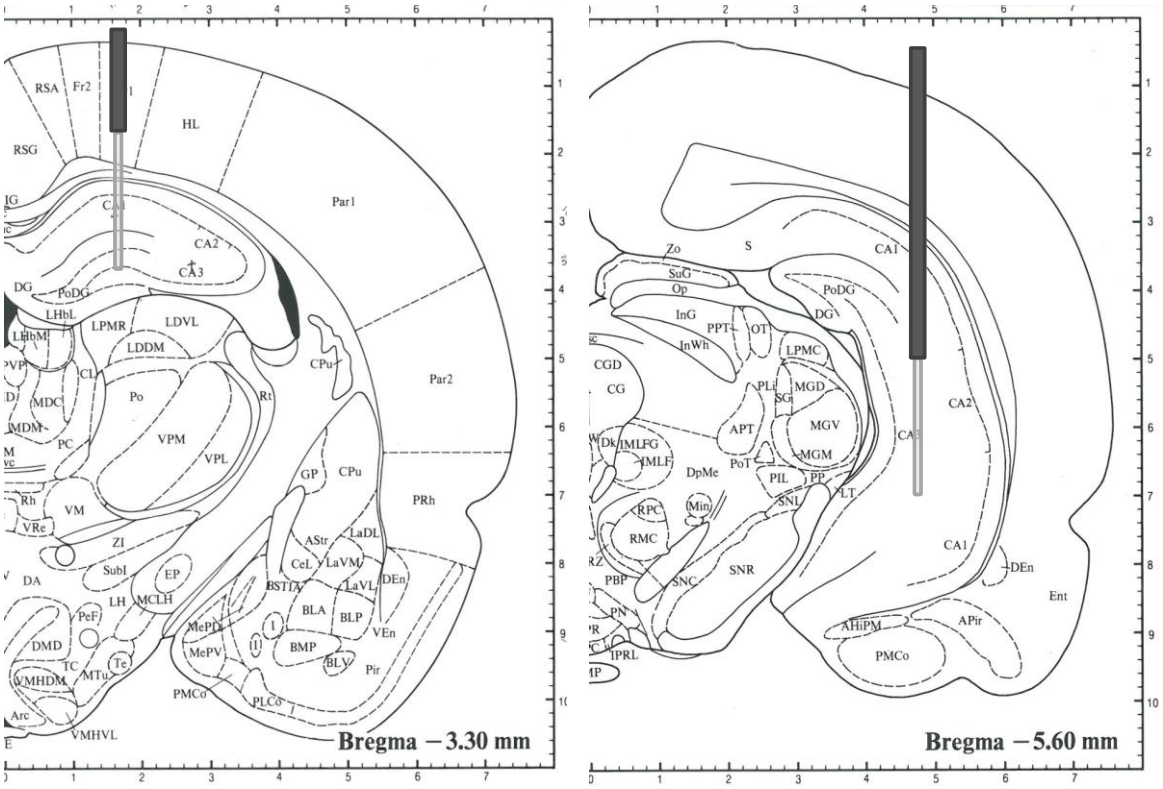

Figure 3.4: Diagram of the two brain regions of the hippocampus, the left is the CA1 and right CA3. Dark rectangle represents the guide cannula and the open rectangle represents the microdialysis probe. Image taken with permission from [15].

3.3 MDA from Local Dosing of 3-MPA

3.3.1 MDA Reaction Modification

For the reaction the same MDA:TBA:acid ratio of 8:2:1 as described in Chapter 2 was used, but because samples were split between multiple methods (including a nitrite/nitrate method) only 5 µL of sample was allocated for this method. To keep the same ratio as previous 1.875 µL of the TBA/acid mixture would have to be added to the 5 µL of sample making a total volume of 6.875 µL. However, under these reaction conditions, there was a large increase in the contaminant in the blank. This was believed to be a result of evaporation from heating such a small volume. To increase the volume without altering the reaction ratio, the TBA and sulfuric acid were mixed (40:20) and then diluted in half with water. Then, 3.75 µL of that mixture was added to the 5 µL of MDA standard or sample in a 200 µL microcentrifuge tube. This did alleviate the large peak from the impurity in the blank, but at the expense of loss in sensitivity from dilution. All other parameters as described in Chapter 2 were not changed.

3.3.2 Delivery of 3-MPA through Microdialysis Probe

Ringer's solution was perfused for 1 hour after probe implantation prior to the start of basal collection. All animal experiments used a perfusion flow rate of 1 µL/min and samples were collected over 10 minute intervals. After the collection of 1 hour of basal (6 samples), the perfusate was switched to a 3-MPA solution (10, 1, or 0.1 mM in Ringer's solution) and perfused for 50 minutes. Following the 3-MPA perfusion period the inlet was reconnected to Ringer's solution and allowed to perfuse for 4 hours. For control experiments the inlet tubing was removed and reattached from the syringe to simulate switching between Ringer's solution and 3-MPA solutions. All samples were stored at -80°C until analyzed. At the completion of the experiment the animals were

euthanized via isoflurane inhalation overdose. Rat brains were harvested and stored in neutral buffered formalin solution for histological evaluation.

3.3.3 Varying 3-MPA Concentrations between Regions

3-MPA was dosed at 3 different concentrations (10, 1 and 0.1 mM) in order to correlate the lipid peroxidation to convulsant dosed. We hypothesized that with every 10 fold increase in 3-MPA there would be a 10 fold increase in MDA. A correlation between glutamate and GABA with the concentration of 3-MPA dosed was anticipated. Previous work in our laboratory developing the local dosing model used only 10 mM 3-MPA in the CA1 region [13]. Therefore, 3-MPA was dosed in both the CA1 and CA3 regions at varying concentrations in order to better understand the local dosing model and relate the data here to previous experiments.

3.3.4 Statistical Difference in MDA between Dosing Regimens

In the CA3 region, the 10 mM 3-MPA perfusion showed significant ($p<0.001$) increases compared to control MDA 20 minutes after the start of perfusion and remained high for 3 hours after dosing had stopped (Figure 3.5). MDA steadily increased throughout the 3-MPA perfusion reaching a maximum of about 7 μM and decreased following the cessation of 3-MPA perfusion; however, never returning to control levels. The 1 and 0.1 mM 3-MPA perfusions showed similar increases in MDA both reaching maxima of 1500 nM; however, these data did not show significant differences when compared to control using the Tukey multiple comparison test [16]. The 10 mM 3-MPA dose was statistically different from both the 1 and 0.1 mM during the perfusion through 30 minutes post 3-MPA perfusion.

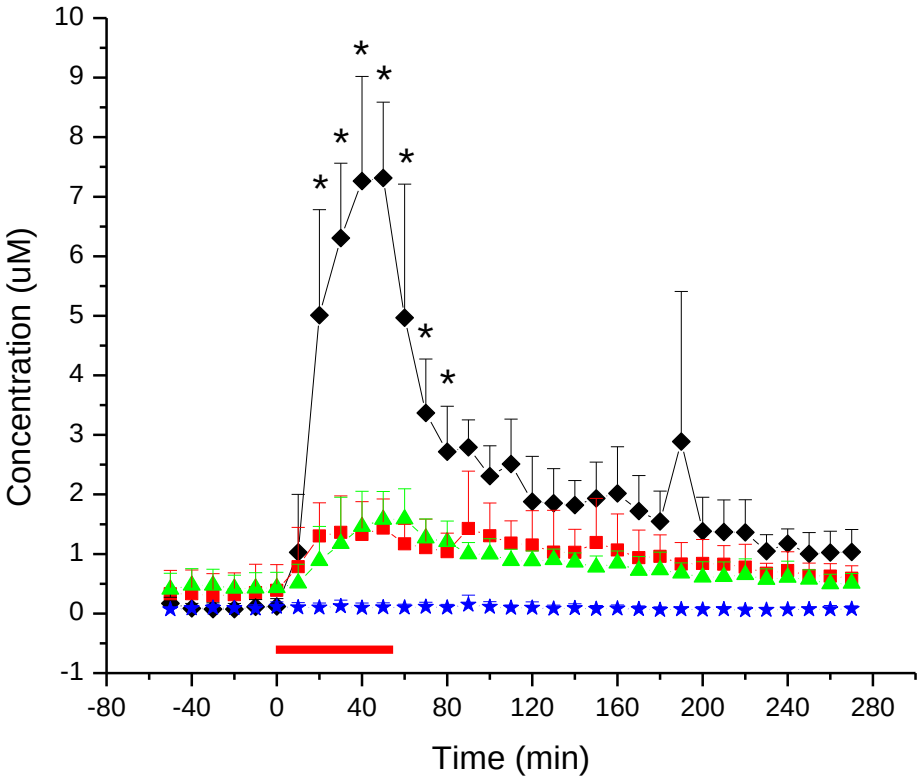

Figure 3.5: Time plots of MDA concentration recovered in microdialysate samples from hippocampus CA3 region as a function of concentration. 3-MPA perfusions experiments of 10 mM (-♦-) (n=5), 1 mM (-■-) (n=6), 0.1 mM (-▲-) (n=5), and control (-★-) (n=5). Time zero represents the start of 3-MPA perfusion for 50 minutes (indicated by bar). (* $p<0.001$ for 10 mM perfusion by one-way ANOVA $F(3,12) = 0.05$ with Tukey multiple comparison)

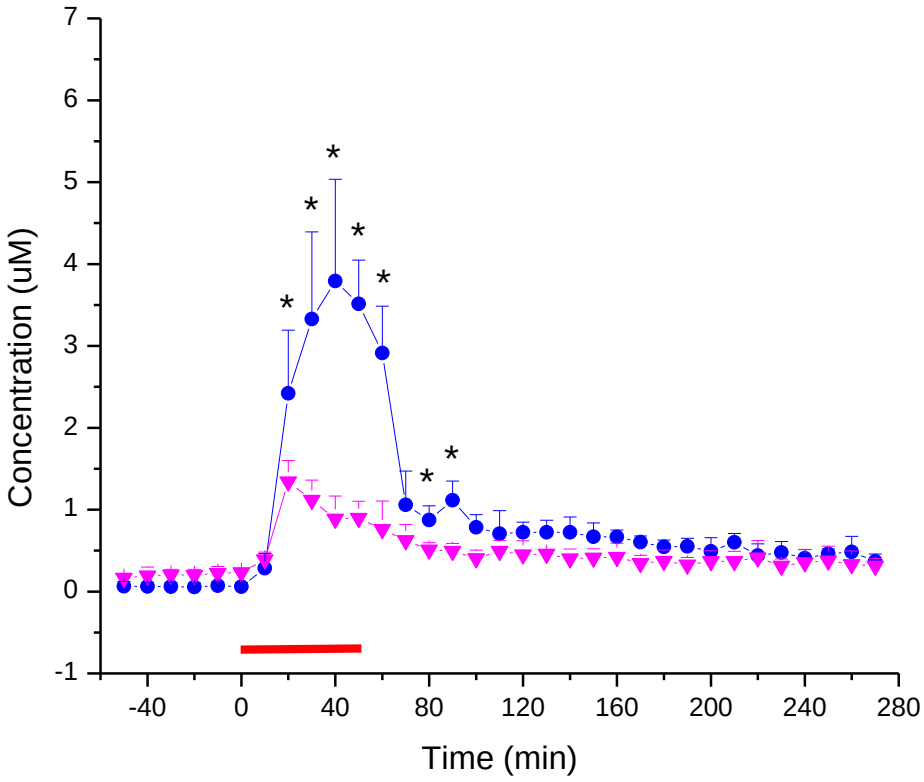

Figure 3.6: Time plots of MDA concentration recovered in microdialysate samples from hippocampus CA1 region as a function of concentration. Time zero represents the start of 3-MPA perfusion for 50 minutes (indicated by bar). 3-MPA perfusions experiments of 10mM (-●-) (n=5), and 1 mM (-▼-) (n=3). (* $p<0.001$ for 10 mM perfusion t-test)

In the CA1 region, the 10 mM 3-MPA perfusion had significant increases during and after perfusion as well as the 1 mM dose (Figure 3.6). MDA did not return to basal in either dosing regimen. Because there were no differences in the 1 mM doses between the two regions as well as between the 1 mM and 0.1 mM within the CA3 region, 3-MPA was not dosed at 0.1 mM to the CA1 region.

3.4 Glu/GABA from Local Dosing of 3-MPA

3.4.1 LC-Fluorescence Method for Glutamate and GABA

Microdialysis samples were analyzed for glutamate and GABA using NDA/CN derivatization reaction [12, 17, 18]. A 1 µL aliquot of sample was added to 2 µL of a 5 mM NaCN and 100 mM Borate (pH 9.2) mixture. To that, 1 µL of 1 mM NDA (in 50% MeOH/water) was added, vortexed and allowed to react in the dark for 30 minutes. A 3 µL injection of sample was separated using a Synergy Hydro-RP 80A 150 x 2.00 mm 4 µm C18 column (Phenomenex) with a two solvent LC gradient system (Shimadzu LC-20AD pumps) consisting of 50 mM ammonium acetate, 5% THF (Solvent A) and MeOH (Solvent B) at a flow rate of 0.350 mL/min. Initial conditions were 45% Solvent B with a linear increase to 60% from 0-7.5 minutes, then an increase to 80% from 7.5-8.5 minutes. Solvent B was held at 80% for 0.5 minutes then returned to 45% for a 2 minute re-equilibration. Derivatives were detected using fluorescence detection (Jasco FP 2020) at 490 nm with excitation at 442 nm. Example chromatograms from hippocampus microdialysis sample can be seen in Figure 3.7.

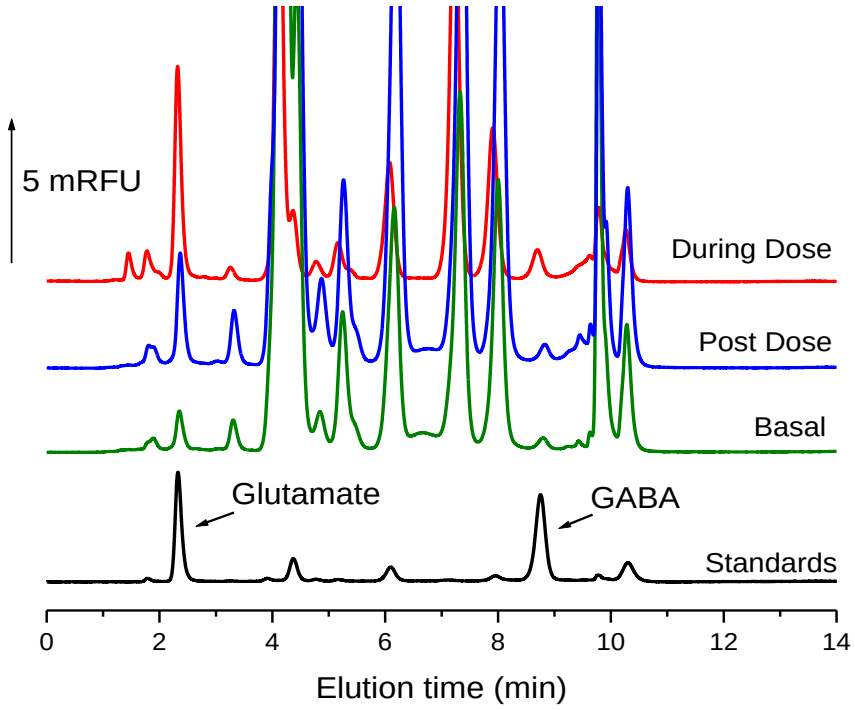

Figure 3.7: LC-fluorescent example chromatograms from NDA/CN derivatization method for amino acids glutamate and GABA (2 µM standards, basal, during 3-MPA dosing, and post 3-MPA dosing dialysate).

3.4.2 Increases in both Glutamate and GABA

Levels of glutamate and GABA were monitored for all three dosing methods in the CA3 region, but only the 10 mM dose showed any statistical changes when compared to controls. Both neurotransmitters increase upon dosing of 10 mM 3-MPA to about 500% basal and remained above basal levels for over 3 hours post dose. Although both neurotransmitters increased from 3-MPA dosing, GABA showed the more statistically significant increase ($p<0.01$) than glutamate ($p<0.05$) during the same time period (Figure 3.8). Microdialysis studies of temporal lobe epilepsy in humans showed increases in glutamate (3 min prior to seizure) and GABA (at the onset of seizure); however, GABA concentrations quickly returned to basal (<10 min post seizure) while glutamate remained elevated (>20 min) [19]. These data are from patients with complex partial epilepsy where the seizures were spontaneous. The delayed increase in GABA would indicate a protective measure against seizures as a result of the elevated glutamate, but it is intriguing that GABA levels decreased after a seizure while glutamate remained high. The results from the research here show that during and post 3-MPA perfusion, GABA remains elevated and follows glutamate very closely. Unfortunately, temporal resolution was sacrificed to allow for enough sample for multiple methods, so it could not be determined if there was a delay in GABA compared to glutamate.

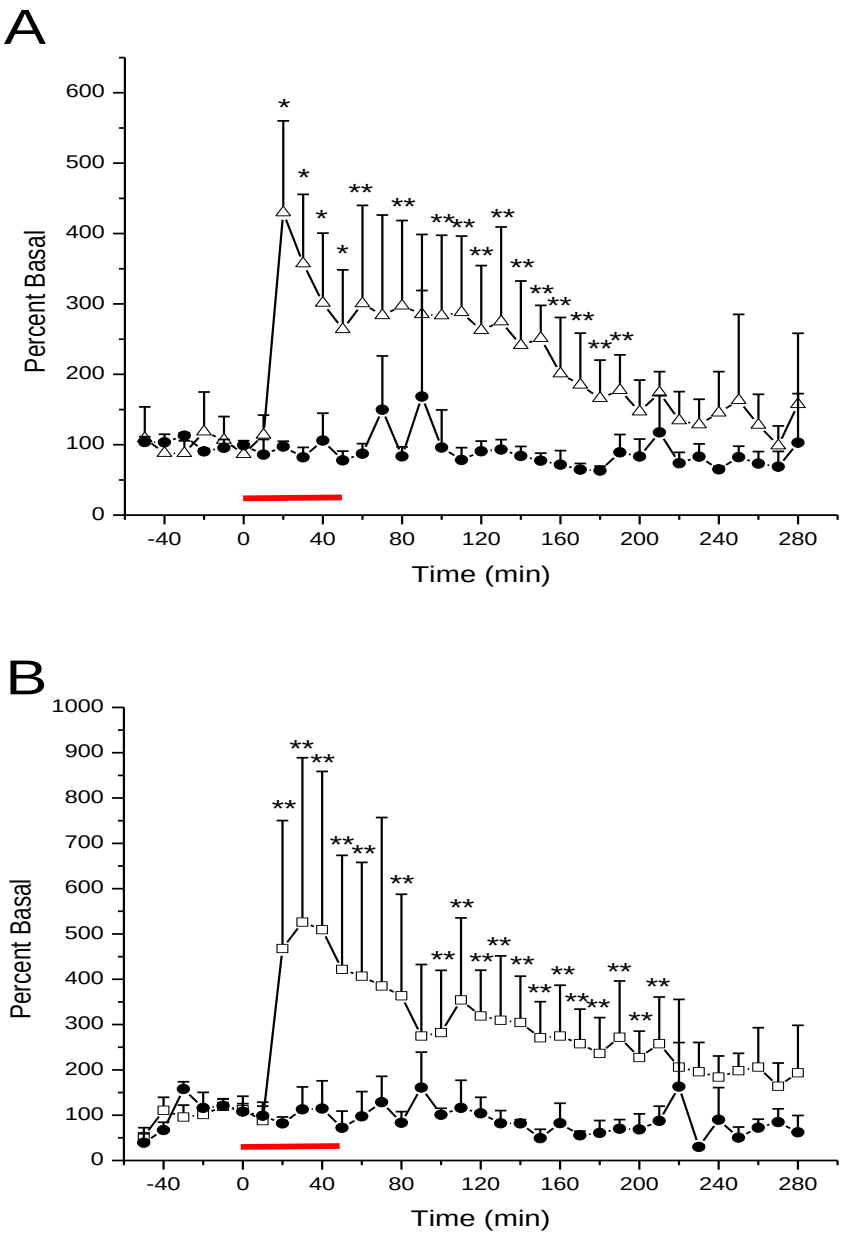

Figure 3.8: Time plots of GABA (A) and glutamate (B) recovered from microdialysate samples from hippocampus CA3 region as a function of percent basal. Time zero represents start of 10mM 3-MPA perfusion for 50 minutes (indicated by bar). (A) Plot of GABA (-Δ-) (n=5) and control (-●-) (n=3). (B) Plot of glutamate (-□-) (n=5) and control (-●-) (n=3). (* $p<0.01$ and ** $p<0.05$ based on t-test)

The increase in extracellular levels of GABA from local dosing of 10 mM 3-MPA was unexpected considering the mechanism of 3-MPA induced seizures. Previous reports have observed a decrease in GABA with *i.v.* or *i.p.* dosing of 3-MPA [20, 21]. This increase could be a result of 3-MPA acting as a competitive inhibitor of GABA transaminase [7] preventing the recycling of GABA through glial cells. This mechanism is not usually seen in animal models because the concentration of 3-MPA required for GABA transaminase inhibition would result in animal death. The *i.v.* or *i.p.* dosing produces global distribution of 3-MPA to the entire brain *via* the blood, while the local dosing through the microdialysis probe is limited by diffusion through the extracellular space. Studies indicate that the local dosing of antiepileptic drugs not only decreased seizure intensity but also limited the severe adverse side effects associated with systemic dosing, providing the possibility of better treatments for epilepsy [22-24]. It is reasonable then, that dosing 3-MPA through the probe could provide a high enough concentration around the probe for inhibition of GABA transaminase without resulting in animal death. However, with GAD inhibition by 3-MPA it has been reported that GABA was not completely depleted in synaptic terminals of hippocampal slices after prolonged 3-MPA dosing, implying a high reuptake of GABA into the neuron [25]. This would indicate that GABA transport to the glial cell is not the predominant route in the brain making it unlikely that the increase in GABA observed here is a result of GABA transaminase inhibition.

3.4.3 GAD Isoforms

It has also been suggested that 3-MPA is selective for the vesicular GAD isoform (GAD65) and does not have an effect on the cytosolic isoform of GAD (GAD67) [26, 27]. If this were the case, the synthesis of GABA responsible for inhibition (*i.e.* synaptic GABA) would still be hindered, allowing excitotoxicity through glutamate buildup, while

intracellular GABA pools would remain unchanged [27]. The observed increase in GABA could be a result of these cytosolic pools being released upon cellular apoptosis. The microdialysis probe was placed in the CA3 region of the hippocampus, which receives mossy fiber input from the dentate gyrus, comprised of a large amount of GABAergic neurons known as basket cells [11]. The increase in extracellular GABA observed could be a result of the apoptosis of these GABAergic neurons as a result of excitotoxicity.

Mathews *et al.* also observed increases in GABA when dosing glutamate, and suggested that extracellular glutamate is transported directly into the inhibitory neuron and converted to GABA for subsequent release [25]. The amount of GABA present could be directly related to the number of inhibitory neurons located around the probe. If the 3-MPA is only inhibiting the GAD65, then uptake of the excess glutamate could be converted to GABA through GAD67 and subsequently released. This could explain the larger GABA increases in the CA3 region (rich with inhibitory neurons) compared to the CA1 (lacking inhibitory neurons) while the changes in glutamate were equal in both regions. It should also be noted that the basal concentrations of GABA in the CA3 region were greater than that of the CA1 region. This would indicate that the CA3 region has a greater threshold for seizure mitigation than the CA1.

3.5 Neuromechanisms

3.5.1 MDA in the Hippocampus

The increases in MDA observed from the CA3 region did not show a linear dose dependence with 3-MPA, which is interesting considering the magnitude between each 3-MPA dose. Dosing of 3-MPA systemically has shown a decrease in NMDA receptor ligand binding in the hippocampus relative to the rest of the brain [28]. Also, with

repetitive doses of 3-MPA NMDA receptor subunits are down regulated [29]. These decreases in NMDA activity would indicate a protective effect in the hippocampus against 3-MPA induced seizures. This could indicate a minimum threshold of glutamate required for excitotoxicity. While there were no changes in glutamate or GABA for the 1 and 0.1 mM 3-MPA dosing, the 10 mM dose resulted in about a 500% increase in both neurotransmitters. Because there is no linear correlation between Glutamate/GABA and 3-MPA it is not surprising that there is not a linear correlation between MDA and 3-MPA.

There was a differential increase ($p<0.001$) in MDA between the CA3 and CA1 regions (Figure 3.9). Dosing 10 mM 3-MPA produced over twice as much MDA in the CA3 region than in the CA1 region based on the area under the curve (AUC) for their respective MDA time plots (Table 3.1). The CA3 region has been shown to have a higher density of cyclooygenase-2 than the CA1 [30, 31] indicating a greater potential for lipid breakdown through the arachidonic acid cascade, ultimately producing more MDA. Interestingly, the 1 mM dosing produced similar maximum responses in both regions (Figure 3.10). As stated above, this could be due to similar protective effects throughout the hippocampus. However, the AUC for the 1 mM dose in the CA3 region is again about twice as much as that from the CA1 region. Taken together the CA3 region may be more susceptible to lipid peroxidation and therefore at greater risk to oxidative damage.

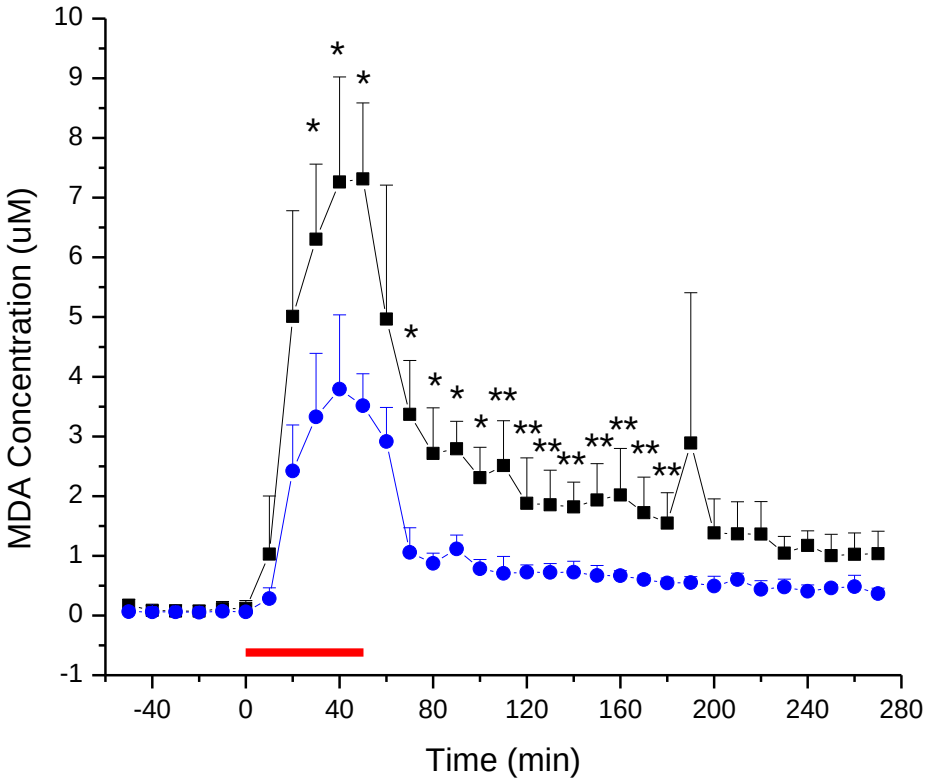

Figure 3.9: Time course of MDA recovered from 10 mM 3-MPA perfusion in the two regions of the hippocampus, CA3 (- ■ -) (n=5) and CA1 (- ● -) (n=5). Time zero represents the start of the 10 mM 3-MPA perfusion for 50 minutes (indicated by bar). (* $p<0.001$ and ** $p<0.02$ based on t-test)

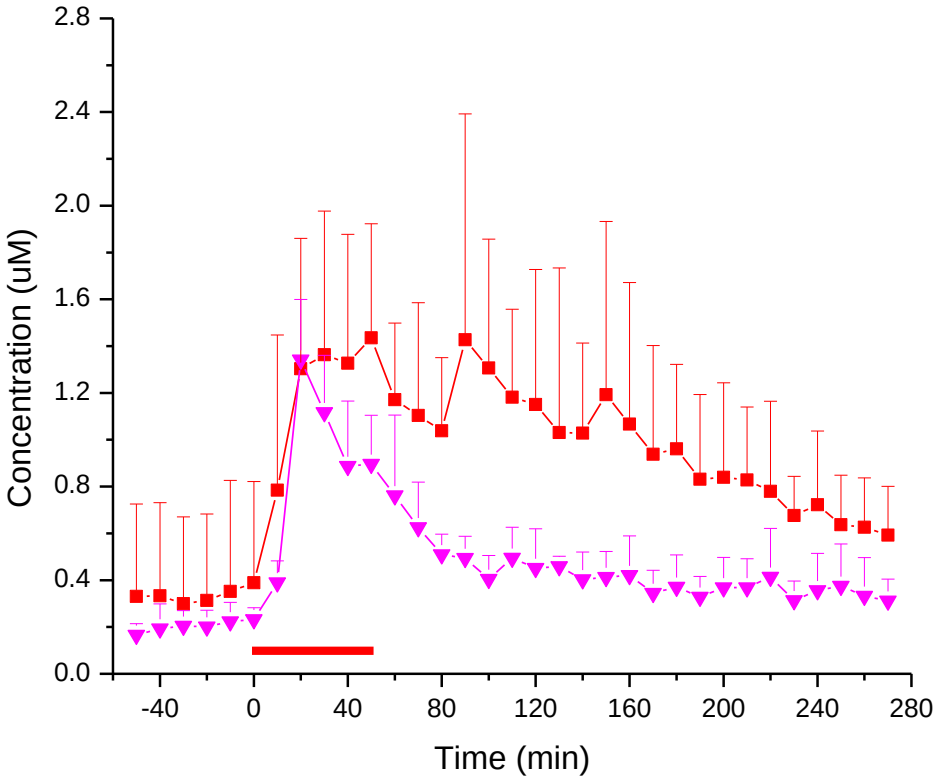

Figure 3.10: Time course of MDA recovered from 1 mM 3-MPA perfusion in the two regions of the hippocampus, CA3 (- ■ -) (n=6) and CA1 (- ▼ -) (n=4). Time zero represents the start of the 10 mM 3-MPA perfusion for 50 minutes (indicated by bar). (No statistical difference was calculated between regions for 1 mM dose)

Region	CA3		CA1	
3-MPA Dose	10 mM	1 mM	10 mM	1 mM
Maximum MDA	7 ± 1 µM	1.4 ± 0.5 µM	4 ± 1 µM	1.3 ± 0.3 µM
AUC	707,000	290,000	300,000	150,000

Table 3.1: Data from microdialysis plots for both hippocampus regions CA1 and CA3.

3.5.2 GABAergic Neuronal Projections

When L-*trans*-pyrrolidine-2,4-dicarboxylic acid (PDC), a Glu/Asp uptake blocker, was dosed through a microdialysis probe in the cortex there was an observed increase in MDA production resulting from elevated extracellular glutamate [14]. Interestingly, when PDC was administered to the thalamus by microinjection there was an observed increase in Glu, Asp, and GABA through microdialysis sampling [32]. This work was performed on genetic absence epilepsy rats and suggests that increases in GABA could result in absence of seizures by lowering membrane potentials. The same group also observed increases in both glutamate and dopamine when dosing PDC through the microdialysis probe suggesting that dopamine release can be regulated by glutamate efflux possibly influencing further neuronal excitation [33]. The local dosing of 3-MPA may result in a cyclical effect where increased glutamate produces MDA, resulting in neuronal degradation and release of GABA that drops membrane potentials furthering excitotoxicity from glutamate.

Work by Meurs *et al.* was performed where three different chemical convulsants were dosed through the microdialysis probe into the hippocampus: a muscarinic agonist, $GABA_A$ receptor antagonist, and glutamate agonist [34]. Glutamate and GABA increased during seizures in all three groups. Their findings along with the results here suggest that GABA and glutamate levels are responsive to neuronal stimulation rather than the pharmacology of the chemical convulsant [34].

3.5.3 Enzymatic Pathways Leading to MDA

Studies shown a high density of cyclooxygenase (COX)-2 around the CA3 region of the hippocampus compared to the CA1 [30, 31, 35]. COX-2, the inducible isoform of COX, is primarily responsible for inflammation and synthesizes prostaglandins

from arachidonic acid in the brain. COX-2 is upregulated during synaptic activity [31] and it has been correlated with oxidative stress [36, 37]. Inhibition of COX-1 and -2 have led to a retarding of seizure intensity in an animal kindling model [35]. When 3-MPA is dosed the increase in glutamate could cause an upregulation of COX-2 leading to excess lipid peroxidation. The large increase in MDA associated with the 10 mM 3-MPA dose could be related, in part, to the increased activity of COX-2 in the CA3 region.

Recently, Abdel-Zaher *et al.* dosed ciprofloxacin to induce seizures in mice and examined the resulting oxidative stress [38]. They observed increases in glutamate, MDA and nitric oxide (via nitrite) upon dosing of ciprofloxacin. Interestingly, when aminoguanidine was administered prior to ciprofloxacin, MDA and nitric oxide production were mitigated while glutamate remained elevated. Because aminoguanidine is a nitric oxide synthase inhibitor nitric oxide levels should drop back to control; however, the excitotoxicity from elevated glutamate could still lead to increased MDA versus control.

Abdel-Zaher *et al.* also observed enhanced production of nitric oxide and MDA with the pretreatment of L-arginine while glutamate did not change from ciprofloxacin alone [38]. L-arginine is the primary substrate for nitric oxide synthase. These findings would indicate that MDA production is more closely related to the nitric oxide pathway rather than glutamate excitotoxicity. Of course this work was done using a general seizure model in mice with whole brain homogenates indicating that individual brain sections, such as the hippocampus, could have other mechanisms leading to MDA synthesis. Nevertheless, these findings indicate MDA production in the brain is correlated to some extent with nitric oxide synthase.

3.6 Conclusion

Although the exact cellular mechanisms leading to MDA production in the brain still remain unclear, evidence indicates a differential response to 3-MPA within the hippocampus. The CA3 region produced over twice as much MDA as compared to the CA1 region with local dosing of 3-MPA. Also, a differential release of GABA between the two regions was observed, with the CA3 releasing more than the CA1. Microdialysis sampling allowed for the spatial and temporal resolution to both sample and dose within these two regions.

3.7 References

1. http://www.epilepsyfoundation.org/ (accessed 2011).
2. Kwan, P.; Brodie, M. J., Early identification of refractory epilepsy. *N. Engl. J. Med.* **2000,** *342* (5), 314-319.
3. Shin, E. J.; Jeong, J. H.; Chung, Y. H.; Kim, W. K.; Ko, K. H.; Bach, J. H.; Hong, J. S.; Yoneda, Y.; Kim, H. C., Role of oxidative stress in epileptic seizures. *Neurochem. Int.* **2011,** *59* (2), 122-137.
4. Golden, T. R.; Patel, M., Catalytic Antioxidants and Neurodegeneration. *Antioxid. Redox Signal.* **2009,** *11* (3), 555-569.
5. Waldbaum, S.; Patel, M., Mitochondria, oxidative stress, and temporal lobe epilepsy. *Epilepsy Res.* **2010,** *88* (1), 23-45.
6. Berg, A. T.; Scheffer, I. E., New concepts in classification of the epilepsies: Entering the 21st century. *Epilepsia* **2011,** *52* (6), 1058-1062.
7. Lamar, C., Mercaptopropionic Acid. A Convulsant that Inhibits Glutamate Decarboxylase. *J. Neurochem.* **1970,** *17* (2), 165-&.
8. Schneider, P. G.; Arnaiz, G. R. D., Area-dependent CNS membrane response of muscarinic receptor to convulsant 3-mercaptopropionic acid. *Mol. Chem. Neuropathol.* **1997,** *32* (1-3), 213-221.
9. Spencer, S. S., Neural networks in human epilepsy: Evidence of and implications for treatment. *Epilepsia* **2002,** *43* (3), 219-227.
10. de Lanerolle, N. C.; Lee, T. S., New facets of the neuropathology and molecular profile of human temporal lobe epilepsy. *Epilepsy Behav.* **2005,** *7* (2), 190-203.
11. Paxinos, G., *The Rat Nervous System* Third ed.; Elsevier, Inc: London, 2004.
12. Crick, E. W. In Vivo Microdialysis Coupled with Electrophysiology for the Neurochemical Analysis of Epileptic Seizures. Univeristy of Kansas, Lawrence, 2007.
13. Mayer, A. Local Dosing in a 3-Mercaptopropionic Acid Chemically-Induced Epileptic Seizure Model with Microdialysis Sampling. University of Kansas, Lawrence, 2010.
14. Yang, C. S.; Tsai, P. J.; Lin, N. N.; Kuo, J. S., Elevated extracellular glutamate concentrations increased malondialdehyde production in anesthetized rat brain cortex. *Neurosci. Lett.* **1998,** *243* (1-3), 33-36.
15. Paxinos, G.; Watson, C., *The Rat Brain in Sterotaxic Coordinates*. 2nd ed.; Harcourt Brace Jovanovich: San Diego, 1986.
16. Glass, G. H., KD, *Statistical Methods in Education and Psychology*. 3rd ed.; Allyn & Bacon: Needham Heights, MA, 1996.
17. Clarke, G.; Mahony, S.; Malone, G.; Dinan, T. G., An isocratic high performance liquid chromatography method for the determination of GABA and glutamate in discrete regions of the rodent brain. *J. Neurosci. Methods* **2007,** *160* (2), 223-230.
18. Hemmati, P.; Shilliam, C. S.; Hughes, Z. A.; Shah, A. J.; Roberts, J. C.; Atkins, A. R.; Hunter, A. J.; Heidbreder, C. A., In vivo characterization of basal amino acid levels in subregions of the rat nucleus accumbens: effect of a dopamine D-3/D-2 agonist. *Neurochem. Int.* **2001,** *39* (3), 199-208.
19. During, M. J.; Spencer, D. D., Extracellular Hippocampal Glutamate and Spontaneous Seizure in the Conscious Human Brain *Lancet* **1993,** *341* (8861), 1607-1610.
20. Crick, E. W.; Osorio, I.; Bhavaraju, N. C.; Linz, T. H.; Lunte, C. E., An investigation into the pharmacokinetics of 3-mercaptopropionic acid and

development of a steady-state chemical seizure model using in vivo microdialysis and electrophysiological monitoring. *Epilepsy Res.* **2007,** *74* (2-3), 116-125.
21. Kehr, J.; Ungerstedt, U., Fast HPLC Estimation of Gamma-Aminobutyric Acid in Microdialysis Perfusates - Effect of Nipecotic and 3-Mercaptopropionic Acids. *J. Neurochem.* **1988,** *51* (4), 1308-1310.
22. Broer, S.; Backofen-Wehrhahn, B.; Bankstahl, M.; Gey, L.; Gernert, M.; Loscher, W., Vigabatrin for focal drug delivery in epilepsy: Bilateral microinfusion into the subthalamic nucleus is more effective than intranigral or systemic administration in a rat seizure model. *Neurobiol. Dis.* **2012,** *46* (2), 362-376.
23. Hamil, N. E.; Cock, H. R.; Walker, M. C., Acute down-regulation of adenosine A1 receptor activity in status epilepticus. *Epilepsia* **2012,** *53* (1), 177-188.
24. Stein, A. G.; Eder, H. G.; Blum, D. E.; Drachev, A.; Fisher, R. S., An automated drug delivery system for focal epilepsy. *Epilepsy Res.* **2000,** *39* (2), 103-114.
25. Mathews, G. C.; Diamond, J. S., Neuronal glutamate uptake contributes to GABA synthesis and inhibitory synaptic strength. *J. Neurosci.* **2003,** *23* (6), 2040-2048.
26. Engel, D.; Palmer, I.; Schulze, K.; Frahm, C.; Jarry, H.; Ahnert-Hilger, G.; Draguhn, A., Plasticity of rat central inhibitory synapses through GABA metabolism. *J. Physiol.-London* **2001,** *535* (2), 473-482.
27. Dericioglu, N.; Garganta, C. L.; Petroff, O. A.; Mendelsohn, D.; Williamson, A., Blockade of GABA synthesis only affects neural excitability under activated conditions in rat hippocampal slices. *Neurochem. Int.* **2008,** *53* (1-2), 22-32.
28. Giraldez, L.; Girardi, E., Modification of H-3 MK801 binding to rat brain NMDA receptors after the administration of a convulsant drug and an adenosine analogue: A quantitative autoradiographic study. *Neurochem. Res.* **1998,** *23* (10), 1327-1336.
29. Auzmendi, J.; Gonzalez, N.; Girardi, E., The NMDAR subunit NR2B expression is modified in hippocampus after repetitive seizures. *Neurochem. Res.* **2009,** *34* (5), 819-826.
30. Breder, C. D.; Dewitt, D.; Kraig, R. P., Characterization of Inducible Cyclooxygenase in Rat-Brain *J. Comp. Neurol.* **1995,** *355* (2), 296-315.
31. Yamagata, K.; Andreasson, K. I.; Kaufmann, W. E.; Barnes, C. A.; Worley, P. F., Expression of a Mitogen-Inducible Cyclooxygenase in Brain Neurons - Regulation by Synaptic Activity and Glucocorticoids. *Neuron* **1993,** *11* (2), 371-386.
32. Parrot, S.; Sauvinet, V.; Riban, V.; Depaulis, A.; Renaud, B.; Denoroy, L., High temporal resolution for in vivo monitoring of neurotransmitters in awake epileptic rats using brain microdialysis and capillary electrophoresis with laser-induced fluorescence detection. *J. Neurosci. Methods* **2004,** *140* (1-2), 29-38.
33. Bert, L.; Parrot, S.; Robert, F.; Desvignes, C.; Denoroy, L.; Suaud-Chagny, M. F.; Renaud, B., In vivo temporal sequence of rat striatal glutamate, aspartate and dopamine efflux during apomorphine, nomifensine, NMDA and PDC in situ administration. *Neuropharmacology* **2002,** *43* (5), 825-835.
34. Meurs, A.; Clinckers, R.; Ebinger, G.; Michotte, Y.; Smolders, I., Seizure activity and changes in hippocampal extracellular glutamate, GABA, dopamine and serotonin. *Epilepsy Res.* **2008,** *78* (1), 50-59.
35. Tanaka, S.; Nakamura, T.; Sumitani, K.; Takahashi, F.; Konishi, R.; Itano, T.; Miyamoto, O., Stage- and region-specific cyclooxygenase expression and effects of a selective COX-1 inhibitor in the mouse amygdala kindling model. *Neurosci. Res.* **2009,** *65* (1), 79-87.
36. Madrigal, J. L. M.; Moro, M. A.; Lizasoain, I.; Lorenzo, P.; Fernandez, A. P.; Rodrigo, J.; Bosca, L.; Leza, J. C., Induction of cyclooxygenase-2 accounts for

restraint stress-induced oxidative status in rat brain. *Neuropsychopharmacology* **2003,** *28* (9), 1579-1588.

37. Rao, R. S.; Medhi, B.; Khanduja, K. L.; Pandhi, P., Correlation of seizures and biochemical parameters of oxidative stress in experimentally induced inflammatory rat models. *Fundam. Clin. Pharmacol.* **2010,** *24* (3), 325-331.
38. Abdel-Zaher, A. O.; Afify, A. H. M.; Kamel, S. M.; Farghaly, H. M.; El-Osely, G. M.; El-Awaad, E. A. M., Involvement of glutamate, oxidative stress and inducible nitric oxide synthase in the convulsant activity of ciprofloxacin in mice. *Eur J Pharmacol* **2012,** *685* (1-3), 30-37.

Chapter 4

LC/MS Method Development for Eicosanoids

Introduction

Enzymes involved in the inflammatory response facilitate the lipid oxidation process. Cyclooxygenase (COX), in particular, is involved in the metabolism of arachidonic acid (AA) synthesizing a class of eicosanoids known as prostaglandins. COX is a heme containing enzyme with two catalytic sites; the first adding two oxygen molecules to AA to form the hydroxyendoperoxide prostaglandin G_2, and the second site which reduces PGG_2 to prostaglandin H_2, a precursor for several prostaglandins (Figure 4.1) [1]. Studies of pro-inflammation have shown increases in 6-keto-prostaglandin $F_{1\alpha}$ [2, 3], prostaglandin E_2, D_2, and 8-iso prostaglandin $F_{2\alpha}$ [4], and thromboxane B_2 [2]. Research has shown that PGE plays a role in neurotransmission and plasticity via PGE receptors (EP) in the hippocampus [5, 6]. These EP receptors activate adenyl cyclase (increasing cAMP) or release intracellular Ca^{2+} [6] leading to glutamate release and further synaptic activity. In this instance PGE synthesis and EP receptor activity acts as a positive feedback loop for COX-2 expression [5], which can be greatly exacerbated during a seizure event. Also, the free radical isoprostane 8-iso$PGF_{2\alpha}$ has become a marker for the non-enzymatic oxidation of arachidonic acid [7-9]. Figure 4.1 shows the metabolites of interest in the arachidonic acid cascade. The main mechanism of lipid peroxidation proposed here involves COX, therefore the lipooxygenase product leukotriene B_4 (LTB) was used as a general marker of stress.

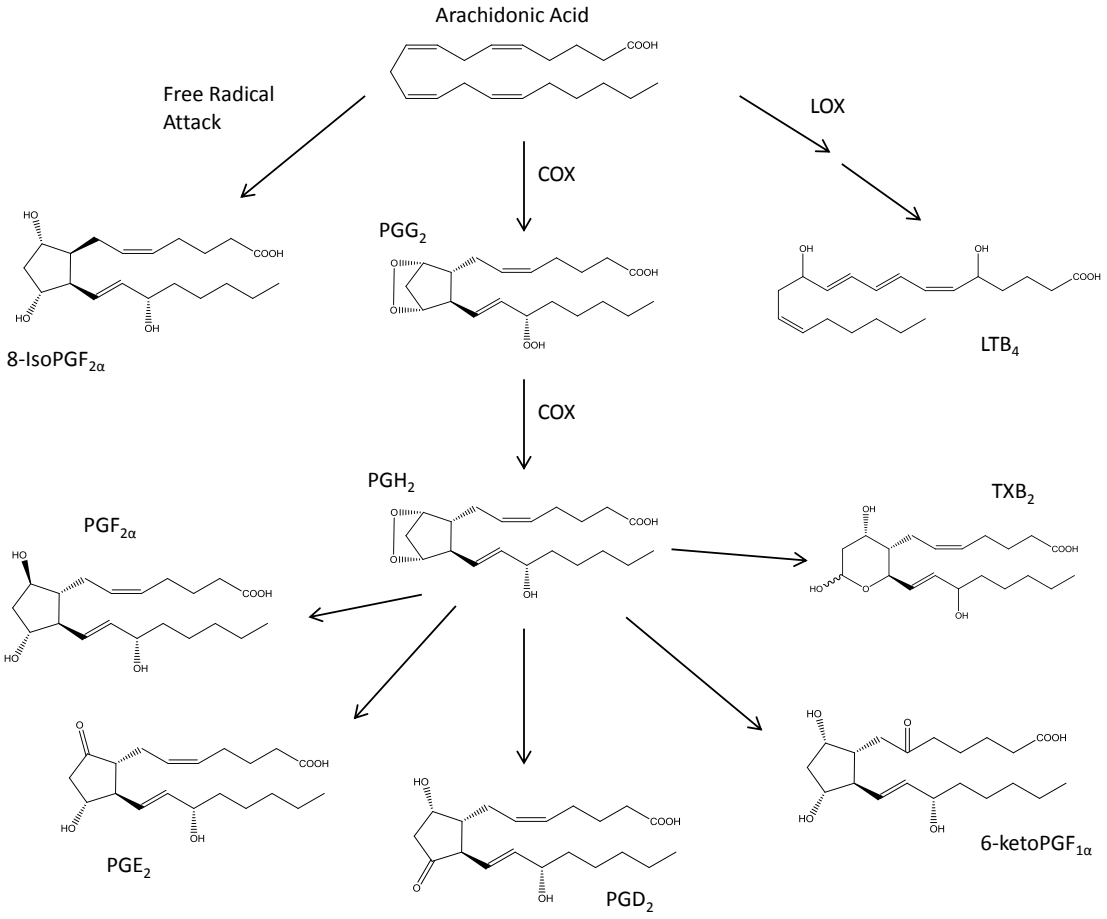

Figure 4.1: Eicosanoids of interest involved in the arachidonic acid cascade. Adapted from (Sang, N 2006).

Methods used to evaluate eicosanoids typically involve immunoassays [3, 4, 7, 10], fluorescent labeling [11] or LC-MS [12, 13]. Immunoassays, however, can only facilitate the detection of one analyte at a time, and for the purpose of this study too much dialysate would be required to monitor every compound of interest. Previous microdialysis methods used for prostaglandins have involved high flow rates (~5 µL/min) and long collection intervals (>20 minutes) [8, 13].

Eicosanoids are difficult to detect using spectrometric methods because they do not have the structural characteristics to allow for UV/Vis absorbance or fluorescence detection. Derivatizing agents such as 1-pyrenyldiazomethane (PDAM) [11] and 9-anthryldiazomethane (ADAM) were attempted but because of the bulkiness of the fluorophore, a separation of prostaglandin isomers was not attainable. The use of a mass spectrometer, which does not require derivatization, is a more appropriate technique from this application. Here, an LC separation coupled with mass spectrometry detection was developed for the detection of 7 eicosanoids; 6-ketoprostaglandin $F_{1\alpha}$ (6-keto), thromboxane B_2 (TXB), 8-isoprostaglandin $F_{2\alpha}$ (8-iso), leukotriene B_4 (LTB) and prostaglandins F_2, E_2, and D_2 (PGF, PGE, and PGD respectively).

4.1 Mass Spectrometry

Mass spectrometry (MS) is a secondary separation technique for gaseous phase ions. Analytes are ionized by an ionization source then separated based on their mass to charge ratio (*m/z*) in a mass analyzer and detected. Ionization sources are appropriate for analytes based on chemical characteristics (*e.g.* volatility, functional groups, *etc*.). Mass analyzers use electrostatic forces to separate ions with an exact *m/z* so they can be individually detected. The resolution at which mass analyzers detect ions is based on the following equation:

$$R = \frac{M}{\Delta M} \qquad (1)$$

There are two ways to calculate resolution [14]. The first involves the resolution between two peaks where the valley between the two ions is 10% of either one. In this case, ΔM is the difference between the two masses and M is the mass of the larger peak [15]. The second is calculated for a single peak by its full width at half maximum height (FWHM). Here M is the mass number of the peak and ΔM is the width of the peak [14].

4.1.1 Ionization

To incorporate MS with LC separations, ionization techniques such as electrospray ionization (ESI) were developed which facilitate the volatilization of ions from the aqueous solutions [16, 17]. ESI is a soft ionization technique where solvent continually flows through a nebulizing tip with a positive voltage applied across it adding excess protons to the solution droplets (if a negative voltage is applied, the solution becomes void of protons) [18]. The excess protons will protonate molecules with basic functional groups, while a negative voltage will deprotonate acidic functional groups. The solvent droplets are evaporated using gas (*e.g.* nitrogen) before entering the mass analyzer. There are two schools of thought as to exactly how ions enter the gas phase; the charge residue model (CRM) and the ion desorption model (IDM) [14]. In the CRM model, as the droplets shrink the charge density on the surface reaches the Rayleigh instability limit and the Coulombic repulsive forces exceed the surface tension causing an explosion creating gas phase ions [18]. According to the IDM, as droplets shrink the surface charge becomes great enough to overcome the cohesive forces within the droplet causing an ion to be ejected [19]. Figure 4.2 diagrams the processes involved in ESI.

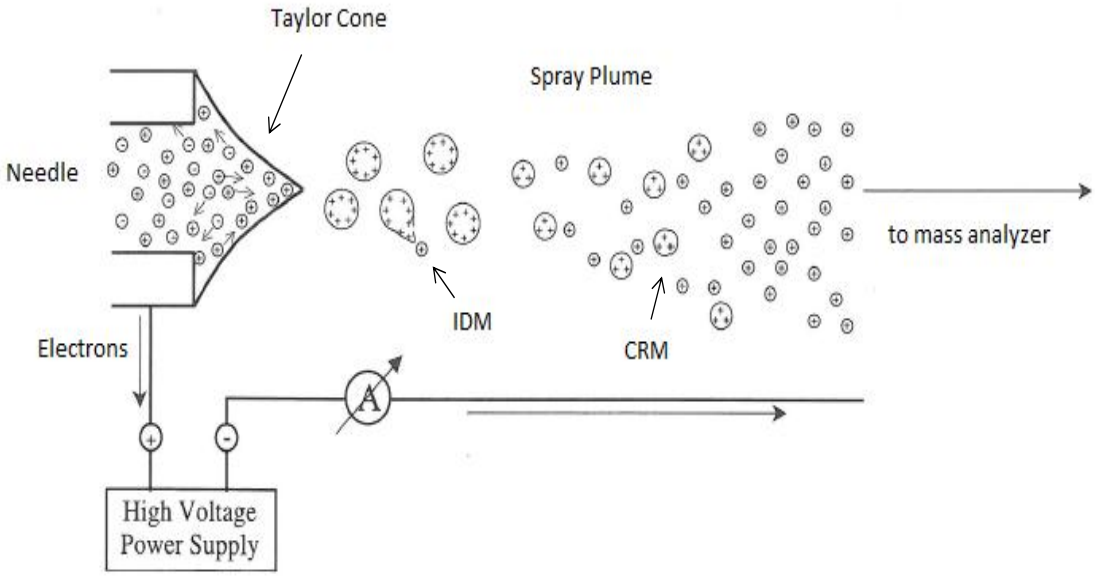

Figure 4.2: Electrospray ionization in positive ion mode with Taylor Cone formation at the needle tip. Examples of both charge residue model (CRM) and ion desorption model (IDM) of gaseous ions is shown. Taken with permission from [20] (pg 2)

4.1.2 Mass Analyzers

Mass analyzers use electric and magnetic fields to manipulate gaseous ions from the inlet to the detector. Analyzers are under high vacuum (about 10^{-5} torr) in order to prevent inadvertent collisions from other species. Analyzers can scan through a range of *m/z* (allowing one *m/z* at a time to be detected) producing a mass spectrum or can be selective to allow only one ion to be detected. Common mass analyzers include time-of-flight (TOF), quadrapole, ion trap, and ion cyclotron resonance.

A 3D ion trap is in a donut shape and consists of three electrodes; one ring and two endcaps while a linear ion trap (used here) is cylindrical "box" made up of four quadrapoles [21]. For analysis the ion trap is first filled with ions, and then it uses isolation waveforms to eject the ions sequentially for MS1 analysis (Figure 4.3). An ion trap can also use the isolation waveforms to eject all ions except the *m/z* of interest. The trap can then induce fragmentation of the isolated ion (usually with an inert gas), followed by an MS2 analysis ejecting all product ions for detection. Unlike other mass analyzers, the ion trap has the ability to perform repeated MS experiments (isolate, fragment, isolate, fragment, *etc.*) so long as there are ions remaining in the trap. MS experiments where specific parent/product ion pairs (transitions) are detected can be used to greatly increase selectivity and sensitivity for an analyte [22]. These types of experiments are known as single reaction monitoring (SRM), or multiple reaction monitoring (MRM) in the case of several product ions, and will be used here for the detection of arachidonic acid metabolites.

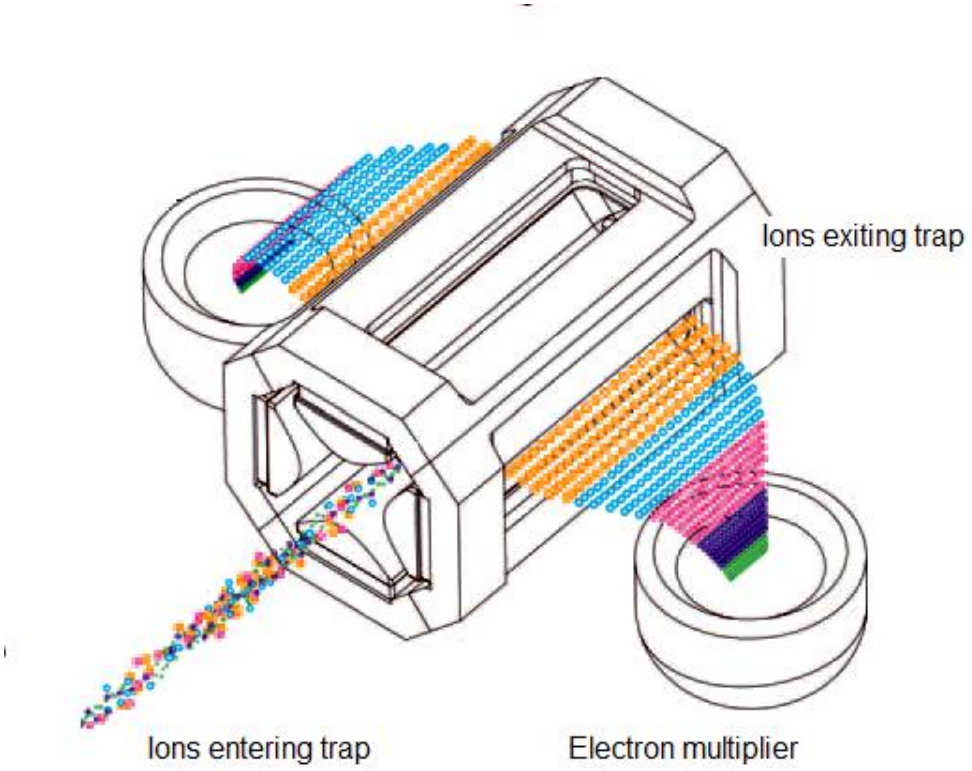

Figure 4.3: Illustration of the linear ion trap with dual detector systems used in this method (Thermo Scientific website product support bulletin [23])

4.2 Methods

4.2.1 Chemicals

All of the PGs were purchased from Cayman Chemicals (Ann Arbor, MI) are easily dissolved in organic solvent (methanol, ethanol, DMSO, *etc.*) and can be diluted with water at lower concentrations. Stock solutions of either 100 or 50 µM were made for each analyte in methanol. Any dilutions made were no greater than 1:20. Large dilution factors led to the more hydrophobic species (*i.e.* LTB) falling out of solution. HPLC grade acetonitrile (ACN), methanol, and the salts for Ringer's solution were purchased from Fisher (Fair Lawn, NJ). Ringer's solution composition was: 147 mM NaCl, 3 mM KCl, 1 mM $MgCl_2$, and 1.2 mM $CaCl_2$. Acetic acid (>99.99%) and 3-mercaptopropionic acid (3-MPA) was purchased from Sigma-Aldrich (St. Louis, MO). All solutions were made using nanopure water obtained from a Millipore Advantage A10 purification system (Billerica, MA).

4.2.2 LC Conditions

A two solvent gradient system consisting of Shimadzu LC20 ADxr pumps and CBM-20A system controller were used for prostaglandin separation. Solvent A was of 0.05% acetic acid and solvent B 0.05% acetic acid in ACN. The initial conditions were 30% solvent B with a flow rate of 0.200 mL/min with the column oven (Shimadzu CTO-10A) set at 30 °C. A two-step linear gradient was employed: 0 to 6.5 minutes solvent B increased from 30 to 54%, then from 6.5 to 9 minutes solvent B increased from 54 to 80%. Solvent B was held at 80% for 30 seconds and for re-equilibration dropped back down to 30% from 9.5 to 9.8 minutes and held from 9.8 to 12 minutes. A Phenomenex Kinetex XB-C18 column with dimensions of 100 x 2.1 mm ID, and 1.7 µm particle size was used. Prior to injections, a 10 µL syringe was rinsed with 80% ACN followed by

25% ACN (rinsing with only 25% ACN lead to sample carry over). After rinsing, 5 µL of sample/standard were injected into a Rheodyne 7725i manual injector fitted with a 10 µL sample loop. All lines and fittings pre-column were stainless steel and post-column were 0.25 x 0.005 inch (OD x ID) PEEK tubing.

4.2.3 MS Conditions

MS analysis was performed on a Thermo LTQ-XL linear iontrap mass spectrometer. Each analyte was individually tuned using high flow rate flow-injection analysis with Thermo LTQ Tune software. A 500 µL Hamilton syringe was filled with an individual standard (~20 µM) and placed into a syringe pump set at 5 µL/min. The syringe was split into the LC line using a T-junction for a total flow of 0.200 mL/min. The mobile phase composition was equivalent to that during the expected elution time for the given analyte. For each MS segment, the Sheath Gas was set at 25, Auxiliary Gas set at 2, Ion Spray Voltage set at -3.5 kV and Capillary Temperature set at 275 °C.

LC-MS method development and analysis was performed using Xcalibur software. During runs, the diverter valve was set to the waste position for the first and last 2 minutes. Seven MS segments were used for the method. Segments 1 and 7 were the waste segments (2 min each) and set for MS1 with a scan range of 295-390 *m/z*. Segment 2 (1.61 min) had 2 scan events: 1) SRM 369 to 315 *m/z* for 6-keto and 2) SIM 105 *m/z* for 3-MPA. Segment 3 (0.75 min) had 2 scan events: 1) MRM 353 to 273, 299, and 309 *m/z* for 8-isoPGF and 2) MRM 369 to 169 and 195 *m/z* for TXB. Segment 4 (0.45 min) had 1 scan, MRM 353 to 273, 299, and 309 *m/z* for PGF. Segment 5 (1.51 min) had 1 scan: MRM 351 to 233, 315, and 333 *m/z* for PGE and PGD. Segment 6 (3.66 min) had 1 scan: MRM 335 to 195 and 317 *m/z* for LTB. Table 4.1 is a summary of the MS settings for each segment and subsequent transitions.

Segment	Time (min)	Parent ion (m/z)	Isolation width (m/z)	CID	Product ions (m/z)
2	1.61	369	4.0	40	315
-	-	105	-	-	-
3	0.75	353	3.0	30	273, 299, 309
-	-	369	5.0	40	169,195
4	0.45	353	3.0	30	273, 299, 309
5	1.51	351	4.0	40	233, 315, 333
6	3.66	335	3.5	30	195, 317

Table 4.1: MS/MS settings for scans from individual segments

4.2.4 Microdialysis Application

4.2.4.1 *In Vitro*

In vitro experiments were performed to evaluate these eicosanoids for microdialysis sampling for the eventual application to the 3-MPA seizure model from Chapter 3. A CMA 12 2 mm probe with MW cutoff of 20 kDa with a perfusate flow rate of 1 µl/min was used.

The *in vitro* experiment involved moving the microdialysis probe between solutions of Ringer's and eicosanoid standards (sample switching); this is a strict recovery experiment. The "sample" vials were heated to ~37 °C and lightly stirred. The microdialysis probe was initially placed in the Ringer's solution sample for 1 hour then moved to a solution of 50 nM eicosanoids for 1 hour followed by a solution of 100 nM and then back to the Ringer's solution. The process was repeated, however, in reverse order (100 nM, 50 nM, and then Ringer's).

4.3.4.2 *In Vivo* Animal Model

The same animal procedure as described in Chapter 3 was used here. Briefly, rats were anesthetized using a subcutaneous cocktail (ketamine (67.5 mg/kg), xylazine (3.4mg/kg), acepromazine (0.67 mg/kg)). A lateral incision was made exposing the skull, and a CMA 12 microdialysis guide cannula (CMA, N. Chelmsford, MA) was slowly implanted into the rat's hippocampus CA3 region at stereotaxic coordinates -5.6 A/P, +4.8 L/M, and -5.0 D/V according to The Rat Brain in Stereotaxic Coordinates 2nd Ed (Paxinos and Watson). A CMA 12 2 mm microdialysis probe (CMA, N. Chelmsford, MA), which had been flushed with Ringer's solution for 1 hour, was placed through the guide cannula into the hippocampus.

All animal experiments were performed using male Wistar rats (Charles River) that had been housed under a 12 hour day/night cycle and given free access to food and water. All experiments were performed in the morning to account for diurnal fluctuations. All animal experiments were performed in accordance with the local Institutional Animal Care and Use Committee and follows the principles stated in the Guide for the Care and Use of Laboratory Animals (National Academy of Sciences, 1996). All chemical solutions used for microdialysis experiments were diluted in Ringer's solution.

4.3 Separation

4.3.1 Column Selection

Reverse phase separation using a C18 stationary phase is the most appropriate conditions for the separation of eicosanoids. The make-up of the bonded phase had a dramatic effect on the efficiency of 6-keto. The type of silica used and the end-capping would dictate the broadness of the 6-keto peak at a much larger degree than the other compounds. This was interesting because 6-keto was the first peak to elute, and usually in LC broadening is more pronounced with later eluting compounds. The Luna C18 (2) column from Phenomenex gave the best peak shape and efficiency, most likely because it has the smoothest silica surface compared to other columns. However, with the Luna column, run times were over 30 minutes and there was large amount a noise, possibly from column bleed. A new technology, the Kinetex column from Phenomenex, using solid core particles (limiting multiple paths) was implementing to help decrease the run times. The Kinetex column not only decreased the run time to less than 10 minutes, but it also had less noise and maintained the peak integrity of 6-keto.

4.3.2 Mobile Phase

Reports using LC-MS to detect eicosanoids have used negative ion mode with either formic or acetic acid [12, 13]. The production of negative ions under acidic conditions is not ideal; therefore, both acidic and basic mobile phases were evaluated along with varying organic solvents. Aqueous solutions (Solvent A) attempted consisted of 0.05 % acetic acid, 0.1 % formic acid, or 10 mM ammonium acetate, with organic solvent (Solvent B) of either acetonitrile or methanol. The use of formic acid leads to diminished signal with negative ion mode [13] and therefore was not used. The two optimal mobile phases for acidic and basic conditions were 0.05% acetic acid/ACN and 10 mM ammomium acetate/MeOH respectively. Using the acetic acid mobile phase TXB and 8-IsoPGF were unable to be resolved chromatographically. While using the ammonium acetate mobile phase all analytes were resolved chromatographically; however, the signal from 6-KetoPGF was diminished. Because TXB and 8-iso have different *m/z*'s (369 and 353 respectively) the acetic acid/ACN mobile phase was chosen because of the better detection of 6-keto.

4.3.3 Gradient Profile

Since the range of hydrophobicity between the eicosanoids would lead to excessively long retention times using an isocratic system, a gradient profile was employed. A single linear gradient (30-55% for 0-15 min) produced sufficient resolution for all analytes. To reduce run times but not lose resolution, a 2 point linear gradient was used, which only decreased the retention time of LTB making the entire analysis less than 15 min (including re-equilibration).

4.4 Tandem MS

4.4.1 Full-Scan MS1

For initial identification and method development the mass spectrometer was set at scan mode covering the range of the PGs and possible adducts (*m/z* 300-400). This mode was also used when adjusting the gradient or varying mobile phases to identify peaks.

4.4.2 MRM Development

Once peaks were identified from the MS1 analysis (including the co-eluting TXB and 8-IsoPGF) the MS was set for collision induced dissociation (CID) on isolated parent ions. Arbitrary CID units of 22 were initially used for all parent ions as this was adequate to product fragmentation with flow injection analysis. The product ions were scanned and individual ion chromatograms that had the best S/N were selected for MRM. The selected ion transitions can be seen in Table 4.1. Figures 4.4 – 4.10 are CID product spectra for each eicosanoid.

4.4.3 S/N Optimization

Several parameters of the ion trap were adjusted to optimize S/N including; max injection time, collision induced dissociation (CID) intensity, and ion isolation width. For testing of the optimization parameters, a 50 nM standard mix was made by diluting stock solutions of each eicosanoid in Ringer's solution. It was assumed that each setting was independent from one another and therefore each was optimized separately on different days. Max injection time was found to be optimum around 400 milliseconds. Shorter injection times lead to increased noise and higher detection limits (trace smoothing with boxcar averaging did not provide better signal to noise than longer injection time). The optimum collision energy for each compound was found to be between 30 and 40 units. Finally, an isolation width of about 3.0 Da afforded the best S/N.

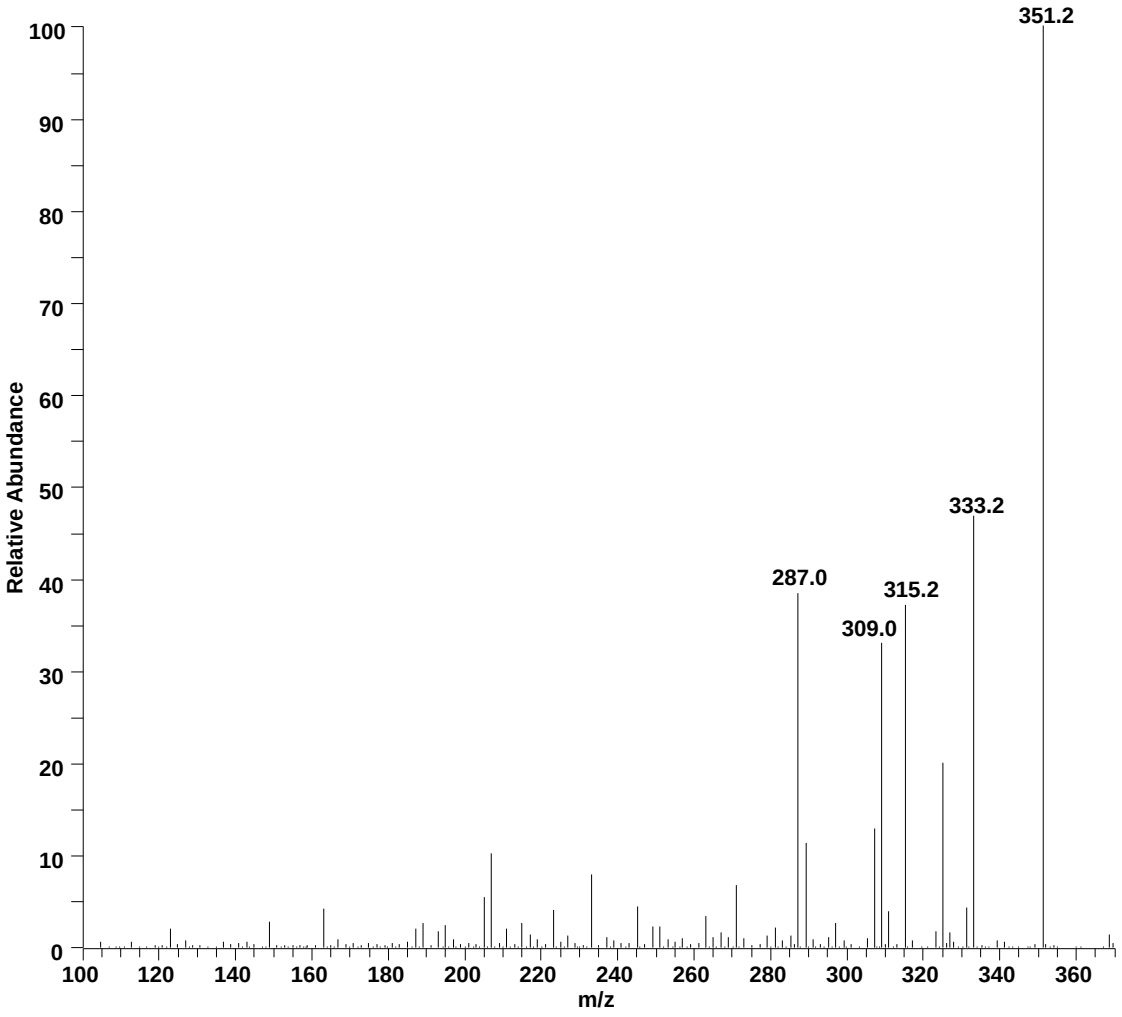

Figure 4.4: CID spectrum for 6-ketoPGF, precursor ion 369 *m/z*

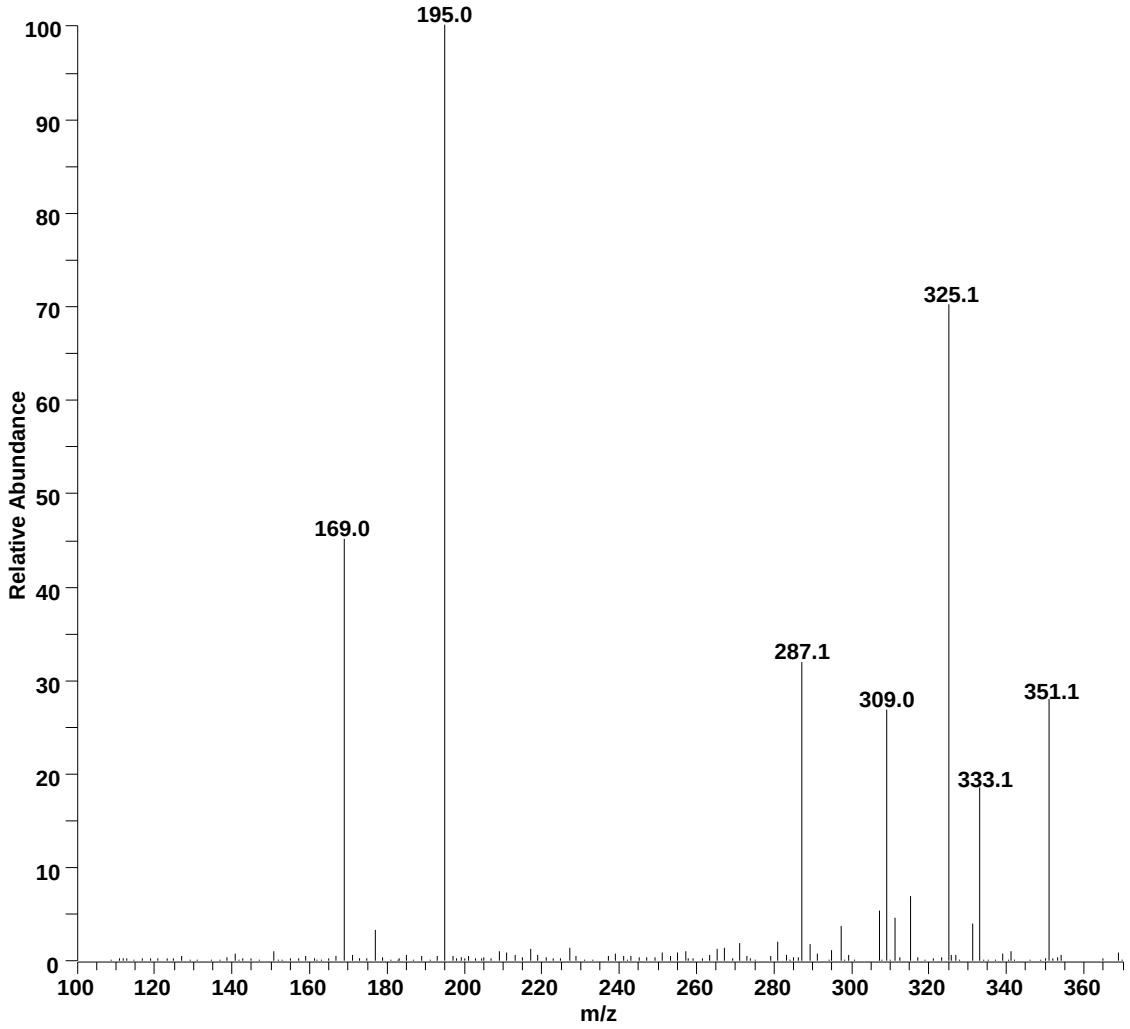

Figure 4.5: CID spectrum for TXB, precursor ion 369 *m/z*

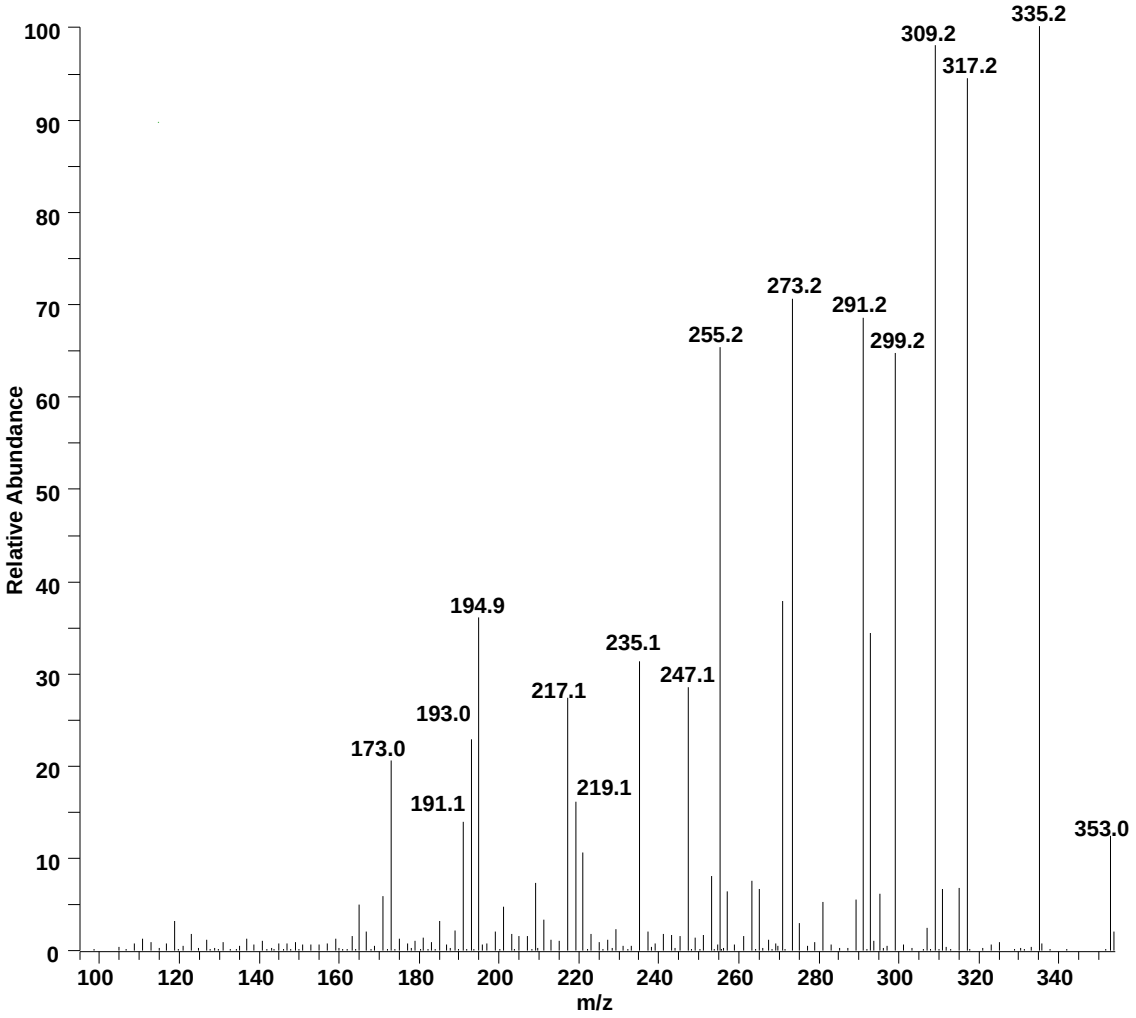

Figure 4.6: CID spectrum for 8-isoPGF, precursor ion 353 *m/z*

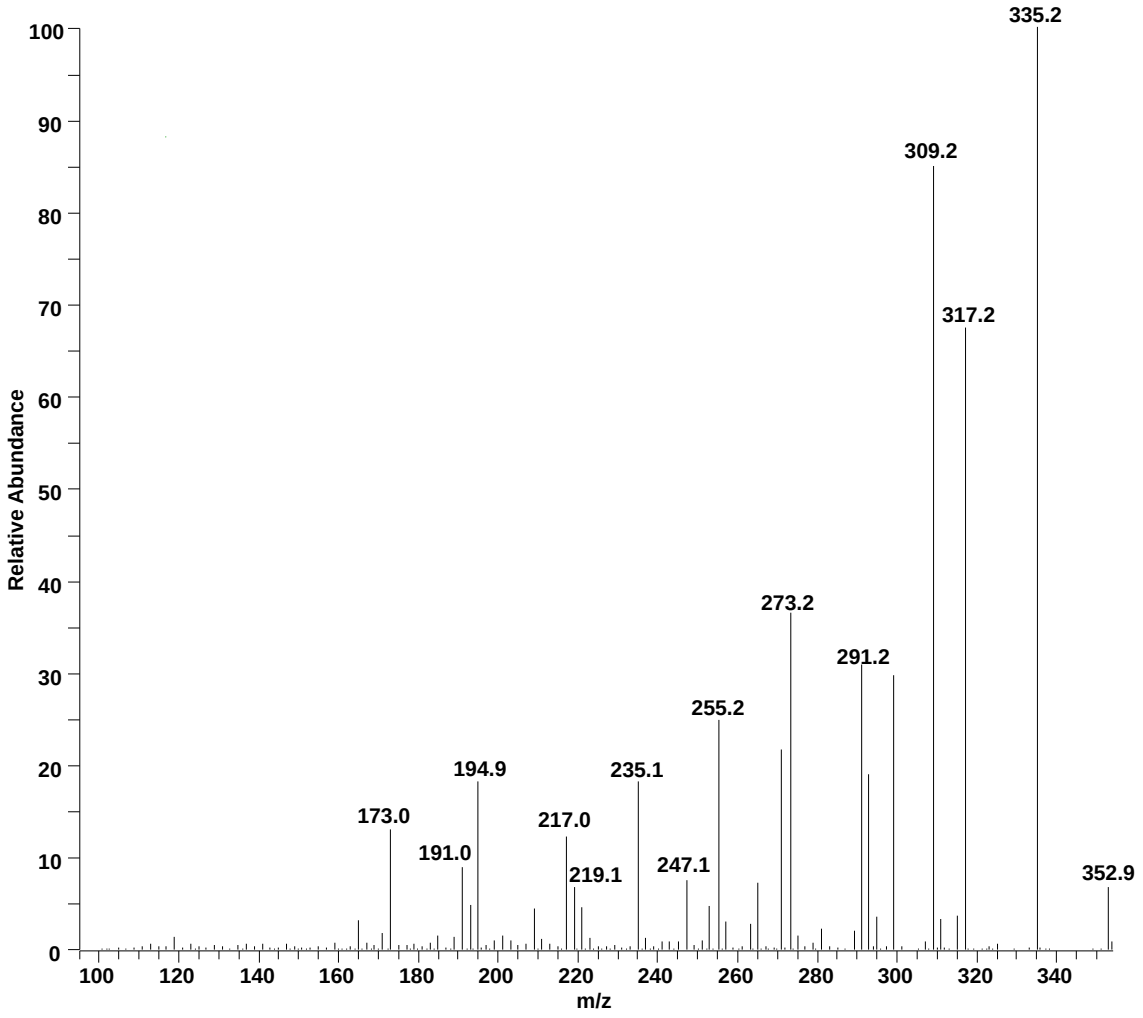

Figure 4.7: CID spectrum for PGF, precursor ion 353 *m/z*

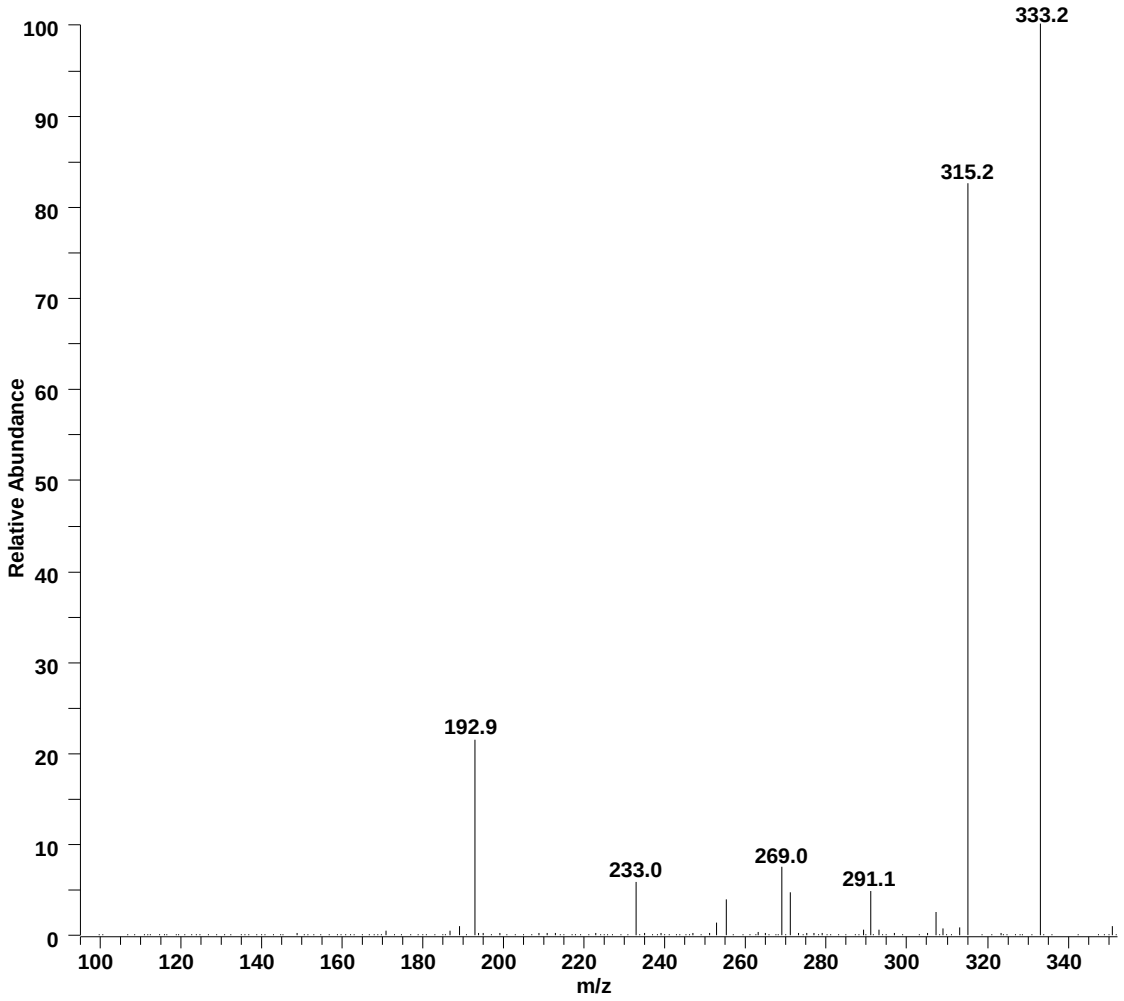

Figure 4.8: CID spectrum for PGE, precursor ion 351 *m/z*

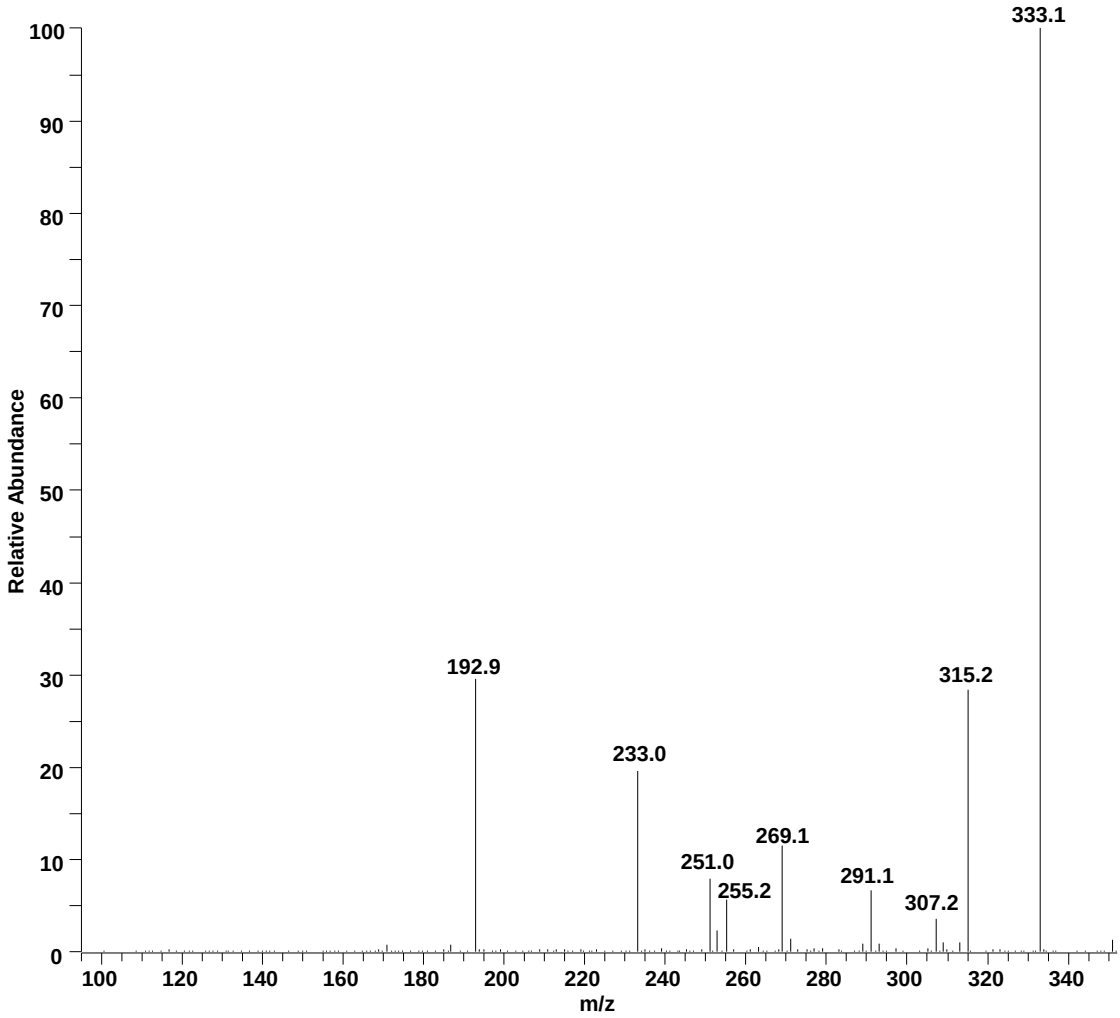

Figure 4.9: CID spectrum for PGD, precursor ion 351 *m/z*

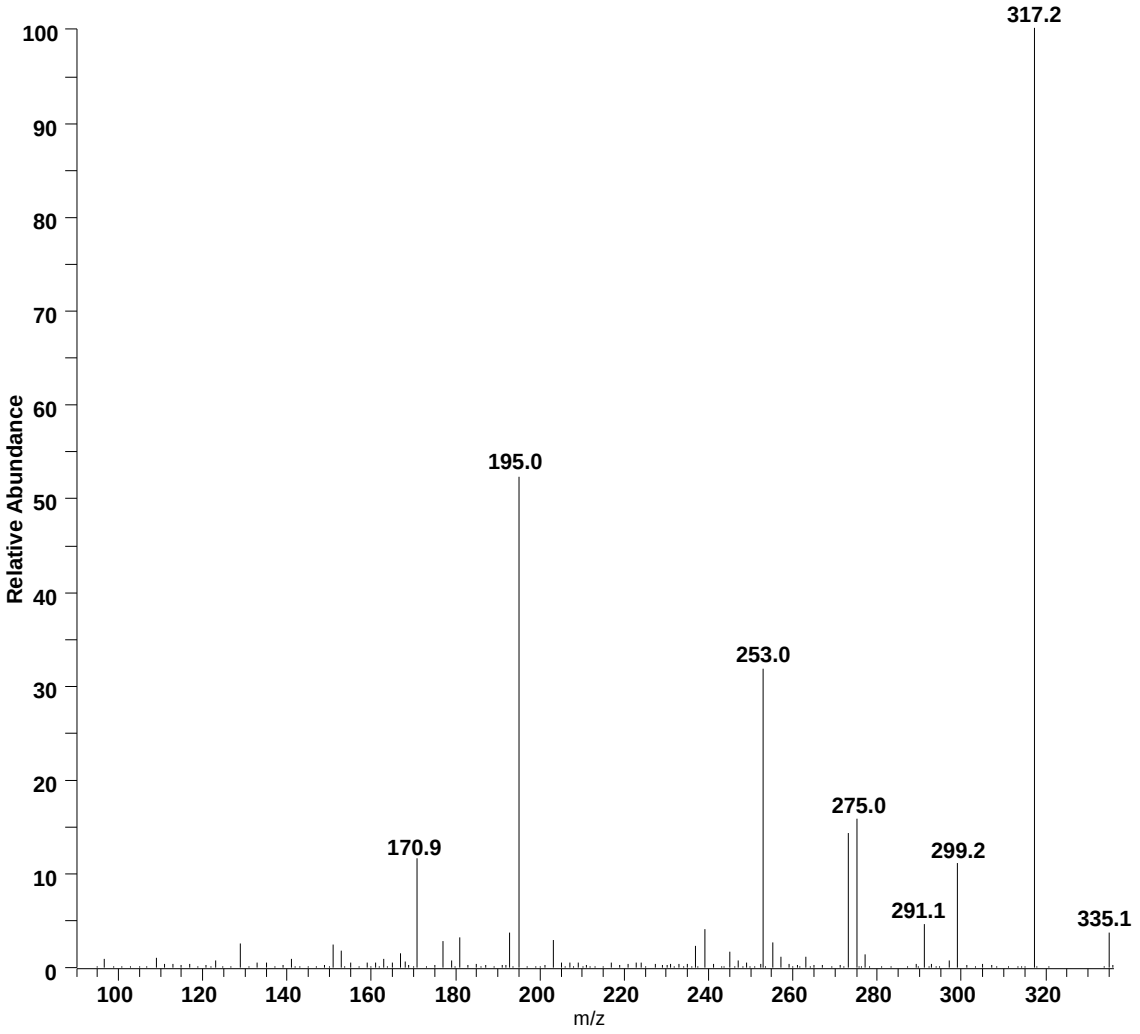

Figure 4.10: CID spectrum for LTB, precursor ion 335 *m/z*

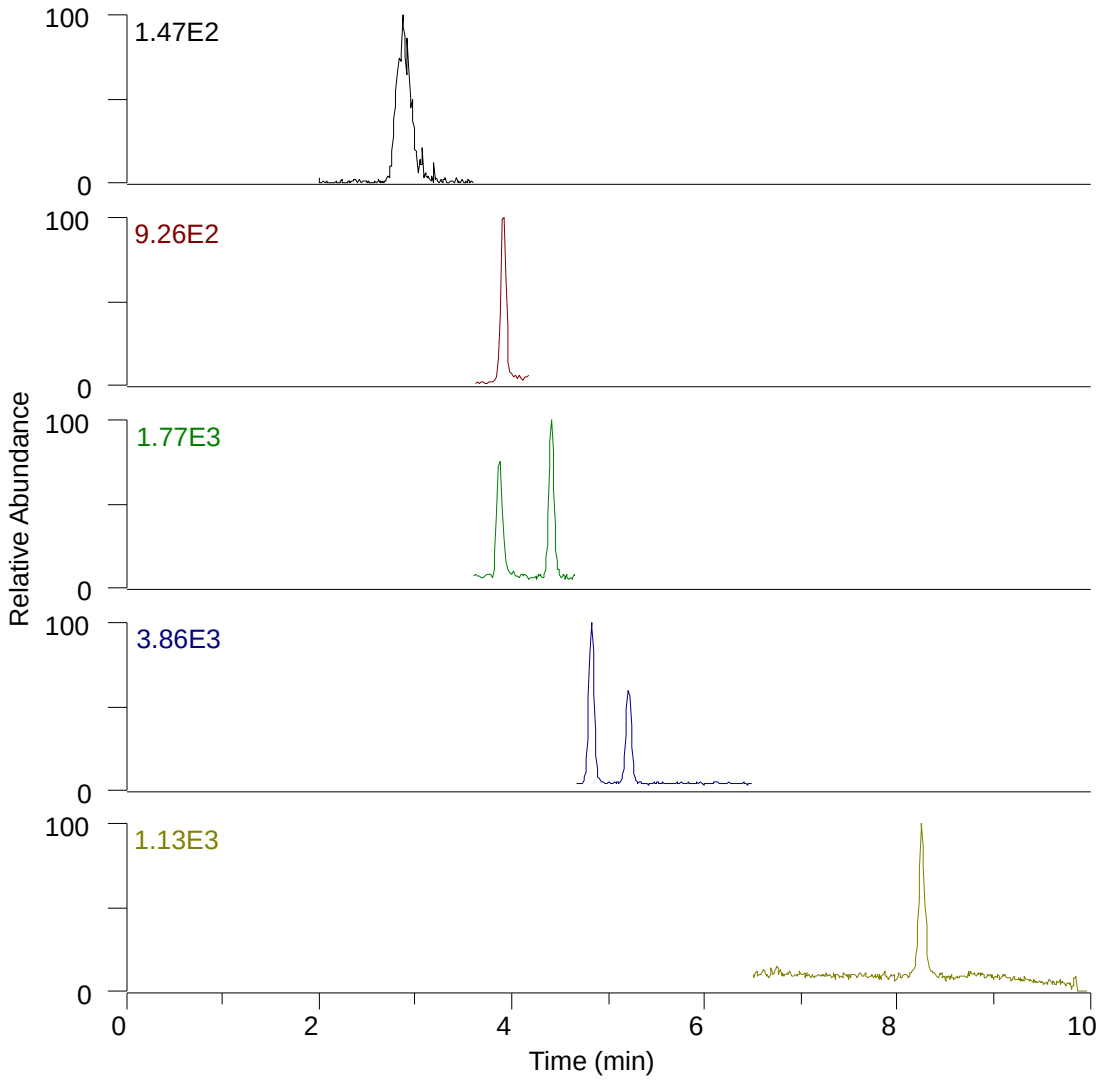

Figure 4.11: Extracted ion chromatograms of 10 nM standards for each eicosanoid. MS conditions were optimum for each standard

Each scan was set with the optimal settings for its respective analyte, and Figure 4.11 is the resulting extracted ion chromatograms of 10 nM standards under these optimal conditions. The limits of detection (S/N=3) was about 1 nM (~1.5 pg) for each prostaglandin and 5 nM (~8 pg) for LTB. These detection limits are not as good as immunoassays (fg/mL) [4, 10], but they are similar to other LC/MS methods [12, 13].

4.5 Validation

4.5.1 Ionization Suppression

The high salt concentration of microdialysis samples can lead to ionization suppression during LC-MS analysis. During flow-injection analysis and LC-MS modes using negative ionization mode, molecular ions of $[M-H]^-$ and $[M+Cl^-]^-$ were observed. To evaluate ionization suppression vs. elution time, two gradients were employed one where the majority of analytes eluted before 6 min and the other where all analytes eluted after 6 minutes. A 1 µM mixture of standards was run under each condition and peak areas were used to determine if elution time effected ionization suppression (Figure 4.12). The peak areas of analytes with the early eluting gradient were decreased compared to those of the longer retention, but this difference was not significant. With no distinct advantage to longer retention of the analytes the early elution gradient was chosen because it gave the best peak resolution.

To test the effect of ionization suppression, two sets of 50 nM standards were made; one in Ringer's solution and one in nanopure water. Both sets were injected repeatedly (n=5) with standards in water first to avoid salt carryover. All the analytes except LTB were statistically ($p<0.001$) different between water and Ringer's solution (Figure 4.13). Standards prepared in Ringer's solution had a decrease in signal between 12-21% compared to standards prepared in water.

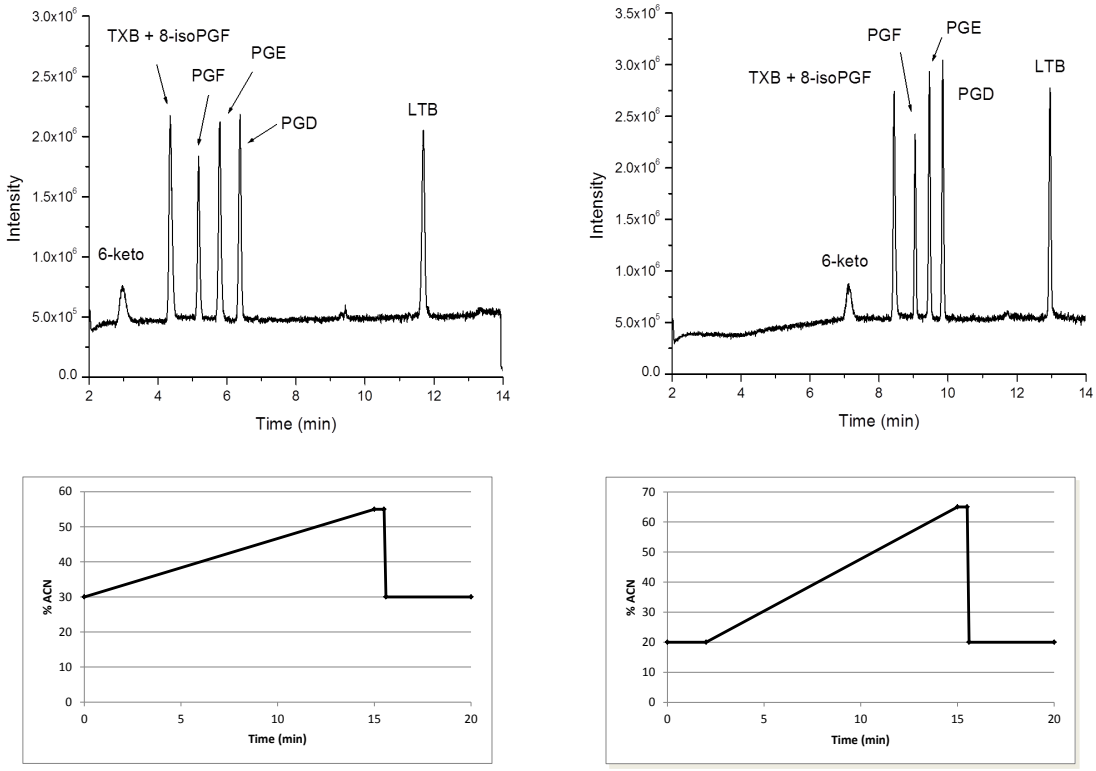

Figure 4.12: Total ion chromatograms (with gradient profiles) of 1 µM eicosanoid mixtures in Ringer's solution to examine the effects of ionization suppression with elution time

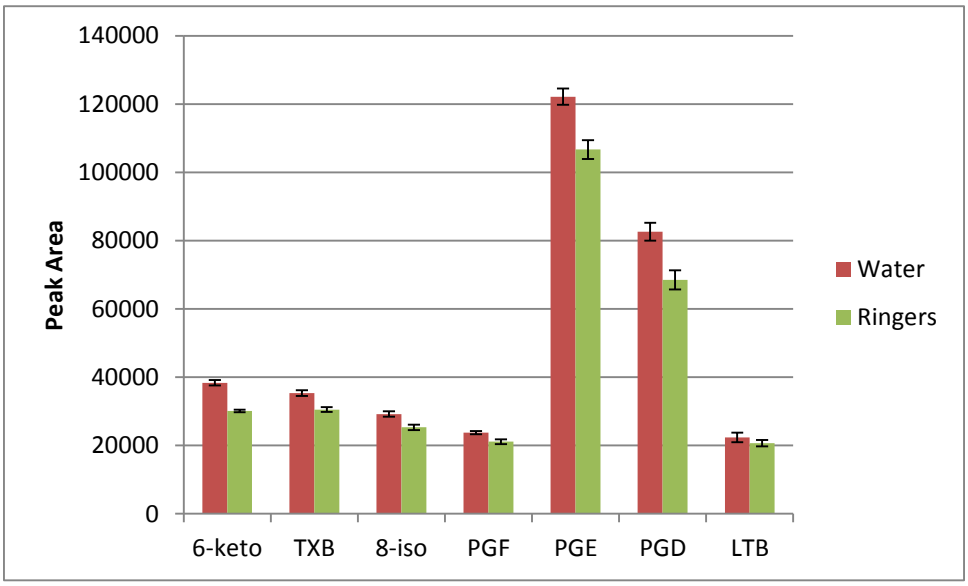

Figure 4.13: Ionization depression. Average peak areas of standards diluted in water and Ringer's solution (n=5). Only LTB was not statistically different between the two matrices, for all others, $p<0.001$.

4.5.2 Reproducibility

To determine intra-day reproducibility, a 100 nM standard was injected repeatedly throughout a day (n=7) (Table 4.2). Solutions of 1000 and 10 nM were also injected repeatedly and there appeared to be no concentration dependence on peak elution or area. For inter-day reproducibility, a 100 nM standard mixture was made and injected repeatedly (n=4) on four separate days (Table 4.3). Again, solutions of 1000 and 10 nM were also made and injected repeatedly. It should be noted the difference between the intra- and inter-day reproducibility was due to adjustments to the system parameters. Between the two experiments the LC and MS settings were adjusted in order to decrease run time and improve limits of detection.

A freeze-thaw experiment was performed where a 100 µM standard mixture was made in Ringer's solution and aliquoted into separate microcentrifuge tubes to be stored at -20 °C for zero, one, and two days. There was an observable decrease in response after the standard mixture had been frozen (Figure 4.14A); this was not the case when standards were diluted in water. It was believed that the high salt concentration from the Ringer's solution caused the eicosanoids to fall out of solution.

In an attempt to prevent this problem, standards were diluted in Ringer's solution containing 1 mM hydroxylpropyl-β-cyclodextrin. As previously performed, a 100 µM mixture (with 1 mM cyclodextrin) was made and aliquoted into separate microcentrifuge tubes and frozen. The decrease in response from freezing was alleviated with cyclodextrin; however, there was still a significant decrease for some of the eicosanoids (Figure 4.14B). Because of this drop in response (both with and without cyclodextrin) all samples collected from either *in vitro* or *in vivo* were analyzed on the day collected and not frozen.

	Time		Peak Area	
	Avg ± STD	CV (%)	Avg ± STD	CV (%)
6-Keto	3.01 ± 0.02	0.8	5300 ± 100	2
TXB	4.12 ± 0.01	0.3	8100 ± 300	4
8-Iso	4.09 ± 0.01	0.3	8200 ± 200	2
PGF	4.66 ± 0.01	0.3	6300 ± 200	3
PGE	5.104 ± 0.008	0.1	19200 ± 200	0.8
PGD	5.52 ± 0.01	0.3	11600 ± 200	2
LTB	8.736 ± 0.005	0.06	16500 ± 900	5

Table 4.2: Intra-day reproducibility of retention times and peak areas for a 100 nM standard mixture of the seven eicosanoids (n=7).

	Time		Peak Area	
	Avg ± STD	CV (%)	Avg ± STD	CV (%)
6-Keto	3.11 ± 0.03	1	6600 ± 400	6
TXB	4.62 ± 0.05	1	8800 ± 600	7
8-Iso	4.57 ± 0.05	1	9500 ± 500	5
PGF	5.42 ± 0.05	1	7900 ± 500	6
PGE	6.05 ± 0.06	0.9	25000 ± 2000	8
PGD	6.65 ± 0.06	0.9	13000 ± 1000	8
LTB	9.73 ± 0.02	0.2	14000 ± 2000	12

Table 4.3: Inter-day reproducibility of retention times and peak areas of a 100 nM standard mixture of the seven eicosanoids (4 days, n=14)

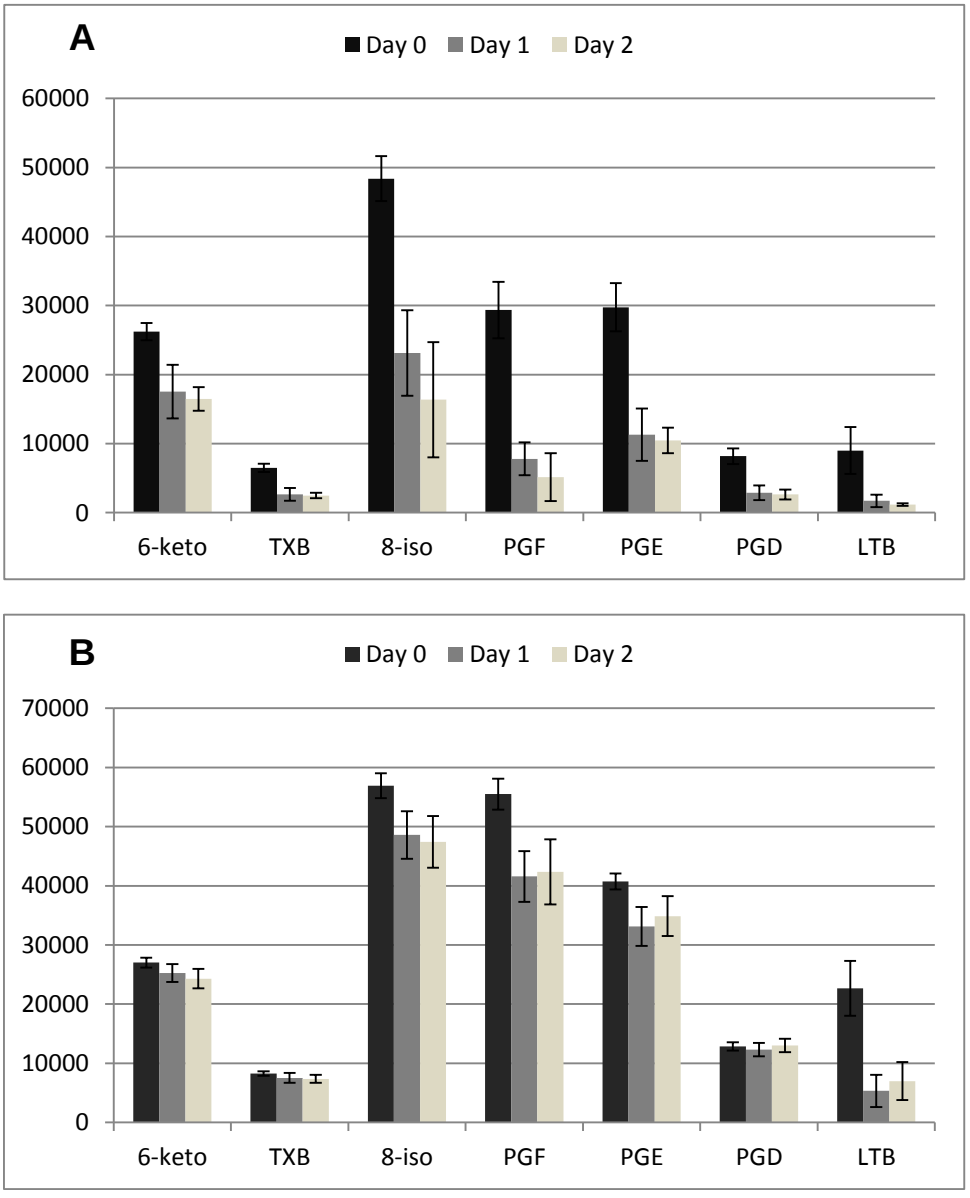

Figure 4.14: Freeze-thaw data comparing 100 μM standards in Ringer's solution (A) and in Ringer's solution with 1 mM hydroxypropyl-β-cyclodextrin (B).

4.6 Microdialysis

4.6.1 *In Vitro* Sample Switching

All the prostaglandins demonstrated good recoveries when switching the probe between standard solutions. LTB, however, had delayed responses compared to the prostaglandins when switching the probe between the sets of solutions (Figure 4.15). These data would indicate that LTB has some type of interaction with the probe. Previous reports of the effects of various membrane materials on leukotriene recovery showed that the more hydrophobic membranes (such as poly(arylene ether sulfone) used here) had lower mass transfer coefficients than the hydrophilic membranes [24]. The delay in response from sample switching seen with LTB is most likely due to adsorption to the membrane surface. Table 4.4 shows the recoveries for each compound during the specified solution, and these results are comparable to previous reports [24, 25]

4.6.2 *In Vivo* 3-MPA Local Dosing

The 3-MPA local dosing model from Chapter 3 was used in order to correlate to the MDA results. An MS^1 single ion monitoring (SIM) scan of 105 *m/z* [M-H]- was added to the LC-MS method in order to detect 3-MPA in the dialysate samples. Similar to previous work in our laboratory [26], 3-MPA delivery reached a steady state during the last 30 minutes of dosing, then had an exponential decay after dosing was terminated (Figure 4.16). The average total delivery of 3-MPA to the hippocampus was 39.0 ± 0.8 µg (n=3) as determined by subtracting the mass in the perfusate from the mass in the dialysate for each point during delivery.

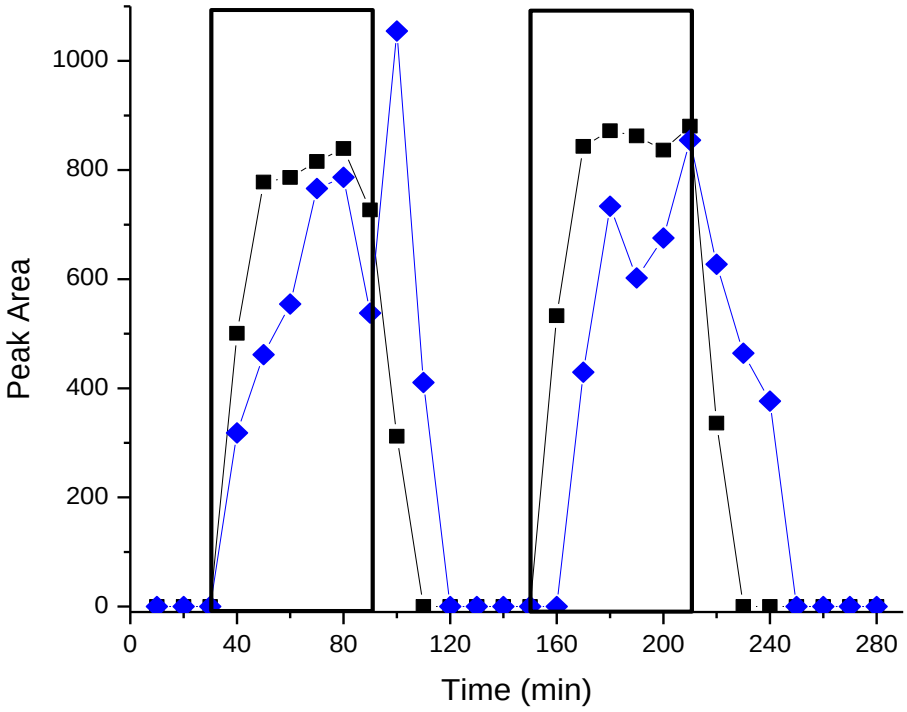

Figure 4.15: Time plots of *in vitro* sampling switching experiment comparing 6-keto (-■-) and LTB (-◆-). Each box represents time frame when the microdialysis probe was in 50 nM standard solution, for all other time points the probe was in Ringer's solution. Note the time delay in LTB reaching zero detection between solutions.

Sample Vial	6-keto	TXB	8-Iso	PGF	PGE	PGD	LTB
1st 50	8.3 ± 0.6	12.7 ± 0.9	13 ± 1	14.9 ± 0.7	17 ± 1	24 ± 1	40 ± 10
1st 100	8.7 ± 0.5	12 ± 1	12.3 ± 0.7	14.3 ± 0.6	19.3 ± 0.4	22 ± 1	33 ± 1
2nd 50	7.3 ± 0.5	12.2 ± 0.4	11.2 ± 0.9	12.4 ± 0.6	15.9 ± 0.3	22.9 ± 0.7	42 ± 2
2nd 100	10.8 ± 0.4	16.8 ± 0.9	15.6 ± 0.5	18.4 ± 0.6	26 ± 2	30 ± 1	42 ± 4
3rd 50	7.6 ± 0.9	13 ± 1	11 ± 1	13.8 ± 0.9	18.0 ± 0.8	26 ± 3	49 ± 5

Table 4.4: Percent recoveries for eicosanoids during the sample switching *in vitro* experiment. Averages and deviations are based the time intervals in each specified solution, excluding the first 10 minute sample.

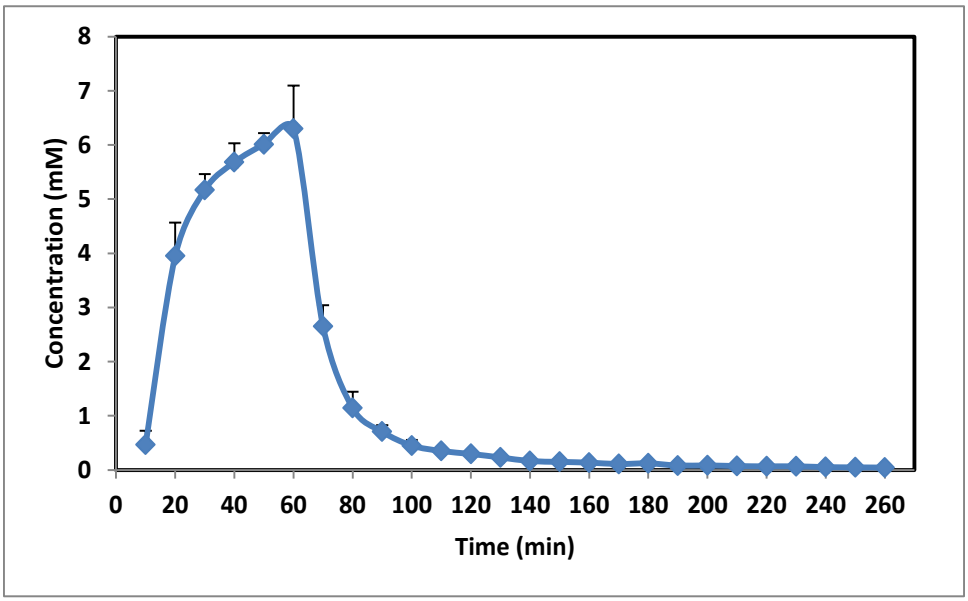

Figure 4.16: Estimated concentration of 3-MPA in dialysate samples from the hippocampus (n=3). Dosing started at the 10 minute time point and ended after the 50 minute time point.

Of the seven analytes, only four were detectable in basal samples; PGF, PGE, PGD and TXB. Interestingly, 8-iso, the free radical byproduct from COX, was not detectable in any sample during the experiment and neither was LTB. 6-Keto was more difficult to detect (in part from its peak shape) and could be detected more sporadically than the other prostaglandins. There was a decrease in all prostaglandins during 3-MPA dosing followed by a rebound back to basal for PGF and PGD and to elevated levels for TXB and PGE (Figure 4.17). Patel *et al.* [25] observed increases in TXB (3 to 4 times basal) and 6-keto (2 times basal) in the hippocampus following 20 minutes of ischemia; however, there were no changes in 6-keto with either 8 or 12 minutes of ischemia. The changes in TXB post 3-MPA dose seen here were similar to those from Patel *et al*. The decrease of the four previously mentioned prostaglandins during 3-MPA dosing was quite unexpected considering the amount of MDA produced with this same model in the same region (Chapter 3).

A possible explanation for the noticeable decrease in the prostaglandins is that while dosing, there is such an enormous amount of excitotoxicity occurring that all the accessible lipids are being oxidized into secondary products such as MDA. There have been reports of free radical products such as isoPGE and isoPGD (that were not studied here) to suggest other possible mechanisms that are independent of COX but still lead to the formation of prostaglandins [27, 28].

Another class of lipids termed the endocannabinoids, in particular arachidonoylethanolamide (AEA) and 2-arachidonoylglycerol (2-AG), are arachidonic acid ester derivatives released from phosphatidylinositol-4,5-biphosphate by phospholipase C [29]. Theses cannabinoids can still be metabolized by COX (similar to arachidonic acid) to produce oxidative prostaglandin esters which can further oxidize and breakdown into MDA [30].

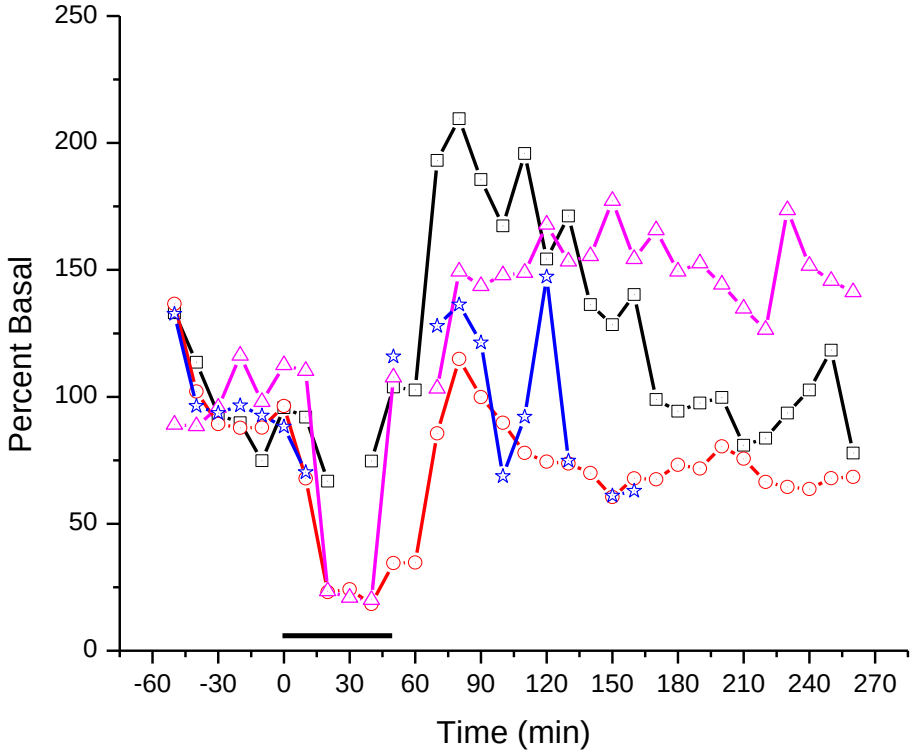

Figure 4.17: Response of TXB (-□-), PGF (-○-), PGE (-△-) and PGD (-☆-) to 3-MPA local dosing in the hippocampus CA3 region. Solid bar represents 50 minutes of 3-MPA dosing.

Toscano *et al* reported a decrease in GABA mediated inhibition with COX-2 knockout mice compared to wild type [31]. This relationship indicates a protective mechanism within the hippocampus and could provide another explanation to the results seen here. As stated in Chapter 3, GABA increased to a greater extent in the CA3 than CA1 regions with 3-MPA local dosing, and there is a higher localization of COX-2 in the CA3 than CA1. It is possible then, that the decrease in prostaglandins observed during 3-MPA dosing could be an effect of GABA suppressing COX activity.

In another study, the same group observed increases in PGF_2, TXB_2, PGD_2 and PGE_2 one hour after *i.p.* injections of kainate or NMDA in COX-2 knockout mice versus wild type [32]. More interestingly though, they found that while seizure intensity between either the kainate or NMDA dosed mice were the same, the quantities of prostaglandins produced were not. This demonstrates that the levels of prostaglandins correlate with neuronal damage and not the severity of the seizure [32].

Studies have demonstrated the induction of COX-2 involves two mechanisms; a rapid response to tissue damage (within 1 hour) followed by an excitotoxicity induction from stimulation (about 4 hours) [33]. The results here may be an after effect of the initial damage caused by probe implantation and not only from 3-MPA dosing. To determine if this is the case, experiments with a longer wait time before 3-MPA dosing or with awake-animals should be performed.

4.7 Conclusion

Here the coupling of HPLC with mass spectrometry allowed for separation and detection of seven eicosanoids including two sets of stereoisomers. Mass spectrometry is a powerful technique with a high degree of selectivity not afforded by traditional spectrometric methods and was best suited for the detection of eicosanoids. This

method provided linearity over 3 orders of magnitude with detection limits of about 1 nM for prostaglandins and 5 nM for LTB. The application of this method to microdialysis samples from local dosing of 3-MPA in the hippocampus CA3 region revealed unpredicted results. During 3-MPA dosing, prostaglandins decreased compared to basal which is the opposite result as MDA from the same model.

4.8 References

1. Phillis, J. W.; Horrocks, L. A.; Farooqui, A. A., Cyclooxygenases, lipoxygenases, and epoxygenases in CNS: Their role and involvement in neurological disorders. *Brain Res. Rev.* **2006,** *52* (2), 201-243.
2. Lazarewicz, J. W.; Salinska, E., N-Methyl-D-Aspartate-Evoked Release of Cyclooxygenase Products in Rabbit Hippocampus - An In-Vivo Microdialysis Study. *J. Neurosci. Res.* **1995,** *40* (5), 660-666.
3. Ma, T. C.; Zhu, X. Z., Effects of intrahippocampal infusion of interleukin-6 on passive avoidance and nitrite and prostaglandin levels in the hippocampus in rats. *Arzneimittelforschung* **2000,** *50* (3), E227-E231.
4. Pepicelli, O.; Fedele, E.; Berardi, M.; Raiteri, M.; Levi, G.; Greco, A.; Ajmone-Cat, M. A.; Minghetti, L., Cyclo-oxygenase-1 and-2 differently contribute to prostaglandin E-2 synthesis and lipid peroxidation after in vivo activation of N-methyl-D-aspartate receptors in rat hippocampus. *J. Neurochem.* **2005,** *93* (6), 1561-1567.
5. Chen, C.; Bazan, N. G., Lipid signaling: Sleep, synaptic plasticity, and neuroprotection. *Prostaglandins Other Lipid Mediat.* **2005,** *77* (1-4), 65-76.
6. Sang, N.; Chen, C., Lipid signaling and synaptic plasticity. *Neuroscientist* **2006,** *12* (5), 425-434.
7. Ercegovac, M.; Jovic, N.; Simic, T.; Beslac-Bumbasirevic, L.; Sokic, D.; Djukic, T.; Savic-Radojevic, A.; Matic, M.; Mimic-Oka, J.; Pljesa-Ercegovac, M., Byproducts of protein, lipid and DNA oxidative damage and antioxidant enzyme activities in seizure. *Seizure* **2010,** *19* (4), 205-210.
8. Pepicelli, O.; Fedele, E.; Bonanno, G.; Raiteri, M.; Ajmone-Cat, M. A.; Greco, A.; Levi, G.; Minghetti, L., In vivo activation of N-methyl-D-aspartate receptors in the rat hippocampus increases prostaglandin E-2 extracellular levels and triggers lipid peroxidation through cyclooxygenase-mediated mechanisms. *J. Neurochem.* **2002,** *81* (5), 1028-1034.
9. Yin, H. Y.; Havrilla, C. M.; Gao, L.; Morrow, J. D.; Porter, N. A., Mechanisms for the formation of isoprostane endoperoxides from arachidonic acid - "Dioxetane" intermediate versus beta-fragmentation of peroxyl radicals. *J. Biol. Chem.* **2003,** *278* (19), 16720-16725.
10. Malmberg, A. B.; Yaksh, T. L., Cyclooxygenase Inhibition and the Spinal Release of Prostaglandin E(2) and Amino-Acids Evoked by Paw Formalin Injection - A Microdialysis Study in Unanesthetized Rats. *J. Neurosci.* **1995,** *15* (4), 2768-2776.
11. Schneede, J.; Mortensen, J. H.; Kvalheim, G.; Ueland, P. M., Capillary Zone Electrophoresis with Laser-Induced Fluorescence Detection for Analysis of Methylmalonic Acid and other Short-Chain Dicarboxylic-Acids Derivatized with 1-Pyrenyldiazomethane. *J. Chromatogr. A* **1994,** *669* (1-2), 185-193.
12. Masoodi, M.; Eiden, M.; Koulman, A.; Spaner, D.; Volmer, D. A., Comprehensive Lipidomics Analysis of Bioactive Lipids in Complex Regulatory Networks. *Anal. Chem.* **2010,** *82* (19), 8176-8185.
13. Schmidt, R.; Coste, O.; Geisslinger, G., LC-MS/MS-analysis of prostaglandin E-2 and D-2 in microdialysis samples of rats. *J. Chromatogr. B* **2005,** *826* (1-2), 188-197.
14. Dass, C., *Principles and Practice of Biological Mass Spectrometry*. John Wiley & Sons, Inc: New York, 2001.

15. Silverstein, R. M.; Webster, F. X., *Spectrometric Identification of Organic Compounds*. 6th ed.; Wiley & Sons, Inc: Hoboken, 1998.
16. Cech, N. B.; Enke, C. G., Practical implications of some recent studies in electrospray ionization fundamentals. *Mass Spectrom. Rev.* **2001,** *20* (6), 362-387.
17. Robb, D. B.; Covey, T. R.; Bruins, A. P., Atmospheric pressure photoionisation: An ionization method for liquid chromatography-mass spectrometry. *Anal. Chem.* **2000,** *72* (15), 3653-3659.
18. Fenn, J. B.; Mann, M.; Meng, C. K.; Wong, S. F.; Whitehouse, C. M., Electrospray Ionization for Mass-Spectrometry of Large Biomolecules. *Science* **1989,** *246* (4926), 64-71.
19. Smith, R. D.; Loo, J. A.; Edmonds, C. G.; Barinaga, C. J.; Udseth, H. R., New Developments in Biochemical Mass-Spectrometry - Electrospray Ionization. *Anal. Chem.* **1990,** *62* (9), 882-899.
20. Cappiello, A., *Advances in LC-MS Instrumentation*. Elsevier: Amsterdam, 2007; Vol. 72.
21. Bredy, R.; Bernard, J.; Chen, L.; Montagne, G.; Li, B.; Martin, S., An introduction to the trapping of clusters with ion traps and electrostatic storage devices. *J. Phys. B-At. Mol. Opt. Phys.* **2009,** *42* (15).
22. Kitteringham, N. R.; Jenkins, R. E.; Lane, C. S.; Elliott, V. L.; Park, B. K., Multiple reaction monitoring for quantitative biomarker analysis in proteomics and metabolomics. *J. Chromatogr. B* **2009,** *877* (13), 1229-1239.
23. Scientific, T. Radial Ejection and Dual Detection on Thermo Scientific LTQ Series Linear Ion Trap Mass Spectrometers 2012, p. 1. http://www.thermoscientific.com/ecomm/servlet/techresource?storeId=11152&langId=-1&taxonomy=4&resourceId=89010&contentType=Product+Support+Bulletins&productId=11960637#.
24. Sun, L.; Stenken, J. A., Improving microdialysis extraction efficiency of lipophilic eicosanoids. *J. Pharm. Biomed. Anal.* **2003,** *33* (5), 1059-1071.
25. Patel, P. M.; Drummond, J. C.; Mitchell, M. D.; Yaksh, T. L.; Cole, D. J., Eicosanoid Production in the Caudate-Nucleus and Dorsal Hippocampus After Forebrain Ischemia - A Microdialysis Study. *J. Cereb. Blood Flow Metab.* **1992,** *12* (1), 88-95.
26. Mayer, A. Local Dosing in a 3-Mercaptopropionic Acid Chemically-Induced Epileptic Seizure Model with Microdialysis Sampling. University of Kansas, Lawrence, 2010.
27. Brose, S. A.; Thuen, B. T.; Golovko, M. Y., LC/MS/MS method for analysis of E-2 series prostaglandins and isoprostanes. *J. Lipid Res.* **2011,** *52* (4), 850-859.
28. Gao, L.; Zackert, W. E.; Hasford, J. J.; Danekis, M. E.; Milne, G. L.; Remmert, C.; Reese, J.; Yin, H. Y.; Tai, H. H.; Dey, S. K.; Porter, N. A.; Morrow, J. D., Formation of prostaglandins E-2 and D-2 via the isoprostane pathway - A mechanism for the generation of bioactive prostaglandins independent of cyclooxygenase. *J. Biol. Chem.* **2003,** *278* (31), 28479-28489.
29. Rouzer, C. A.; Marnett, L. J., Non-redundant functions of cyclooxygenases: Oxygenation of endocannabinoids. *J. Biol. Chem.* **2008,** *283* (13), 8065-8069.
30. Costa, B.; Conti, S.; Giagnoni, G.; Colleoni, M., Therapeutic effect of the endogenous fatty acid amide, palmitoylethanolamide, in rat acute inflammation: inhibition of nitric oxide and cyclo-oxygenase systems. *Br. J. Pharmacol.* **2002,** *137* (4), 413-420.

31. Toscano, C. D.; Ueda, Y.; Tomita, Y. A.; Vicini, S.; Bosetti, F., Altered GABAergic neurotransmission is associated with increased kainate-induced seizure in prostaglandin-endoperoxide synthase-2 deficient mice. *Brain Res. Bull.* **2008,** *75* (5), 598-609.
32. Toscano, C. D.; Kingsley, P. J.; Marnett, L. J.; Bosetti, F., NMDA-induced seizure intensity is enhanced in COX-2 deficient mice. *Neurotoxicology* **2008,** *29* (6), 1114-1120.
33. Adams, J.; CollacoMoraes, Y.; deBelleroche, J., Cyclooxygenase-2 induction in cerebral cortex: An intracellular response to synaptic excitation. *J. Neurochem.* **1996,** *66* (1), 6-13.

Chapter 5

Conclusions and Future Directions

5.1 Conclusions

Two analytical methods were developed to monitor lipid peroxidation in animal models of oxidative stress using microdialysis sampling. First developed was a CE-fluorescence method for the detection of MDA. This method provided a range of linearity of over 2 orders of magnitude with LOD of 25 nM. The second method was an LC-MS/MS method for the detection of seven products of the arachidonic acid cascade; 6-keto$PGF_{1\alpha}$, TXB_2, 8-iso$PGF_{2\alpha}$, PGF_2, PGE_2, PGD_2, and LTB_4. The method had a range of linearity of 3 orders of magnitude for all analytes with detection limits of around 1nM.

These methods were applied to a focal seizure animal model previously used in our laboratory [1]. In this model, 3-MPA was dosed through the microdialysis probe for 50 minutes directly into the CA3 or CA1 regions of the hippocampus. 3-MPA is an inhibitor of glutamate decarboxylase, preventing the synthesis of GABA from glutamate creating an excitatory state in the brain. Excitotoxicity from glutamate can cause cell death and has been related to several disease states such as Alzheimer's, Parkinson's, and Amyotrophic Lateral Sclerosis [2].

Shortly after the start of 3-MPA dosing there were increases in MDA ultimately reaching a maximum of 7 µM in the CA3 and 4 µM in the CA1 region at the end of the 10 mM 3-MPA perfusion. MDA began to decrease after dosing, but never returned to basal levels. Dosing 1 and 0.1 mM 3-MPA also produced an increase in MDA although there was not a linear relationship between 3-MPA concentration and MDA production. It was postulated that the difference in MDA between the two regions in the hippocampus was

due to greater localization of COX-2 in the CA3 than in the CA1. COX-2 is the inducible isoform of COX catalyzing the synthesis of prostaglandins from arachidonic acid. If there is more COX-2, then there is more oxidation of poly-unsaturated lipids leading to more MDA formation.

3-MPA local dosing also produced increases in glutamate and GABA in both regions of the hippocampus. Interestingly, changes in glutamate were the same between regions while there was a greater increase in GABA in the CA3 than the CA1 region. This difference in GABA between regions was attributed to a greater number of GABAnergic neurons located about the CA3 region in the dentate gyrus.

The only arachidonic acid metabolites detected in the CA3 region were TXB, PGF, PGE and PGD. During 3-MPA dosing, there was an unexpected decrease in all four prostaglandins. It was postulated that this decrease was due to free radical attack on the prostaglandins as a result of the excitotoxicity from glutamate ultimately forming MDA in the process.

Although the exact mechanism to which lipid peroxidation occurs during 3-MPA local dosing is not yet fully understood, the degree of damage in the hippocampus has become more clear. It is evident that both glutamate and GABA play key roles to the extent of peroxidation. It has also become clear that lipid peroxidation occurs very rapidly during times of elevated glutamate and it is possible that this initial insult could have lasting effects on the structure and function of the hippocampus. Furthermore, the observation of MDA never returning to basal levels is indicative of continuing oxidation long after the cessation of stress. Lipid peroxidation plays a predominant role in oxidative stress events, and the ability to limit this type of damage could aid in the survival of tissue surrounding the area of insult.

5.2 Future Directions

The next step for this project is to continue the evaluation of the aforementioned prostaglandins in the CA1 region of the hippocampus. To further clarify the mechanisms associated here, modulating agents would be perfused. For example, dosing of selective inhibitors for either COX or PLA through the probe could help determine if the increase in MDA observed resulted from of the oxidation of prostaglandin metabolism or release of unsaturated fatty acids. Also, there have been reports of other isoprostanes related to PGE and PGD formed during oxidative stress [3]. These isoprostanes (8-isoPGE and 8-isoPGD) were observed in liver and urine. It would be interesting if either of these isoprostanes could be detectable in this 3-MPA model.

Another interesting study would be to see if the hippocampus is communicating within itself during 3-MPA dosing. In this experiment, two probes would be implanted, one in each region (the distance between implantation sites is large enough for both probes) and 3-MPA would then be dosed into one region at a time. Of course 3-MPA would have to be monitored in both regions to determine if there was either diffusion through the brain causing a response or if it was from signaling between regions. This may help elucidate the plausibility of the inhibitory surround theory [1], as well as the propagation of damage through the hippocampus.

It is possible that the increase in glutamate and GABA observed could have been diminished from the anesthesia used, as ketamine is a known NMDA antagonist [4]. Other reports have also demonstrated depressed glutamate stimulation with volatile anesthesia (*i.e.* isoflurane), disrupting NMDA transmission [5]. Previous work done in this laboratory showed differences between glutamate and GABA with local dosing of 3-MPA in several regions of the brain [1]. It is possible that the anesthesia could have

mitigated the damage caused thereby lessening MDA formation. Also, studies have demonstrated the generation of COX-2 involves two mechanisms: a rapid response to tissue damage (within 1 hour) followed by an excitotoxic induction from stimulation (about 4 hours) [6]. The results of MDA and the prostaglandins may be an after effect of the damage caused by probe implantation and the initial increase in COX-2 and not from the excitotoxicity of 3-MPA dosing. Therefore awake-animal studies would be needed in order to exclude other possible mechanisms.

References

1. Mayer, A. Local Dosing in a 3-Mercaptopropionic Acid Chemically-Induced Epileptic Seizure Model with Microdialysis Sampling. University of Kansas, Lawrence, 2010.
2. Mattson, M. P., Excitotoxic and excitoprotective mechanisms - Abundant targets for the prevention and treatment of neurodegenerative disorders. *Neuromol. Med.* **2003,** *3* (2), 65-94.
3. Gao, L.; Zackert, W. E.; Hasford, J. J.; Danekis, M. E.; Milne, G. L.; Remmert, C.; Reese, J.; Yin, H. Y.; Tai, H. H.; Dey, S. K.; Porter, N. A.; Morrow, J. D., Formation of prostaglandins E-2 and D-2 via the isoprostane pathway - A mechanism for the generation of bioactive prostaglandins independent of cyclooxygenase. *J. Biol. Chem.* **2003,** *278* (31), 28479-28489.
4. Olney, J. W.; Labruyere, J.; Wang, G.; Wozniak, D. F.; Price, M. T.; Sesma, M. A., NMDA Antagonist Neruotoxicity - Mechanism and Prevention. *Science* **1991,** *254* (5037), 1515-1518.
5. Martin, D. C.; Plagenhoef, M.; Abraham, J.; Dennison, R. L.; Aronstam, R. S., Volatile Anesthetics and Glutamate Activation of N-Methyl-D-Aspartate Receptors. *Biochem. Pharmacol.* **1995,** *49* (6), 809-817.
6. Adams, J.; CollacoMoraes, Y.; deBelleroche, J., Cyclooxygenase-2 induction in cerebral cortex: An intracellular response to synaptic excitation. *J. Neurochem.* **1996,** *66* (1), 6-13.